NEW MEXICO GEOLOGY

ISSN 0196-948X
Volume 22, No. 3, August 2000

NM Bureau of Mines & Mineral Resources
New Mexico Tech
Earth Science for the 21st Century
Science and Service

Field and microstructural observations from the Capilla Peak area, Manzano Mountains, central New Mexico

by *Joseph R. Marcoline*, *Steven Ralser**, and *Laurel B. Goodwin*, Department of Earth and Environmental Science,New Mexico Institute of Mining and Technology, Socorro, New Mexico 87801
*Corresponding author (ralser@nmt.edu)

FIGURE 1—Capilla Peak area, Manzano Mountains, central New Mexico.

Abstract

Proterozoic rocks in the Capilla Peak area preserve evidence, at all scales, for multiple deformation events. The dominant north-northeast-striking, east-dipping foliation (S_2), with a downdip mineral lineation, overprints an older foliation. In schists and metarhyolites, S_2 is a crenulation cleavage, whereas in quartzites, S_2 is a mylonitic fabric. Two generations of amphibole are preserved in amphibolites, an older, core-forming actinolite and a younger hornblende. The hornblende defines the S_2 foliation.

Microstructures in the quartzite mylonites vary from fine grained and equigranular to monocrystalline ribbons. All quartzite mylonites have a strong *c*-axis crystallographic preferred orientation. The quartzite mylonite microfabric and the presence of hornblende in the amphibolites indicate that deformation associated with D_2 occurred under upper greenschist to lower amphibolite facies conditions. Kinematic indicators associated with the S_2 foliation (e.g. S-C surfaces, porphyroclast systems) dominantly indicate an east-side-up sense of shear. A minority (ca 5%) record a west-side-up sense of shear. This variation in sense-of-shear indicators is interpreted to suggest a strain history that reflects general shear (simple shear plus flattening strain). The Proterozoic rocks exposed in the Capilla Peak area are interpreted to represent a part of a large, lower amphibolite facies, ductile shear zone, which was active at ca 1.4 Ga.

Introduction

The Proterozoic tectonic history of the southwestern United States is complex, with deformation and/or metamorphic events occurring at ca 1.65 Ga, 1.4 Ga, and 1.0 Ga (Karlstrom and Bowring, 1988; Grambling et al., 1989; Heizler et al., 1997). In New Mexico, the timing of deformation events is generally constrained to be contemporaneous with or younger than plutonism associated with crustal accretion at 1,750–1,650 Ma and older than the comparatively undeformed 1,400–1,450 Ma plutons. The timing of regional deformation has, in the past, generally been considered to accompany accretion of the continental crust at ca 1.65 Ga (e.g. Karlstrom and Bowring, 1988; Bauer and Williams, 1994), with only minor deformation accompanying metamorphism and pluton emplacement at ca 1.4 Ga. However, more recent observations have shown that deformation at ca 1.4 Ga is extensive and regional in nature, often completely overprinting the structures associated with deformation at 1.65 Ga (Lanzirotti et al., 1996; Marcoline et al., 1999; Williams et al., 1999; Ralser, 2000).

Locally, the timing of individual deformation events can be more accurately tied down. In central New Mexico the timing of deformation can be constrained in a number of areas. In the Magdalena Mountains, for instance, Bauer and Williams (1994) demonstrated deformation at ca 1,660 Ma. In the Manzano Mountains (Fig. 1), two phases of deformation are constrained to be younger than the 1,656 ± 10 Ma Monte Largo granodiorite (U/Pb zircon, Bauer et al., 1993), which is strongly deformed. The comparatively undeformed 1,427 ± 10 Ma

Also in this issue

New Mexico Science Fair Bureau award winners p. 64
2001 NMGS Fall Field Trip call for papers p. 65
Rockhound State Park p. 66
Charles H. Maxwell (1923–2000) p. 72
Thesis abstracts p. 75
Geographic names p. 85
Book review p. 86
Service/News p. 87
Upcoming meetings p. 88

Coming soon

Oil and gas activities in 1999
Geologic history, stratigraphy, and paleontology of SAM Cave, north-central New Mexico
Manzano Mountains State Park

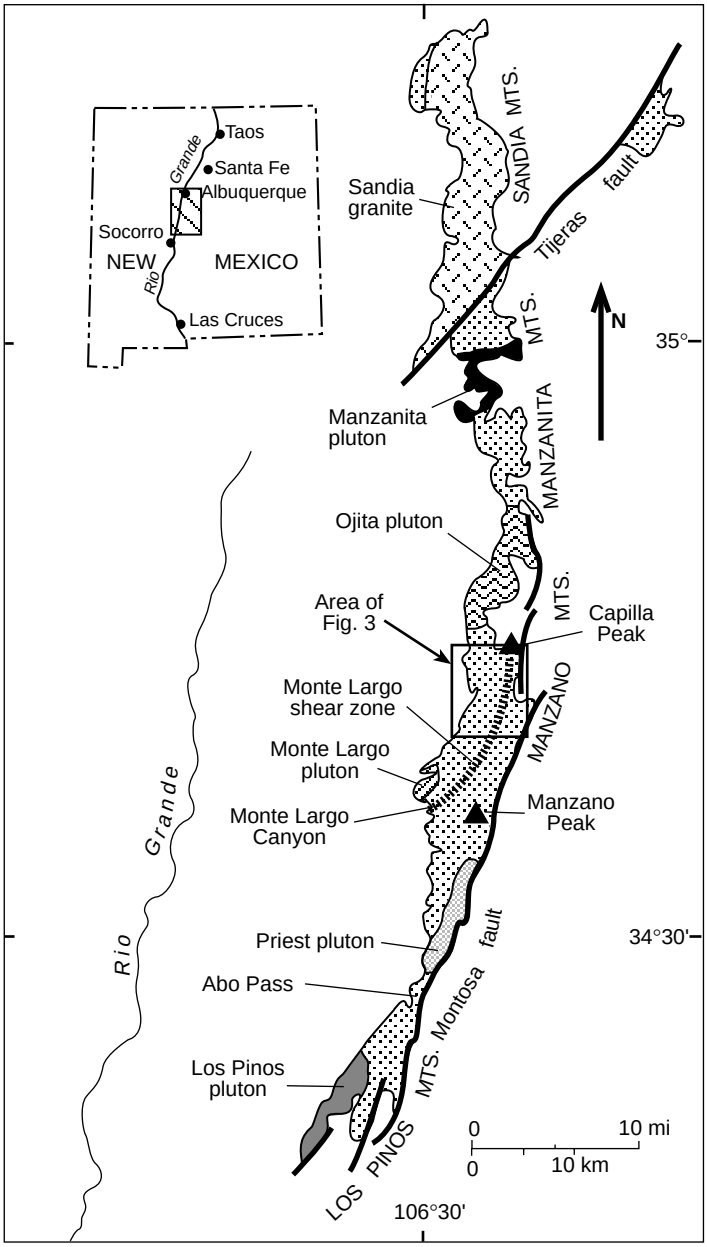

FIGURE 2—Location map, showing simplified geology of the Manzano Mountains (modified from Bauer et al., 1993).

Priest pluton (U/Pb zircon, Bauer et al., 1993) is interpreted to have intruded late syntectonic to the younger phase of deformation. This interpretation is supported by the presence of a strongly deformed granitic dike that has a U/Pb age of 1,438 ± 6 Ma (Ralser et al., 1997). Detailed $^{40}Ar/^{39}Ar$ geochronologic studies in the Capilla Peak area, in the central Manzano Mountains (Fig. 2), also suggest that the dominant structural fabric formed during 1.4 Ga tectonism (Marcoline, 1996; Marcoline et al., 1996, 1999). Localized deformation in the Priest pluton is related to the Grenville orogeny at ca 1,000 Ma (Heizler et al., 1997).

In this paper, we summarize structural relationships and deformation conditions in the Proterozoic rocks in the Capilla Peak area. Our goal is to document the structural relationships in this area in order to better understand the character and significance of 1.4 Ga deformation in New Mexico. This area straddles the northern extent of the Monte Largo shear zone (MLSZ; Bauer, 1983; Thompson et al., 1991), which separates lower amphibolite facies rocks in the south from upper greenschist facies rocks to the north (Thompson et al., 1991, 1996).

Location and regional geology

The Manzano Mountains are an eastward-tilted fault block composed primarily of Proterozoic metasedimentary, metavolcanic, and plutonic rocks. The mountain range is approximately 70 km long and 15 km wide and defines the eastern margin of the Rio Grande rift between the Manzanita Mountains and Abo Pass (Fig. 2). The study area is in the central Manzano Mountains, located between Capilla Peak and Trigo Canyon (Figs. 2, 3).

Three major lithologic units are recognized in the Capilla Peak area (Stark, 1956; Stark and Dapples, 1946; Reiche, 1949; Bauer, 1982): the Blue Springs Schist, the Whiterock quartzite, and the Sevilleta Metarhyolite. The Blue Springs Schist is composed of intensely folded metasiltstones, phyllites, and muscovite-chlorite schists (Stark 1956; Bauer 1982). Boudinaged quartzites within the Blue Springs Schist are now interpreted as transposed sedimentary layers but were initially believed to be saddle reefs (Stark, 1956).

The Whiterock quartzite consists of a series of quartzite mylonites interlayered with rocks of the Blue Springs Schist and Sevilleta Metarhyolite. These quartzite mylonites represent localized high-strain zones within a larger deformation zone (Marcoline, 1996). In Monte Largo Canyon these quartzite mylonites define the MLSZ (Bauer, 1983; Thompson et al., 1991), where it crops out as a discrete 3-m-wide shear zone.

The Sevilleta Metarhyolite (Stark and Dapples, 1946), is exposed predominately on the east side of the range in the Capilla Peak area (Fig. 3). The metarhyolite is pink to brown, well foliated, and lineated. In lower strain areas, the metarhyolite contains 1–2 mm equidimensional quartz and feldspar phenocrysts. Amphibolite layers (1–20 m wide and 400 m long) occur within the Sevilleta Metarhyolite and are interpreted to be deformed and metamorphosed early mafic dikes (Stark and Dapples, 1946). The amphibolites are petrologically complex, containing two amphibole phases, hornblende and actinolite, along with plagioclase, biotite, quartz, epidote, and minor amounts of titanite and Fe–Ti oxides. The mineral assemblages in different amphibolites all indicate formation under amphibolite grade conditions (Marcoline et al., 1999).

The stratigraphic relationships between these units are unclear, although it is

NEW MEXICO GEOLOGY

Science and Service

ISSN 0196-948X
Volume 22, No. 3, August 2000

Editors: Jane C. Love, Nancy S. Gilson, Bonnie Frey, and Susan Voss
Cartographers: Kathryn E. Glesener and Leo Gabaldon

Published quarterly by
New Mexico Bureau of Mines and Mineral Resources
a division of New Mexico Institute of Mining and Technology

Subscriptions: Issued quarterly, February, May, August, November; subscription price $10.00/calendar year.

Editorial Matter: Articles submitted for publication should be in the editor's hands a minimum of five (5) months before date of publication (February, May, August, or November) and should be no longer than 20 typewritten, double-spaced pages. All scientific papers will be reviewed by at least two people in the appropriate field of study. Address inquiries to Jane C. Love, Editor of *New Mexico Geology*, New Mexico Bureau of Mines and Mineral Resources, Socorro, New Mexico 87801-4796.

Circulation: 1,000

Printer: University of New Mexico Printing Services

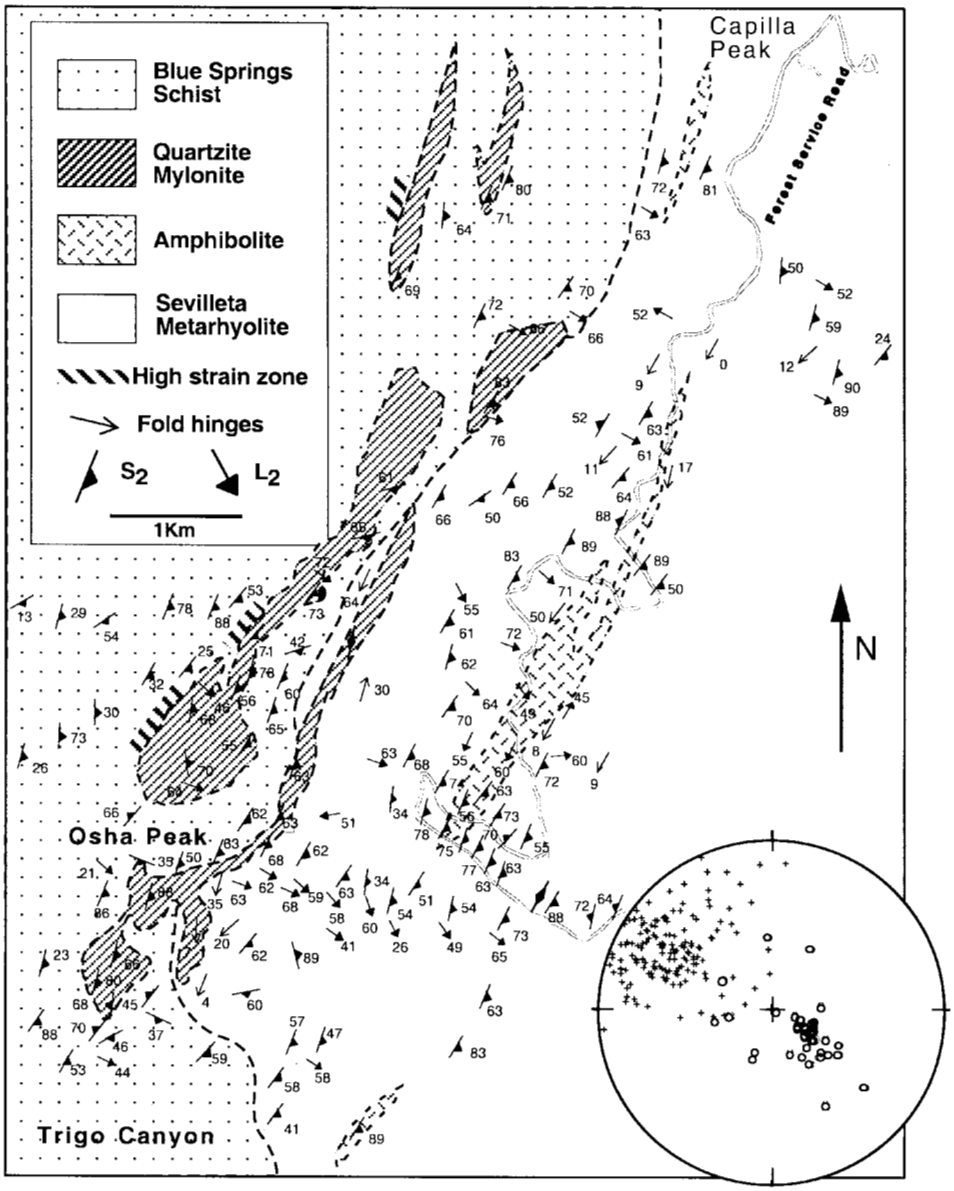

FIGURE 3—Geologic map of the Capilla Peak area showing the distribution of units, the main foliation (**S_2**), and lineation (**L_2**). Poles to foliation (**+**)and mineral lineations (**o**) are plotted on a lower hemisphere equal area projection.

believed that the Sevilleta Metarhyolite is the oldest unit, based on Rb–Sr isochrons with an age of 1,700 ± 58 Ma (Bolton, 1976) and a U–Pb zircon age of 1,680 Ma (Bowring et al., 1983).

Structure

The dominant structure in the central Manzano Mountains is a pervasive, northeast-striking, steeply southeast-dipping foliation (S_2; Fig. 3). In the schistose units, this foliation is a crenulation cleavage, cutting a well-defined earlier foliation (S_1). In the non-schistose units, S_2 is the main foliation. As this S_2 foliation is interpreted to have formed during tectonism at 1.4 Ga (Marcoline et al., 1999; Ralser, 2000), it will be described in detail in this paper. The macrostructural and microstructural nature of this foliation will be described from west to east (Blue Springs Schist, quartzite mylonites, Sevilleta Metarhyolite, amphibolites) in the following sections. We will describe *c*-axis crystallographic preferred orientations observed in the quartzite mylonites in the final part of this section.

Macrostructural relationships

S_2 exhibits significant variation in character and orientation in the Blue Springs Schist. In the phyllites and quartz-rich zones of the muscovite-chlorite schists, S_2 is a well-developed planar foliation, striking approximately 030° and dipping from 60° to 80° southeast. However, in quartz-poor zones of the muscovite-chlorite schist, the S_2 orientation is variable. S_2 anastamoses around the numerous folded quartz layers, with strikes ranging from 0° to 50° and dips varying from 60° to 90° southeast. Asymmetrical chevron-style crenulations, with limbs 1–3 cm in length and with axial planar S_2, are locally evident. The metasiltstones are characterized by small-scale disharmonic folding of the compositional layering. The S_2 foliation is poorly developed and highly irregular in orientation in the metasiltstones. The foliation is axial planar to the disharmonic folds, which may explain the large variation in orientation of S_2.

Intensely deformed Blue Springs Schist is found in three distinct, narrow zones less than a meter wide, which are characterized by a well-developed, planar S_1 foliation. The most continuous of these high-strain zones is located on the western contact between the quartzite mylonite and the Blue Springs Schist (Fig. 3). Two other highly deformed zones are located along strike within the Blue Springs Schist, adjacent to one of the smaller quartzite mylonite layers. The contacts between the highly deformed zones and the more typical schist are gradational. Away from the highly deformed zones the schist contains abundant quartz-rich layers. Nearer to the deformed zones, the quartz-rich layers become discontinuous and boudinaged. No quartz-rich layers were observed in the high-strain zones.

In quartzite mylonites, S_2 is a strong mylonitic foliation that strikes approximately 025° and dips from 60° to 80° southeast. S_1 is only preserved in lower strain zones as open to isoclinally folded surfaces. The development of S_2 is controlled by mica content in the quartzite mylonites; S_2 is best developed in areas with a higher mica content.

The Sevilleta Metarhyolites are, in general, characterized by a strongly developed north-northeast-striking foliation (S_2) with a locally well developed downdip lineation (Fig. 3). S_1 is only observed in a few locations where S_2 is poorly developed. The S_2 foliation is defined by aligned biotite and lens-shaped quartz and feldspar porphyroclasts. F_2 folds in the metarhyolite plunge shallowly to moderately to the south-southwest and include both small 0.5–1-m isoclinal folds and 3–5-m open folds. An S_2 axial planar foliation is only locally observed in the folded areas.

S_2 in the amphibolite layers ranges from weakly to strongly developed and is typically parallel to the foliation in the surrounding metarhyolite. One amphibolite layer contains distinctive less deformed 'pods' as large as 10 cm in diameter. These pods have length to width ratios ranging from 1:1 to 2:1 and contain 1–3-mm, unaligned, green to black amphibole crystals. A strong foliation wraps around the pods. The pods are sigmoidal in shape and asymmetric with respect to the main foliation, consistently recording east-side-up shearing. Several 0.5–1-m-scale asymmet-

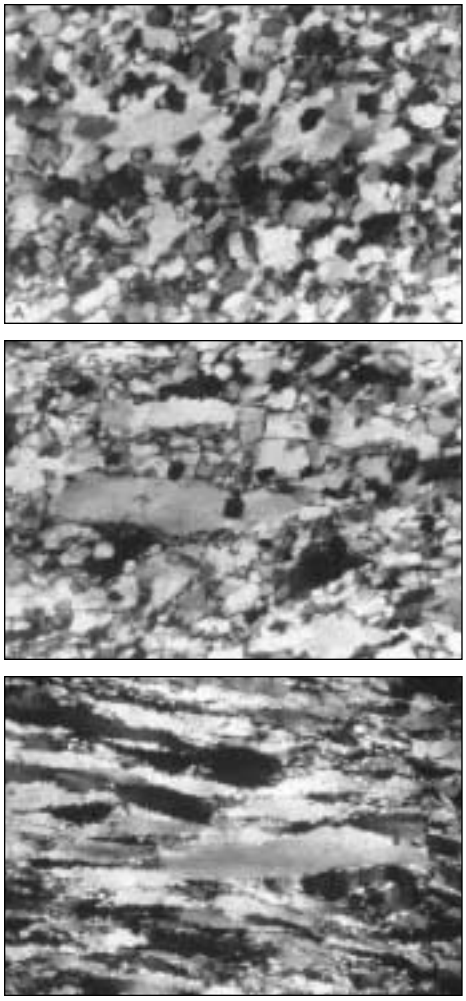

FIGURE 4—Photomicrographs showing the variation in microstructures developed in the quartzite mylonites. Three groups can be recognized based on microstructures. **A**) Group 1 is characterized by equant recrystallized quartz grains 0.1–0.25 mm in size. Note the recrystallized relic grain, and the grain-shape preferred orientation trending from bottom left to top right. **B**) Group 2 is characterized by a bimodal grain-size distribution with large elongate grains parallel to the main foliation and fine equigranular crystals. **C**) Group 3 is characterized by 1–20-mm, slightly undulose monocrystalline quartz ribbons. All photomicrographs normal to the foliation and parallel to the lineation; S_2 is horizontal; width of photos—**A** and **B**, 0.5 mm; **C**, 3 mm.

ric sigmoid-shaped structures within the amphibolite layers are also observed. These structures are similar to the pods but contain an internal foliation parallel to, but weaker than, the surrounding foliation.

Microstructural relationships

The character of the Blue Springs Schist is as variable microscopically as it is at the outcrop scale. In general, the S_2 crenulation cleavage is best developed adjacent to the quartzite mylonites. With better S_2 development, the cleavage-plane spacing decreases. In zones with a large amount of quartz, recrystallized grains preserve a grain-shape preferred orientation at a 45° angle to S_2.

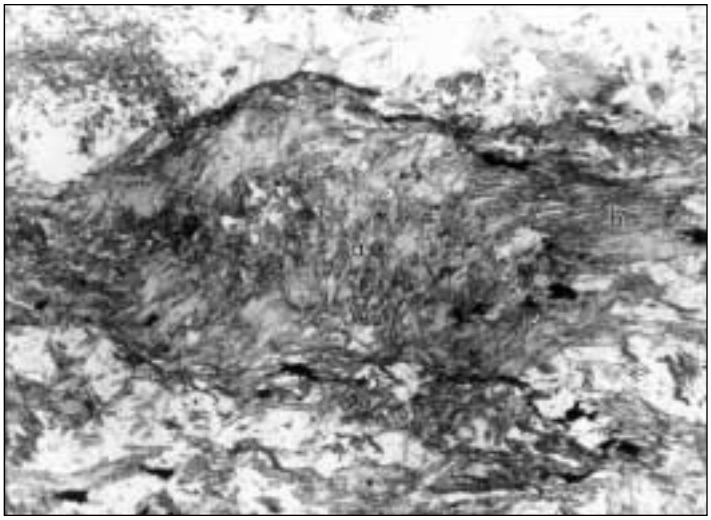

FIGURE 5—Photomicrograph showing two amphibole phases. Actinolite (**a**) forms cores and has inclusion trails nearly perpendicular to the foliation-forming, green euhedral hornblendes (**h**). Width of photo is 4.5 mm; S_2 is horizontal.

The major quartzite mylonite units can be divided into three groups on the basis of microstructures. The first group is characterized by 0.1–0.25-mm, recrystallized quartz grains with a strong to moderate grain-shape preferred orientation that defines a foliation at an angle between 45° and 60° from S_2 (samples ML 11-3, ML 7-15, and ML 6-2; Fig. 4A). The second group of quartzite mylonites is characterized by fine-grained, 0.1–0.25-mm, recrystallized quartz grains with 1–3-mm-long monocrystalline quartz ribbons (samples ML 7-1 and ML 7-3; Fig. 4B). The third group is characterized by 3–20+ mm-long monocrystalline quartz ribbons (samples ML 1-2, ML5-10; Fig. 4C). The ribbons exhibit undulose extinction with minor subgrain formation. S-C fabrics are locally present in the third group of quartzite mylonites. In all mylonite samples, micas are included within the recrystallized quartz grains as well as between grains, indicating a significant degree of grain boundary mobility and suggesting deformation at a high temperature or slow strain rate (e.g. Lister and Dornsiepen, 1982).

The metarhyolites are characterized by 1–2-mm quartz and feldspar porphyroclasts in a fine-grained (0.1–0.25 mm) foliated quartz and feldspar matrix. Although the majority of the feldspar porphyroclasts show orthorhombic symmetry with respect to the foliation (ϕ-type, see Passchier and Trouw, 1996), scattered asymmetric ∂-type porphyroclasts are also present. Asymmetric strain shadows, defined by recrystallized quartz, are developed around feldspar phenocrysts. Although these porphyroclasts show evidence for both west- and east-side-up sense of shear, the latter group is dominant.

The amphibolites exhibit complex microstructures and are dealt with in more detail elsewhere (Marcoline, 1996; Marcoline et al., 1999). They preserve older actinolite and younger hornblende, plagioclase, biotite, quartz, and epidote. The older anhedral actinolite is crosscut and overgrown by the foliation-forming euhedral hornblende (Fig. 5). Actinolite contains inclusion trails that record an older foliation parallel to the crystallographic cleavage planes and nearly perpendicular to the well-defined hornblende foliation. Hornblende both rims the actinolite and defines the S_2 foliation. Hornblende rims and foliation-forming grains show mutual crosscutting relations. The composition of the hornblende is consistent with formation at lower amphibolite facies conditions (Marcoline, 1996; Marcoline et al., 1999).

Quartz *c*-axis crystallographic preferred orientations

In general, *c*-axis crystallographic preferred orientations (CPOs) develop due to a reorientation of crystal axes as a result of dislocation slip (e.g. Hobbs et al., 1976; Van Houtte and Wagner, 1985; Williams et al., 1994). Dislocation slip occurs when the shear stress resolved on the slip plane in a particular slip direction reaches a critical value, the critical resolved shear stress (Hobbs, 1985; Van Houtte and Wagner, 1985). As with microstructural studies, CPO studies cannot provide unique constraints on the deformation conditions, because both intrinsic factors (e.g. temperature, strain rate) and extrinsic factors (e.g. strain history) can influence the development of CPOs (e.g. Hobbs, 1985). Increasing temperature has the same effect as decreasing strain rate. Slip systems that have a high critically resolved shear stress (CRSS) at low temperatures or fast strain rates (e.g. prism slip in quartz) have a much lower CRSS at higher temperatures or slower strain rates. Such changes in the operating slip systems are reflected in the CPOs that develop (e.g. Tullis et al., 1973; Lister and Hobbs, 1980; Schmid and Casey, 1986). The strain history also has a profound effect on the CPOs that develop; with a coaxial strain history, symmetric CPOs develop, whereas with a noncoaxial strain history, asymmetric CPOs develop (e.g. Lister and Hobbs, 1980). The sense of asymmetry can be used to determine the sense of shear (e.g. Schmid and Casey, 1986).

Two hundred *c*-axis orientations were

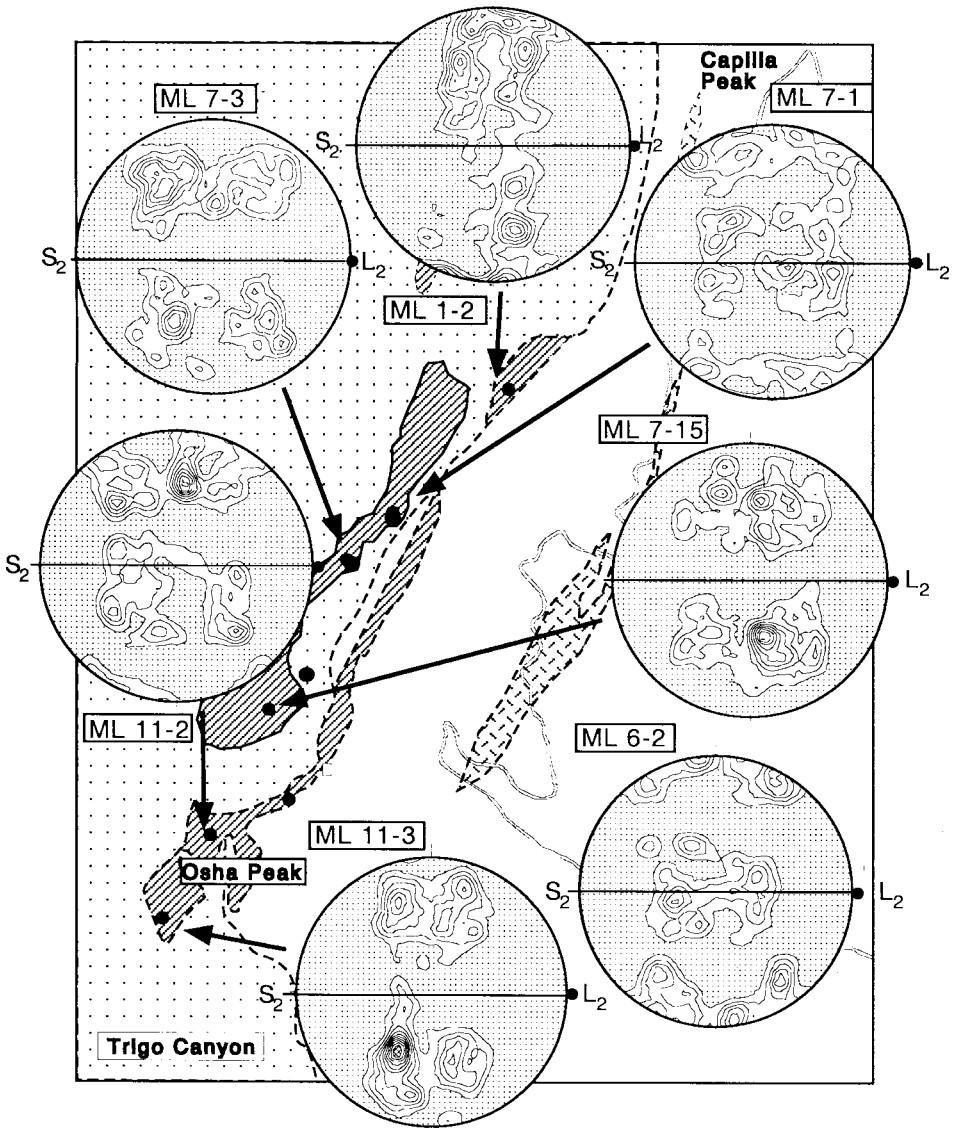

FIGURE 6—Geologic map of the Capilla Peak area showing location of quartzite mylonites where *c*-axes have been measured and showing equal area, lower hemisphere plots of 200 quartz grains. Contours represent multiples of uniform distribution.

measured from thin sections cut perpendicular to the lineation and foliation from each of seven representative quartzite mylonite samples from the Capilla Peak area (Fig. 6). Data were then plotted on equal area, lower hemisphere projections and rotated so that the trace of the foliation is horizontal and the lineation is horizontal and plunging to the right on each plot.

Three different patterns are observed in the quartzite mylonite samples. Incomplete small circle girdles about the pole normal to the foliation are developed in three samples (ML 11-3, ML 7-3, and ML 7-15; Fig. 6). In each girdle, two maxima are symmetrically distributed on either side of the pole to the foliation; however, the size of the maxima on either side of the pole to the foliation vary. Samples ML 6-2, ML 7-1, and ML 11-2 have *c*-axis distributions that range from normal to the foliation to perpendicular to the lineation, within the foliation plane (Fig 6). The maxima in these three samples are relatively symmetric, in both distribution and size, about the pole to the foliation. These plots are different from the first group of plots in that the maxima are located preferentially in the center and in the outer top and bottom portions of the plot. The CPO of sample ML 1-2 differs from those of the other samples, in that a relatively symmetric *c*-axis girdle is approximately normal to the lineation (Fig. 6).

Discussion

D_2 structures are developed throughout the Capilla Peak area and vary from a crenulation cleavage (with wavelengths from 0.5 mm to 5 cm) developed in the Blue Springs Schist to strongly foliated and lineated tectonites developed in the quartzites and metarhyolites. In most places S_1 is not visible. Zones of high strain formed during D_2 (characterized by a well-developed, planar foliation) are localized in the quartzite of the Blue Springs Schist, near the contact between the Blue Springs Schist and the quartzite mylonites, and in the Sevilleta Metarhyolite.

The Monte Largo shear zone (MLSZ) has previously been interpreted as a narrow (3–5 m in width) shear zone characterized by quartzite mylonites (Bauer, 1983; Thompson et al., 1991). This interpretation is based on studies along the southern extent of the MLSZ in Monte Largo Canyon. Our observations along the northern extent of the MLSZ in the Capilla Peak area indicate that deformation associated with the shear zone is more widespread. This increase in width of the deformed zone is related to the number of quartzite layers present, which is greater in the Capilla Peak area (Fig. 3). Deformation associated with the MLSZ is spread over the zone encompassed by the quartzite mylonites.

Deformation under amphibolite facies conditions is indicated by both mineral assemblages and microstructures. The hornblende, which defines the S_2 foliation in the amphibolites and accompanying phases, suggests formation under amphibolite facies conditions (c.f. Spear, 1981; see Marcoline et al., 1999 for a detailed discussion). These hornblendes yield $^{40}Ar/^{39}Ar$ ages of ca 1,400 Ma, indicating that hornblende closed to Ar diffusion and was, therefore, at temperatures around the greenschist/amphibolite facies boundary (~450°–550° C) at ca 1,400 Ma. Other features related to D_2 deformation, in particular microstructures and *c*-axis CPOs, are consistent with lower amphibolite facies deformation. The microstructures in the quartzite mylonites range from fine grained and equigranular to large monocrystalline quartz ribbons. Some areas (e.g. sample ML 11-2) show coexisting zones of monocrystalline quartz ribbons and fine-grained equigranular microstructure. Such microstructures are consistent with deformation at upper greenschist to lower amphibolite facies conditions (Simpson, 1985; Hanmer and Passchier, 1991). Because the pressure and temperature at which deformation took place could not have varied significantly within the small area encompassing the quartzite mylonites, changes in these deformation conditions can not be called on to explain the differences in microstructure observed in the quartzite mylonites. The observed microstructure variations, therefore, must be the result of variations in either strain, strain rate, composition, and/or water content (e.g. Kronenberg, 1981). The mineralogy, including the presence of hydrous phases, is similar in all the quartzite mylonites, suggesting that neither mineralogy nor water content affect the microstructure that developed. All the quartzite mylonites are strongly deformed so a steady state microstructure could have developed. It is, therefore, most likely that

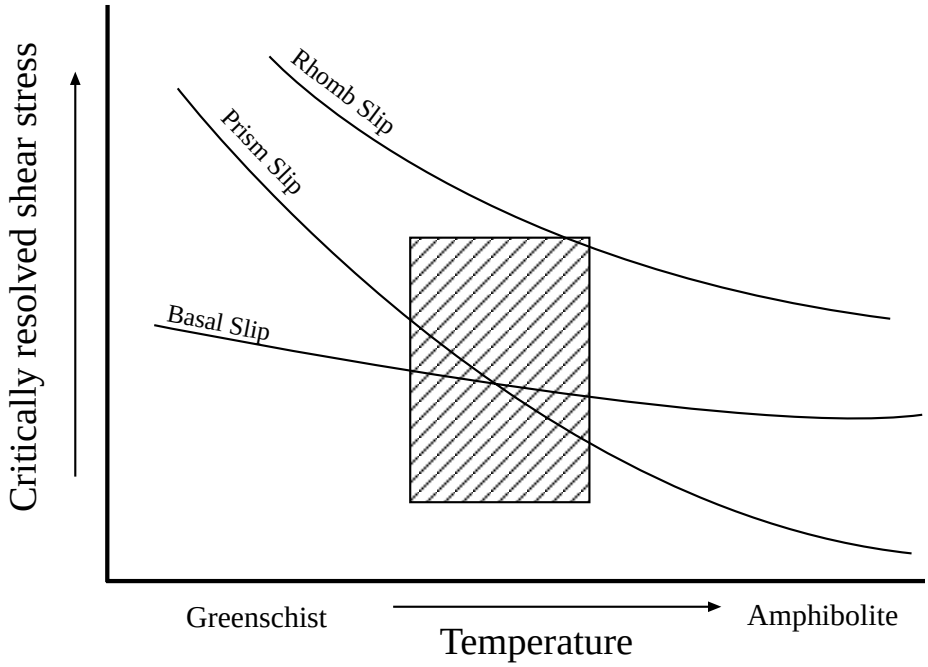

FIGURE 7—Plot of critically resolved shear stress versus temperature (Hobbs, 1985). The shaded area represents the approximate deformation conditions in the Capilla Peak area.

the observed microstructures reflect differences in strain rate rather than the alternatives.

The presence of only ∂-type porphyroclast systems, as opposed to σ-type porphyroclast systems, within the metarhyolites is striking. Previous workers have proposed that the dominance of ∂-type porphyroclast systems indicates that both the strain (rotation) rate was high relative to the recrystallization rate and that there was a component of extensional shear in the deformation (Passchier and Simpson, 1986; Hanmer and Passchier, 1991). Because we observe asymmetric fabrics and porphyroclast systems as well as a nearly orthorhombic symmetry in most quartzite mylonite *c*-axis CPOs, we believe that the observed deformation history resulted from a progressive, general, noncoaxial flow (Simpson and De Paor, 1993). Such an interpretation is consistent with the variable sense of shear determined from kinematic indicators in the Capilla Peak area (e.g. grain-shape preferred orientation, shear bands, asymmetric porphyroclast systems). The majority of these kinematic indicators indicate an east-side-up sense of shear, but approximately 5% of the kinematic indicators indicate a west-side-up sense of shear.

Interpretations from crystallographic preferred orientations

In order to use CPOs to place constraints on the conditions under which deformation took place in the MLSZ, it is necessary to determine which deformation mechanism(s) was (were) operating to form the observed microfabric. A strong CPO indicates that deformation was primarily accommodated by dislocation slip (e.g. Hobbs et al., 1976; Van Houtte and Wagner, 1985), with the operating slip systems a function of the deformation conditions (Fig. 7; e.g. Hobbs, 1985). The most commonly reported slip systems in quartz are basal, prism, and rhomb planes with slip primarily in the <*a*> direction; however, evidence of slip in the <*c*> and <*c*+*a*> directions has also been observed (e.g. Price, 1985). Basal <*a*> slip dominates at greenschist facies conditions, basal <*a*> and prism <*a*> slip show approximately equal activity at amphibolite facies conditions, and prism <*a*> slip dominates at higher-grade conditions (e.g. Hobbs, 1985). Although determination of active slip systems can only be made unequivocally through detailed transmission electron microscope studies, an indication of which slip systems are operative can be obtained from *c*-axis CPOs (e.g. Schmid and Casey, 1986).

The apparent small circle girdles about the pole to the foliation in samples ML 11-3, ML 7-3, and ML 7-15 suggest either a predominantly flattening strain history (c.f. Tullis et al., 1973; Law et al., 1984; Price, 1985) or incomplete development of *c*-axis girdles during plane strain (c.f. compilation of Price, 1985). Compared to the CPO data of Schmid and Casey (1986), the *c*-axis CPOs from these samples suggest that deformation could have been predominantly accommodated by rhomb <*a*> slip. However, at all conditions, basal <*a*> and prism <*a*> slip are easier than rhomb <*a*> slip, suggesting that this interpretation is unlikely (Fig. 7). Alternatively, such *c*-axis CPOs could result from the almost equal activity of basal <*a*> and prism <*a*> slip (c.f. Ralser et al., 1991). Equal activity of basal <*a*> and prism <*a*> slip is consistent with amphibolite-grade conditions.

Only sample ML 1-2 shows a crossed-circle girdle normal to the lineation (Type I girdle of Lister, 1977). Both the CPO and the S-C microstructure of this sample indicate a large component of noncoaxial deformation. The CPOs in the other three samples (ML 6-2, ML 7-1, ML 11-2), consisting of *c*-axis maxima nearly normal to the lineation, both parallel and perpendicular to the foliation, are not as easy to interpret. They may reflect incomplete crossed girdles and, therefore, represent deformation under plane strain. The maxima, both normal to the foliation and in the foliation plane, result from the activity of a combination basal <*a*> and prism <*a*> slip.

Only weak asymmetries are observed in the CPOs. The majority of the samples (ML 11-2, ML 1-2, ML 7-3, ML 7-15, ML 6-2) are defined by the more populated northeast-southwest girdle, suggesting a weak component of east-side-up simple shear. In sample ML 11-3, the northwest-southeast girdle has a higher population than the northeast-southwest girdle and is interpreted to indicate a west-side-up sense of shear. This is consistent with the variability exhibited by other kinematic indicators.

Conclusions

The Proterozoic rocks currently exposed in the Capilla Peak area of the Manzano Mountains were all part of an upper greenschist to lower amphibolite facies, ductile shear zone active at ca 1.4 Ga (see also Marcoline et al., 1999; Ralser, 2000). The dominant north-northeast-striking foliation (S_2) is observed in all lithologic units and overprints at least one older foliation. Deformation related to S_2 is partitioned into high- and low-strain zones. In low-strain zones, deformation is expressed as small-scale folding, and if S_2 is present, it is a poorly defined crenulation cleavage. High-strain zones are characterized by a strong planar foliation, which completely overprints all evidence of the earlier deformation.

The quartzite mylonite microstructures within high-strain zones range from monocrystalline quartz ribbons to fine-grained equigranular crystals. As these quartzite mylonites are interpreted to have formed under similar pressures and temperatures, the observed variations are interpreted to result from changes in strain rate. The strong *c*-axis CPOs are interpreted to have formed predominantly by dislocation slip on basal and prism planes, indicating formation during an upper greenschist- to lower amphibolite-grade deformational event. This is consistent with metamorphic conditions determined from nearby amphibolites, where euhedral horn-

blende (parallel to the S_2 foliation) is interpreted to have formed under amphibolite facies conditions (Marcoline, 1996; Marcoline et al., 1996, 1999).

Kinematic indicators, including microscopic folds, S-C surfaces, asymmetric porphyroclast systems, and *c*-axis CPOs, in general, indicate an east-side-up sense of shear. However, rare porphyroclast systems in the quartzites and the Sevilleta Metarhyolite record a west-side-up sense of shear. These differing kinematic indicators suggest a strain history of progressive, general, noncoaxial flow (c.f. Simpson and De Paor, 1993); i.e. a combination of both simple shear and flattening.

Acknowledgments. This work was supported by National Science Foundation grant EAR-9316474. Critical reviews by E. A. Melis, K. Nielsen, and M. Williams are gratefully acknowledged.

References

Bauer, P. W., 1982, Precambrian geology and tectonics of the southern Manzano Mountains, central New Mexico; *in* Grambling, J. A., and Wells, S. G. (eds.), Albuquerque country II: New Mexico Geological Society, Guidebook 33, pp. 211–216.

Bauer, P. W., 1983, Geology of the Precambrian rocks of the southern Manzano Mountains, New Mexico: Unpublished MS thesis, University of New Mexico; New Mexico Bureau of Mines and Mineral Resources, Open-file Report 339, 145 pp.

Bauer, P. W., Karlstrom, K. E., Bowring, S. A., Smith, A. G., and Goodwin, L. B., 1993, Proterozoic plutonism and regional deformation—new constraints from the southern Manzano Mountains, central New Mexico: New Mexico Geology, v. 15, no. 3, pp. 49–55.

Bauer, P. W., and Williams, M. L., 1994, The age of Proterozoic orogenesis in New Mexico, U.S.A.: Precambrian Research, v. 67, pp. 349–356.

Bolton, W. R., 1976, Precambrian geochronology of the Sevilleta Metarhyolite and the Los Pinos, Sepultura, and Priest plutons of the southern Sandia uplift, central New Mexico: Unpublished MS thesis, New Mexico Institute of Mining and Technology, 57 pp.

Bowring, S. A., Kent, S. C., and Sumner, W., 1983, Geology and U–Pb geochronology of Proterozoic rocks in the vicinity of Socorro, New Mexico; *in* Chapin, C. E., and Callender, J. F. (eds.), Socorro region II: New Mexico Geological Society, Guidebook 34, pp. 137–142.

Grambling, J. A., Williams, M. L., Mawer, C. K., and Smith, R. F., 1989, Metamorphic evolution of Proterozoic rocks in New Mexico; *in* Daly, J. S., Cliff, R. A., Yardley, B. W. D. (eds.), Evolution of metamorphic belts, Proceedings of the 1987 joint meeting of the Metamorphic Studies Group and IGCP project 235, University College, Dublin, Ireland: Geological Society of London, Special Publication 43, pp. 461–467.

Hanmer, S., and Passchier, C., 1991, Shear-sense indicators—a review: Geological Survey of Canada, Paper 90–17.

Heizler, M. T., Ralser, S., and Karlstrom, K. E., 1997, Late Proterozoic (Grenville?) deformation in central New Mexico determined from single-crystal muscovite $^{40}Ar/^{39}Ar$ age spectra: Precambrian Research, v. 84, pp. 1–15.

Hobbs, B. E., 1985, The geological significance of microfabric analysis; *in* Wenk, H. R. (ed.), Preferred orientation in deformed metals and rocks—an introduction to modern texture analysis: Academic Press, Orlando, pp. 463–484.

Hobbs, B. E., Means, W. D., and Williams, P. F., 1976, An outline of structural geology: Wiley, New York, 571 pp.

Karlstrom, K. E., and Bowring, S. A., 1988, Early Proterozoic assembly of tectonostratigraphic terranes in southwestern North America: Journal of Geology, v. 96, pp. 561–576.

Kronenberg, A., 1981, Quartz preferred orientations within a deformed pebble conglomerate from New Hampshire, U.S.A.: Tectonophysics, v. 79, pp. T7–T15.

Lanzirotti, A., Bishop, J. L., and Williams, M. L., 1996, A more vigorous approach to dating mid-crustal processes—U–Pb dating of varied major and accessory metamorphic minerals tied to microstructural processes (abs.): Geological Society of America, Abstracts with programs, 1996 annual meeting, p. A-453.

Law, R. D., Knipe, R .J., and Dayan, H., 1984, Strain path partitioning within thrust sheets—microstructural and petrofabric evidence from the Moine thrust zone at Loch Eriboll, northwest Scotland: Journal of Structural Geology, v. 6, no. 5, pp. 477–497.

Lister, G. S., 1977, Discussion—crossed-girdle *c*-axis fabrics in quartzites plastically deformed by plane strain and progressive simple shear: Tectonophysics, v. 39, pp. 51–54.

Lister, G. S., and Dornsiepen, U. F., 1982, Fabric transitions in the Saxony granulite terrain: Journal of Structural Geology, v. 4, no. 1, pp. 81–92.

Lister, G. S., and Hobbs, B. E., 1980, The simulation of fabric development during plastic deformation and its application to quartzite—the influence of deformation history: Journal of Structural Geology, v. 2, no. 3, pp. 355–370.

Marcoline, J. R., 1996, Field, petrographic, and $^{40}Ar/^{39}Ar$ constraints on the tectonic history of the central Manzano Mountains, central New Mexico: Unpublished MS thesis, New Mexico Institute of Mining and Technology, Socorro, 124 pp.

Marcoline, J., Heizler, M., Goodwin, L. B., Ralser, S., and Clark, J., 1999, Thermal, structural and petrological evidence for 1,400-Ma metamorphism and deformation in central New Mexico: Rocky Mountain Geology, v. 34, pp. 93–119.

Marcoline, J. R., Heizler, M., Ralser, S., and Goodwin, L., 1996, Thermochronologic constraints on Proterozoic deformation and metamorphism in the Manzano Mountains, central New Mexico (abs.): New Mexico Geology, v. 18, no. 2, p. 44.

Passchier, C. W., and Simpson, C., 1986, Porphyroclast systems as kinematic indicators: Journal of Structural Geology, v. 8, no. 8, pp. 831–843.

Passchier, C. W., and Trouw, R. A. J., 1996, Microtectonics: Springer, New York, 289 pp.

Price, G. P., 1985, Preferred orientations in quartzites; *in* Wenk, H. R. (ed.), Preferred orientation in deformed metals and rocks—an introduction to modern texture analysis: Academic Press, Orlando, pp. 385–406.

Ralser, S., 2000, Microstructural constraints on the timing of Proterozoic deformation in central New Mexico: Journal of Metamorphic Geology, v. 18, no. 5, in press.

Ralser, S., Hobbs, B. E., and Ord, A., 1991, Experimental deformation of a quartz mylonite: Journal of Structural Geology, v. 13, no. 7, pp. 837–850.

Ralser, S., Unruh, D. M., Goodwin, L. B., and Bauer, P. W., 1997, Geochronologic and microstructural evidence for 1.4 Ga deformation in the southern Manzano Mountains, NM (abs.): New Mexico Geology, v. 19, no. 2, p. 62.

Reiche, P., 1949, Geology of the Manzanita and north Manzano Mountains, New Mexico: Geological Society of America, Bulletin, v. 60, pp. 1183–1212.

Schmid, S. M., and Casey, M., 1986, Complete texture analysis of commonly observed quartz *c*-axis patterns; *in* Hobbs, B. E., and Heard, H. C. (eds.), Mineral and rock deformation—laboratory studies, the Paterson volume: American Geophysical Union, pp. 263–286.

Simpson, C., 1985, Deformation of granitic rocks across the brittle-ductile transition: Journal of Structural Geology, v. 7, no. 5, pp. 503–511.

Simpson, C., and De Paor, D. G., 1993, Strain and kinematic analysis in general shear zones: Journal of Structural Geology, v. 15, no.1, pp. 1–20.

Spear, F. S., 1981, An experimental study of hornblende stability and compositional variability in amphibolite: American Journal of Science, v. 281, no. 6, pp. 697–734.

Stark, J. T., 1956, Geology of the south Manzano Mountains, New Mexico: New Mexico Bureau of Mines and Mineral Resources, Bulletin 34, 49 pp.

Stark, J. T., and Dapples, E. C., 1946, Geology of the Los Pinos Mountains, New Mexico: Geological Society of America, Bulletin, v. 57, pp. 1121–1172.

Thompson, A. G., Grambling, J. A., and Dallmeyer, R. D., 1991, Proterozoic tectonic history of the Manzano Mountains, central New Mexico; *in* Julian, B., and Zidek, J. (eds.), Field guide to geologic excursions in New Mexico and adjacent areas of Texas and Colorado: New Mexico Bureau of Mines and Mineral Resources, Bulletin 137, pp. 71–77.

Thompson, A. G., Grambling, J. A., Karlstrom, K. E., and Dallmeyer, R. D., 1996, Mesoproterozoic metamorphism and $^{40}Ar/^{39}Ar$ thermal history of the 1.4 Ga Priest pluton, Manzano Mountains, New Mexico: Journal of Geology, v. 104, pp. 583–598.

Tullis, J., Christie, J. M., and Griggs, D. T., 1973, Microstructures and preferred orientations of experimentally deformed quartzites: Geological Society of America, Bulletin, v. 84, no. 1, pp. 297–314.

Van Houtte, P., and Wagner, F., 1985, Development of textures by slip and twinning; *in* Wenk, H. R. (ed.), Preferred orientation in deformed metals and rocks—an introduction to modern texture analysis: Academic Press, Orlando, pp. 233–258.

Williams, M. L., Jercinovic, M. J., and Terry, M. P., 1999, Age mapping and dating of monazite on the electron microprobe—deconvoluting multistage tectonic histories: Geology, v. 27, no. 11, pp. 1023–1026.

Williams, P. F., Goodwin, L. B., and Ralser, S., 1994, Ductile deformation processes; *in* Hancock, P. L. (ed.), Continental deformation: Pergamon Press, New York, pp. 1–27.

The editors wish to correct the erroneous statement: "The Romans used pozzolans found in southeastern France along the Rhine River." from "Uses of fly ash from New Mexico coals," *New Mexico Geology*, v. 22, no. 2, p. 25. A pozzolanic volcanic tuff called Rhenish Trass is mined near the Rhine in western Germany. It is used today in the manufacture of portland cement, and it may have been used by the Romans as

New Mexico Bureau of Mines and Mineral Resources Excellence in Geoscience Award New Mexico Science and Engineering Fair 2000

The New Mexico Bureau of Mines and Mineral Resources presented awards to five young women for their Earth Science exhibits at the New Mexico Science and Engineering Fair held at New Mexico Tech, in Socorro, New Mexico, on April 14–15, 2000. The awards were judged and funded by Bureau staff.

For first place in the Senior Division, Amy Dalness, Deniz Husrev, and Amy Olsen, from Santa Fe High School, received a $50.00 cash award for their team contribution, "Lunar effects on the Earth: Earth tides." Senior Division exhibitor Kira P. Lueth, from Socorro High School, was awarded second place for her exhibit, "Dehydration properties of minerals." She received a $30.00 cash award. First place in the Junior Division went to Diana V. Gonzales, a 9th grader from Wagon Mound Public Schools. Her exhibit titled "Can't retain, must drain" earned her a $25.00 cash award. All winners received subscriptions to *New Mexico Geology* and *Lite Geology* and the opportunity to have their abstracts appear in *New Mexico Geology*.

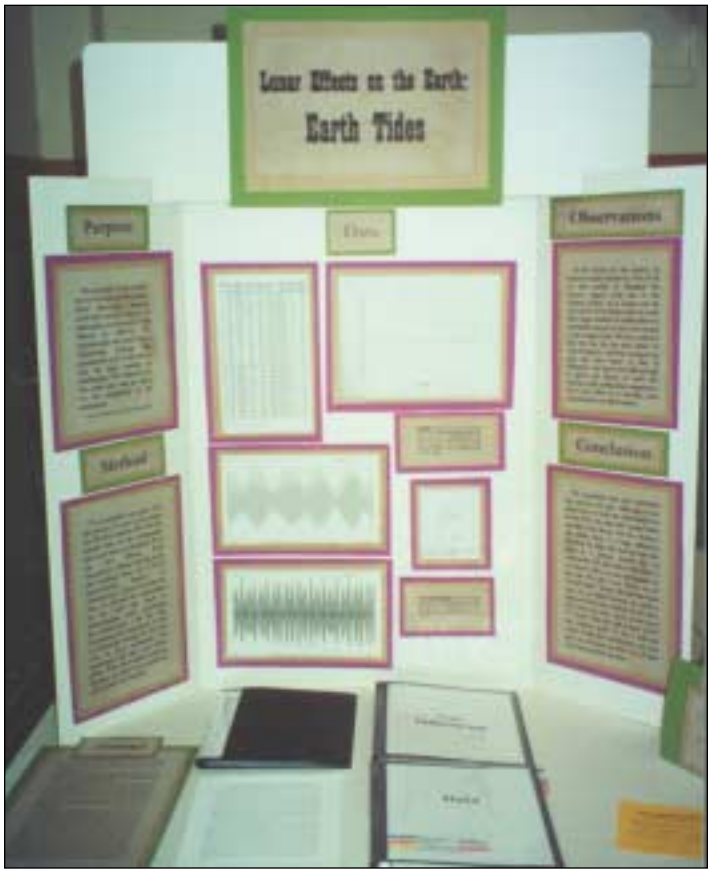

First Place, Senior Division

LUNAR EFFECTS ON THE EARTH: EARTH TIDES by *Amy Dalness, Amy Olsen*, and *Deniz Husrev*, Santa Fe High School, Santa Fe, NM 87505

Abstract—Our project was to determine if there was a relationship between the series of earthquakes in Bernardo, New Mexico, from 1989–91, and Earth tides. We hypothesized that there would be a direct effect on the magnitude of the earthquakes from the Earth tides. Earth tides are the gravitational pull of the moon and, to a lesser extent, the sun on the Earth's landmasses.

Using data from the New Mexico Tech Geophysics Library of the earthquake swarms in Bernardo and Earth-tide read outs from the USGS, we were able to draw our conclusions. We plotted the earthquake data on the Earth-tide readings by day and hour. After doing this, we analyzed the data through tables, graphs, and percentages to find a correlation between the quakes and the tides.

We discovered that we had to make many modifications on our project in order for the results to be logical. We first wanted to exclude the Socorro magma body in and around Socorro, thinking it would effect our results. We thought Bernardo was far enough away to exclude this factor, but were proven wrong when we learned from the USGS that Bernardo is on the edge of the magma body. We concluded that the magma body would, after all, not make a major impact on our results. We also figured that our project would be more accurate if our Earth-tide data had a relatively small time frame that would allow us to analyze the earthquake from hour to hour, not just day to day. The Bernardo swarms seemed to provide a good time frame and a large number of earthquakes to plot.

We concluded that our original theory that Earth tides directly affect the earthquake magnitude was not true; although we did draw some other theories that point at the possibility of there being some relationships. Our initial theory was disproved for a few reasons. When taking the average Earth-tide magnitude, it came out to be approximately 6.23, which is only slightly over the median (our scale was from 120 to -120). When looking at the data and comparing tide magnitude versus number of earthquakes to determine percentage, we found that 20 of the 43 counted earthquakes occurred in a period of "high tide," (which we determined to be anything above or below 50 or -50), which gave us only 47% occurring at high tide. Although we could not determine a direct relationship to magnitude, we did notice a few other things. In a day with a high fluctuation in tide magnitude, a "mini-swarm" occurred when three or more earthquakes shook the Earth in a 24-hour time frame. This became one of our theories; maybe the tides were creating just enough extra stress on the Earth's crust that the almost exact same area could harbor another earthquake. We also believe that Earth tides are constantly effecting earthquakes due to the fact that the Earth is being pushed and pulled every minute. The Earth's crust can fluctuate a matter of a few feet every 6–7 hours. This gave us our "straw on the camel's back" theory. The Earth tides are a constant factor in earthquakes, and we believe that they are not the cause of earthquakes but are a constant factor in their formation.

Conclusions—We concluded that our hypothesis was proven not true. Although it was disproved, we took the information we found from the data and created other theories. One theory was that during a day when there is a huge difference between the high tide and the low tide, there is a greater chance for an earthquake. We also believe that there is a constant effect on the earthquakes by the pull. We call it our "straw on the camel's back" theory. We feel that there must be an effect because the Earth is being moved every minute by the tides. The crust can move up to a foot every 6–7 hours. The tide pull is the final "push" the tension needs to be a full-scale quake. From the information our data gave us, we came up with a lot of ideas and many possible theories.

Second Place, Senior Division

DEHYDRATION PROPERTIES OF MINERALS by *Kira Lueth*, Socorro High School, Socorro, NM 87801

Abstract—This project tested the dehydration properties of some minerals. These minerals were stilbite, hornblende, chabazite, talc, and chrysocolla. The minerals were heated at 200°, 400°, and 600°C. The products were then analyzed by an X-ray diffractometer. The minerals proved the hypothesis, which is, samples that showed loss of water and rehydration showed no signs of structure alteration. Samples that lost water but did not rehydrate showed altered structures. Samples that showed no sign of water loss show no signs of alteration.

Conclusions—The data collected in this experiment supported the hypothesis. The hypothesis was that the H_2O in the minerals would be removed and replaced, but the OH would not. The minerals stilbite, chrysocolla, and chabazite (H_2O minerals) lost water at all the temperatures and regained all or most of it at 200°. At 400° and 600°C, the minerals regained little or no water.

The OH minerals did little in the way of weight change. Any big differences were most likely human error. This lack of change would be because OH is more strongly held in the structure of the molecule and a higher temperature than that used is needed to remove the water.

As shown by the data, it is possible to dehydrate and "rehydrate" minerals. This data was analyzed and the why of it was then tested. After X-raying, it was possible to see why or why not the specimen was able to regain its lost water. The specimens that showed dehydration and rehydration also showed evidence of a structure change. Those that showed no loss of water showed little or no alteration of their structure. Those that dehydrated but did not rehydrate showed massive changes in their structure.

These tests show that when minerals are heated and lose part of their structural water, they may or may not change the rest of their structure. Part of it depends on the type of water. OH, which is held tighter in a mineral structure, will destroy the mineral sample if it is removed. H_2O may or may not alter the structure. If the H_2O is held in a structure such as it is in the zeolites (held loosely in channels), it will only be destroyed by higher temperatures. If it is like chrysocolla,

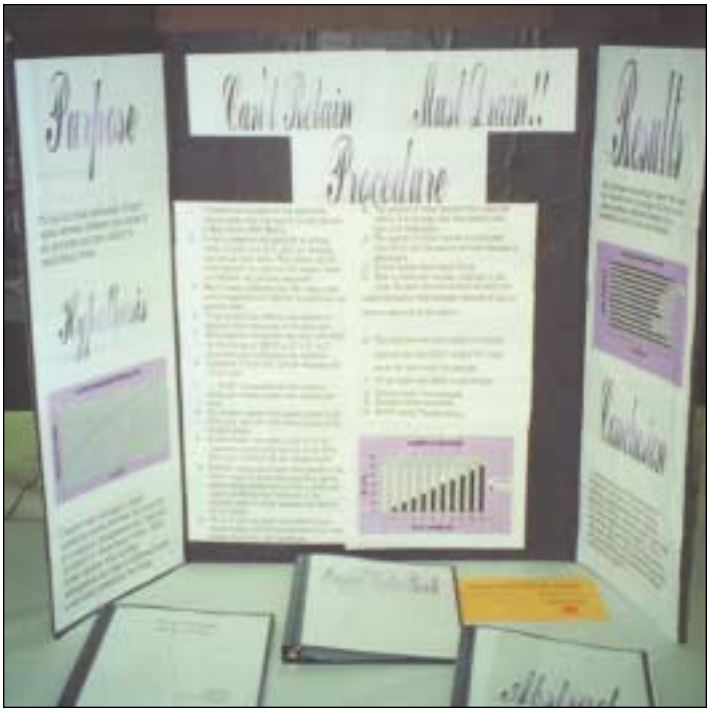

Junior Division

CAN'T RETAIN, MUST DRAIN by *Diana Gonzales*, Wagon Mound Public Schools, Wagon Mound, NM 87752

Purpose—To find out what correlation (if any) exists between different mix ratios of soil particles and their ability to retain / drain water.

Hypothesis—I believe that although a linear correlation exists between the quantity of a singular homogeneous soil type and its ability to drain / retain water, when mixed together with another homogeneous soil type at different ratios a non-linear correlation will exist.

Results—My hypothesis was partially correct. The water that drained from my samples did form a non-linear correlation. However, instead of an exponential curve, a bell curve resulted.

Soil samples were collected on a ranch with help from the Soil Survey of Mora County. Soils are classified into several textural groups. They include sandy clay, silty clay, clay loam, sandy clay loam, silty clay loam, and loamy sand. A sand grain ranges in diameter from 0.05 to 2 mm; a silt particle ranges from 0.002 to 0.05 mm in diameter, and clay is a grain having a diameter less than 0.002 mm. If a grain of sand is as big as a two-story building, a grain of silt would be the size of a tennis ball and a grain of clay would be the size of a grain of sand.

Conclusions—I learned that although clay and sand by themselves have their own water-holding-capability characteristics, when combined, especially when the ratios are closer to each other, they have reduced water-holding capacities. This is because the clay particles are approximately ten times smaller than sand, and they actually reduce the available pore space between the sand particles and reduce the water-holding capacity.

Call for papers: Tucumcari 2001
New Mexico Geological Society 52nd Fall Field Conference

On 26–29 September 2001, the 52nd Fall Field Conference of the New Mexico Geological Society will visit eastern New Mexico and west Texas from the conference's central point in Tucumcari, New Mexico. Three days of field trips will encompass the area from Palo Duro Canyon in west Texas to Santa Rosa, New Mexico. Articles for the conference guidebook are invited in all areas of geoscience relevant to the conference area, which includes all of eastern New Mexico north of Roswell, all of west Texas north of Midland and adjoining areas of Colorado, Kansas and Oklahoma.

Articles must be submitted by 15 January 2001 to be published in the NMGS Guidebook in Fall 2001.

To contribute an article you must send a title and estimated manuscript length (number of double-spaced typescript pages, number of figures) by 30 September 2000 to:

Spencer G. Lucas
New Mexico Museum of Natural History
1801 Mountain Road NW
Albuquerque, NM 87104
Tel: 505-841-2873
FAX: 505-841-2808
Email: slucas@nmmnh.state.nm.us

After receipt of your title and length estimate, you will receive detailed instructions to authors to aid you in preparation of your manuscript.

Rockhound State Park and Spring Canyon Recreation Area

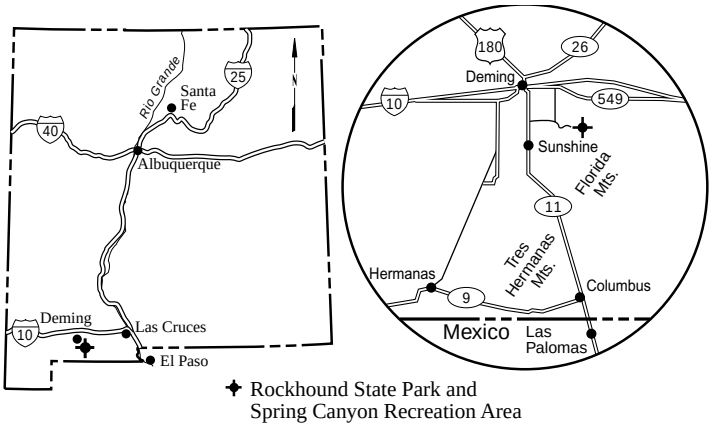

FIGURE 1—Location of Rockhound State Park.

Introduction

Rockhound State Park lies in the Little Florida Mountains southeast of Deming, New Mexico (Fig. 1). It was established in 1966 as the first park in the United States that allowed collecting of rocks and minerals for personal use. Each visitor is allowed to collect as much as 15 lb of rocks and minerals from the 1,100-acre park; mineral dealers are not allowed to collect for sale. Rockhound State Park actually consists of two separate units, the main park and Spring Canyon Recreation Area (Fig. 1). The main park offers covered shelters for camping and picnicking, a group shelter, restrooms with showers, RV dump station, playground, hiking trails, wildlife viewing areas, and rock and mineral collecting areas (Fig. 2, 3). Spring Canyon lies in the northern Florida Mountains, south of the main park, and is open for day use only from Easter through November. Facilities include picnic tables, group shelter, restrooms, and hiking.

The main park (Fig. 4) provides excellent views of the surrounding mountain desert. Basin and Range topography is easily seen in the distance. On a clear day the smokestacks of the Hurley smelter can be seen to the northwest. The Cobre Mountains form

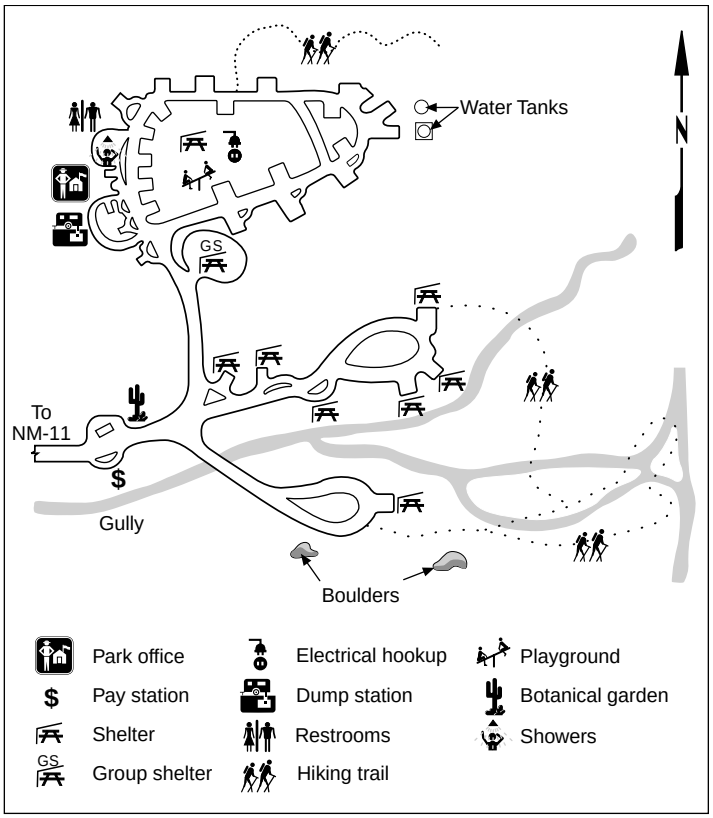

FIGURE 3—Facilities map of Rockhound State Park.

the far northern horizon behind the smokestacks. The Burro Mountains lie to the west-northwest; the Victorio Mountains lie to the west-southwest. The Florida Mountains lie directly to the south of the main state park; Florida Gap separates the two ranges. The Cedar Mountains lie to the south-southwest. The dark mountain north of Deming is called Black Mountain. Spring Canyon in the Florida Mountains is a sheltered canyon (Fig. 5) and

FIGURE 2—View of Rockhound State Park.

FIGURE 4—View of Rockhound State Park from Rockhound Road.

FIGURE 5—Hiker traveling up Spring Canyon Trail. Little Florida Mountains are in the distance.

offers solitude common to many canyons throughout the desert Southwest.

The Florida and Little Florida Mountains are typical of the mountain desert throughout southern New Mexico and Arizona. Elevations range from 4,400 ft along the foothills, where the state park is located, to 7,448 ft at Florida Peak in the Florida Mountains. Water is scarce and limited to wells and hidden springs, but be careful of thunderstorms and flash floods during the summer months! Despite the dry, seemingly inhospitable environment, life abounds. The area is home to many lizards and snakes, deer, antelope, coyotes, and small mammals such as prairie dogs, rabbits, badgers, and many birds (Table 1). Mountain lion and desert bighorn sheep may be seen at the higher elevations of the Florida Mountains. A variety of plants thrive in this environment, including yucca, prickly pear cactus, barrel cactus, ocotillo, creosote bush, mesquite, and hackberry; juniper and scrub oak are common in the canyons.

History

Prehistoric people most likely camped thousands of years ago beneath rocks that provided some shelter from the elements and predators. The Mimbres or Mimbreño Indians settled north of the area about 1200–1150 A.D. Later, Apache Indians moved into the area. The rugged Florida Mountains were well known as Apache strongholds until the mid-1880s. Spanish conquistadors and settlers traveled through the area in the 1500s but did not find the desert environment or the Apache Indians very hospitable. Spanish explorers named the larger mountain range in the 1700s; "Florida" is Spanish for flowery. In the spring after a wet winter, the mountain range is sometimes covered with poppy blossoms, giving rise to its name. The range was shown on Juan Nentwig's map of 1762 as Sierra Floridas (Julyan, 1996). The Little Florida Mountains were named later. In 1804 Col. Manuel Carrasco, a Spanish army officer, began mining the copper at Santa Rita (McLemore, 1996). Mule trains loaded with copper from the mine passed near what is now the state park on their way to Chihuahua in 1804–1834 (Weber, 1980).

After the Mexican War in 1850, the Americans and Mexicans disputed the southern border of New Mexico, including the area in and around what is now known as Deming. President Franklin Pierce appointed James Gadsden to settle the dispute; the Gadsden Treaty purchase was ratified on April 25, 1854, making southern New Mexico officially part of the United States and allowing a southern transportation route across the country (Clemons et al., 1980). The Butterfield Trail was the first route established, and the Butterfield Stage passed north of what is now known as Deming in 1858–1881. It was the longest overland route in its time, beginning in Tipton, Missouri, and ending in San Francisco, California. This was still Apache territory, so travel and settlement were treacherous. Raiding by Apache Indians declined in the mid-1880s when rapid settlement of southern New Mexico occurred.

In 1881, Deming was settled where the Atchinson, Topeka, and Santa Fe (AT&SF) and Southern Pacific (SP) Railroads met, providing the second transcontinental railroad in the United States and the only route open year round. The first settlement, mostly of tents, was 10 mi to the east and called New Chicago; it was relocated for better access to water (Stanley, 1962; Julyan, 1996). The new settlement was named for Mary Anne Deming, the bride of Charles Crocker, who was one of the founders of the Southern Pacific Railroad (Stanley, 1962; Clemons et al., 1980). E. Germain and Company opened the first store in Deming, using old boxcars for storerooms. The El Paso and Southwestern Railroad also came through Deming, making Deming one of the few towns in New Mexico with three depots of three independent railroads. Deming ground water was found to be so pure that it was bottled and shipped to El Paso and other points (Stanley, 1962). Deming quickly grew, becoming a center of agriculture and commerce in southern New Mexico. It also attracted cattle rustlers and other lawless types for a time (Stanley, 1962).

Luna County was established in 1901 from the western portion of Doña Ana County and the eastern portion of Grant County;

TABLE 1—Birds found in the Florida Mountains area. How many can you find in Rockhound State Park and Spring Canyon Recreation Area?

Ash-throated flycatcher	
Barn swallow	
Black phoebe	
Black-chinned hummingbird	
Black-throated sparrow	
Broad-tailed hummingbird	
Brown towhee	
Cactus wren	
Canyon wren	
Common crow	
Common raven	
Curve-billed thrasher	
Eastern meadowlark	
Gambel's quail	
Golden eagle	
Great horned owl	
House finch	
House sparrow	
Ladder-backed woodpecker	
Lesser nighthawk	
Mourning dove	
Pyrrhuloxia	
Red-tailed hawk	
Roadrunner	
Robin	
Rock dove	
Rock wren	
Rufous-crowned sparrow	
Sage sparrow	
Scaled quail	
Turkey vulture	

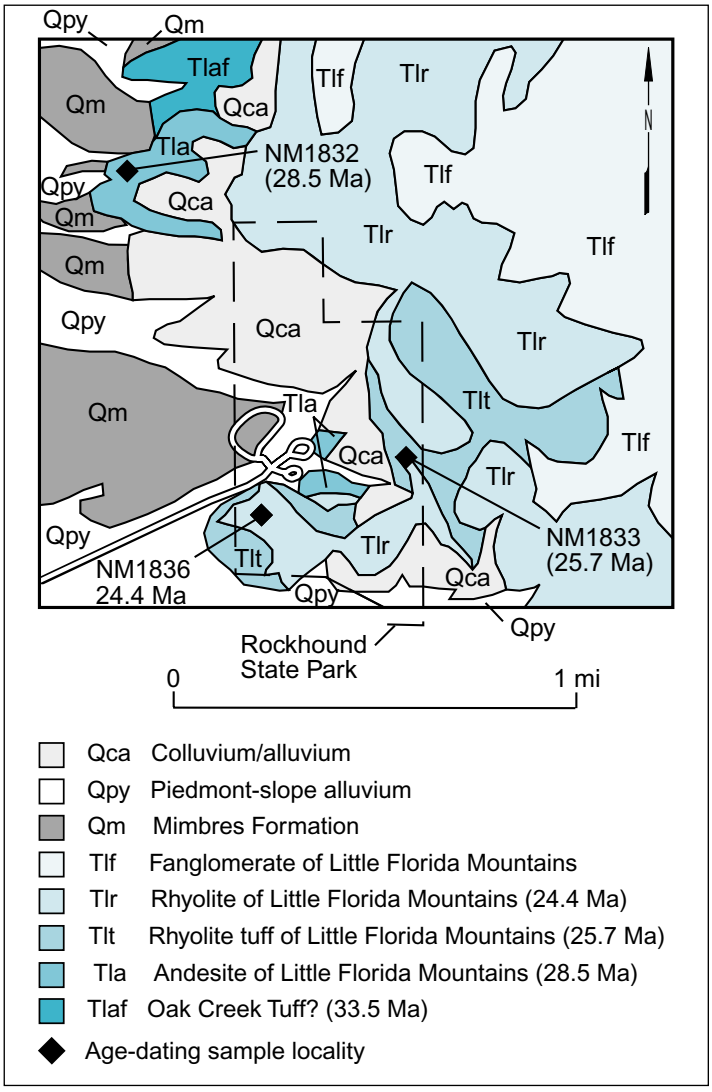

FIGURE 6—Geologic map of the Little Florida Mountains, including Rockhound State Park (simplified from Clemons, 1982).

Deming became the county seat. The county was named for Solomon Luna, who sponsored the new county in the legislature. Camp Cody was established at Deming in 1917 to train troops for World War I. At the end of the war, Camp Cody was operated by the Catholic Sisters of the Holy Cross as a tuberculosis sanitarium for ex-soldiers. In 1939, Camp Cody was destroyed by fire, and the sanitarium closed. The Deming Army Air Base was established in the 1940s for training bombardiers during World War II; it later became the Municipal Deming Airport and Industrial Park. Today agriculture, especially chile, melons, cotton, and pumpkins, light industry, and tourism are the main economic base for Deming.

Geology

Paleozoic through lower Tertiary sedimentary rocks overlie a Cambrian granitic to syenitic pluton in the northern Florida Mountains (Clemons and Brown, 1983; Clemons, 1984, 1998). The rocks at Spring Canyon Recreation Area belong to the Starvation Draw Member of the Rubio Peak Formation and were emplaced about 51–36 m.y. ago (late Eocene to early Oligocene, Clemons, 1982). The Starvation Draw Member consists of volcanic breccias, conglomerates, and lavas of andesitic composition. A rhyolite dike, which cuts the Starvation Draw Member near the head of Spring Canyon, is 25.4 m.y. old (groundmass, $^{40}Ar/^{39}Ar$; unpublished age determination, New Mexico Geochronology Research Laboratory, New Mexico Institute of Mining and Technology).

The Little Florida Mountains consist predominantly of interbedded mid-Tertiary andesitic, dacitic, and rhyolitic ash-flow tuffs and lavas, and volcanic-derived fanglomerates intruded by rhyolite domes and dikes (Fig. 6; Clemons, 1982, 1984, 1998). The earliest evidence of volcanic activity in the Little Florida Mountains are small outcrops of ash-flow tuffs exposed approximately 1 mi north of the state park (Fig. 6) and farther north, near Little Gap. Altered sanidine and biotite from an ash flow near the base of the stratigraphic section at Little Gap give $^{40}Ar/^{39}Ar$ ages of 33.5 m.y. and 32.9 m.y., respectively. This ash flow may correlate with the 33.5 m.y. old Oak Creek Tuff that erupted from the Juniper caldera in the northern Animas Range in the Boot Heel volcanic field in Hidalgo County to the west. During ash-flow eruptions, volcanic ash can travel a great distance from the source vent. In some cases, the ash is still very hot when deposited and can then fuse, or weld, into a very dense, hard layer of rock, such as the ash-flow tuff found in the Little Florida Mountains. The ash-flow tuff is overlain by andesite flows (andesite of Little Florida Mountains) that were probably erupted from shield or stratovolcanoes. The vents of these once-prominent volcanoes are difficult to impossible to find because of local faulting and rapid erosion. The andesites subsequently were intruded by rhyolite domes and covered by rhyolite lavas and tuffs (Fig 6; rhyolite tuff [Tlt] and rhyolite [Tlr] of Little Florida Mountains; Clemons, 1982). Volcanic activity was relatively brief in geologic time; rhyolite and andesite samples from the state park range in age from 28.5 to 24.4 m.y. ($^{40}Ar/^{39}Ar$; unpublished age determination, New Mexico Geochronology Research Laboratory, New Mexico Institute of Mining and Technology). Seismic data suggest that there are only 600 ft of volcanic rock in the subsurface in the area of the state park.

Erosion of the volcanic rocks began during and after eruption. The fanglomerate of Little Florida Mountains was the first of the deposits that formed by erosion of the volcanic rocks and is Miocene in age (Clemons, 1982; Kiely and James, 1988). Dacite flows were erupted onto the fanglomerate of Little Florida Mountains. During and after this brief period of volcanic activity, regional tectonics (i.e. mountain building by block faulting) related to the Rio Grande rift uplifted the Little Florida and Florida Mountains; erosion has since worn the mountains down to their present elevation above the surrounding desert. Wind, water, and ice have continued to break up the rocks through time and to carry fragments downslope forming the gently sloping bajadas or alluvial fans at the base of the mountains. The campground at Rockhound lies on one of these bajadas.

Geothermal ground waters and springs were associated with the volcanic activity. Silica cementation of the younger fanglomerate of Little Florida Mountains indicates that these fluids continued to circulate long after eruption of the volcanic rocks and during their erosion (Kiely and James, 1988).

Manganese-oxide and fluorite veins that cut the fanglomerate of Little Florida Mountains in the northeastern part of the Little Florida Mountains were also formed during this time. These deposits are present where various manganese- and iron-oxide minerals, along with fluorite, barite, calcite, and quartz, are found in the fanglomerate of Little Florida Mountains (Lasky, 1940; Clemons, 1982; Kiely and James, 1988). Hydrothermal fluids that contained high concentrations of manganese and fluorite, along with silica, also formed these mineral deposits. The Manganese mine was one of the larger producing mines in the district. The mines are extremely unsafe, and visitors should not enter the adits. Care is needed around the shafts and prospect pits as well. Fluorite production from epithermal fluorite veins is estimated as 13,428 short tons, mostly from the Spar mine (McAnulty, 1978). Manganese production from epithermal manganese veins is reported as 19,527 long tons of ore and 21,393 long tons of concentrate (Farnham, 1961; McLemore et al., 1996). Production of manganese ceased in 1959 when the Federal government ended its buying program.

Mineral deposits were discovered in 1876 in the Florida Mountains district south of Spring Canyon in the main Florida Mountains. Hydrothermal fluids that created replacement

FIGURE 7—Solid spherulite from Rockhound State Park (photo by Robert Colburn).

deposits in carbonate rocks also formed these deposits. The hot fluids actually dissolved the limestone and dolomite in the carbonate rocks and left cavities that were later filled by precipitation of minerals from the fluids. From 1880 to 1956, 5,000 lbs copper, <10 oz gold, 8,000 oz silver, and >30,000 lbs lead worth approximately $102,000 were produced from carbonate-hosted Pb–Zn and polymetallic vein deposits in the district (McLemore et al., 1996). The Mahoney and Silver Cave mines were the largest metal producers. In addition, 200 short tons of fluorite and 1,421 long tons of 22–30% manganese have been produced from epithermal veins in the district (Farnham, 1961; McLemore et al., 1996).

The basins around the Little Florida and Florida Mountains subsided as the mountains were uplifted. Rain and snow melt from the local mountains, including the Little Florida and Florida Mountains as well as the Cobre Mountains and Black Range north of Deming, percolated through the rocks, migrated into the basins, and formed large reservoirs of ground water that we call aquifers. Today, this ground water is being pumped from the basins surrounding Deming faster than it can be replaced by current rainfall.

Formation of thundereggs and geodes

Gray perlite, thundereggs, geodes, jasper, onyx, agate, crystalline rhyolite, Apache tears (obsidian), and quartz crystals are among the more common rocks and minerals found in the park. Thompsonite, a zeolite, is found in amygdules in quartz latite (Northrop and LaBruzza, 1996). Agate is present in a wide range of colors and is one of the minerals that many visitors collect at Rockhound State Park. Some thundereggs and geodes found at Rockhound contain multicolored agate in addition to well-formed quartz crystals.

The difference between geodes, thundereggs, and concretions can be confusing. “Geodes” are hollow or near-hollow, crystal-lined cavities found in igneous and sedimentary rocks. “Thundereggs,” also known as spherulites, are solid or near-solid nodules formed by magmatic and volcanic processes and are found only in volcanic rocks (Lofgren, 1971). Spherulites are made of radial crystals extending from the center. Prehistoric Indians found solid nodules near Mt. Jefferson and Mt. Hood in Oregon and thought that when the gods or spirits who inhabited the mountains became angry with one another they would hurl nodules at each other with accompanying thunder and lightning. Hence they called these nodules thundereggs (Shaub, 1979). They range in diameter from less than ¼ inch to greater than a foot. “Concretions” are compact accumulations of minerals cemented together to form hard masses in sedimentary rocks. Concretions can be hollow inside, and some concretions contain a loose “nut.” Concretions can be any shape or size, whereas geodes and thundereggs are typically rounded to slightly ovoid.

Many thundereggs found at Rockhound State Park are spherical and consist of two distinct parts: a dark-gray to pinkish outer part and a white, blue, or gray inner part, or core, which is recognizable as agate, chalcedony, and quartz crystals, all forms of the compound SiO_2. In many examples, these two parts can be described as a shell and a filling. However, some thundereggs, or spherulites, do not contain the filling; they are composed of solid dark-gray to pinkish shell material (Fig. 7) or are partly hollow. Geologically distinct processes form the two parts of the thundereggs. The outer part of the thundereggs is formed by complex magmatic processes (i.e. as spherulites), and then the inner part is formed and modified by multiple cycles of late-stage hydrothermal fluids. The processes that form geodes and thundereggs are complex and are controlled by constantly changing physical and chemical conditions, such as temperature, pressure, depth of formation, composition of the magma, composition of the ground water, and composition of the host rocks.

In order to better understand the processes by which the thundereggs form, samples from Rockhound State Park were examined using a specialized microscope called an electron microprobe. The instrument used is a Cameca SX100 microprobe. It produces a beam of electrons that is focused onto a polished sample surface and then allows investigation of the distribution of chemical elements on the sample surface. The exact composition of minerals within a polished sample can also be determined by quantitatively analyzing characteristic electrons emitted from the sample.

Microprobe examination of the "shell" portion of Rockhound spherulites (Fig. 7) shows that they are composed of intergrown crystals of quartz (SiO_2), alkali feldspar ($K,Na)[AlSi_3O_8]$, plagioclase feldspar $Na[AlSi_3O_8]$-$Ca[Al_2Si_2O_8]$, and magnetite (Fe_3O_4). The images from the microprobe show that the spherulites are formed either of intimately intergrown quartz, feldspar, and magnetite or of bands of quartz systematically interspersed with bands of intergrown feldspar and quartz (Fig. 8A and B). This banding produces the concentric structure that is apparent in some spherulites. Quartz veinlets crosscutting the banded structure are also observed (Fig. 8).

The observed patterns of crystal growth in the spherulites suggest that they may have formed during the cooling of the rhyolite lava. Similar spherulitic features were observed in an artificial melt that was rapidly cooled (Jacobs et al., 1992; Dunbar et al., 1995). The temperature of the artificial melt was monitored during the cooling process, and crystallization was observed at high temperatures (1,100°C). Spherulitic growth occurred during this crystallization process, and the internal structure of the artificially produced spherulites was very similar to the internal structure of Rockhound spherulites, although in the artificial melt the phenocryst phases were plagioclase and pyroxene rather than quartz and two feldspars. Furthermore, the feathery and non-equant shapes (Fig. 8) demonstrated by the crystals in the spherulites are very similar to some crystal forms described by Lofgren (1970, 1971) for crystals that grew rapidly at high temperatures. Investigation of spherulitic structures in a rhyolitic dike suggests that the spherulites grew at high temperature (Davis and McPhie, 1996), although another study of very small spherulites with simple internal structure (Akizuki, 1983) suggests that some may be able to form at lower temperature (~200°C). The complex internal structure and rapid-growth crystal morphology suggests that the shell portion of the Rockhound spherulites formed at high temperatures (~700°C), probably very soon after the rhyolitic lava was erupted onto the Earth's surface.

Many spherulites found within the rhyolitic lava are hollow or partially hollow and/or contain a filling of banded agate, chalcedony, and quartz crystals surrounded by the dark-gray to pinkish outer shell. How do the spherulites become hollow? Although this is difficult to demonstrate directly, we speculate that the hollow centers of spherulites are formed by nucleation, coalescence, and expansion of vapor bubbles at high temperature, resulting in

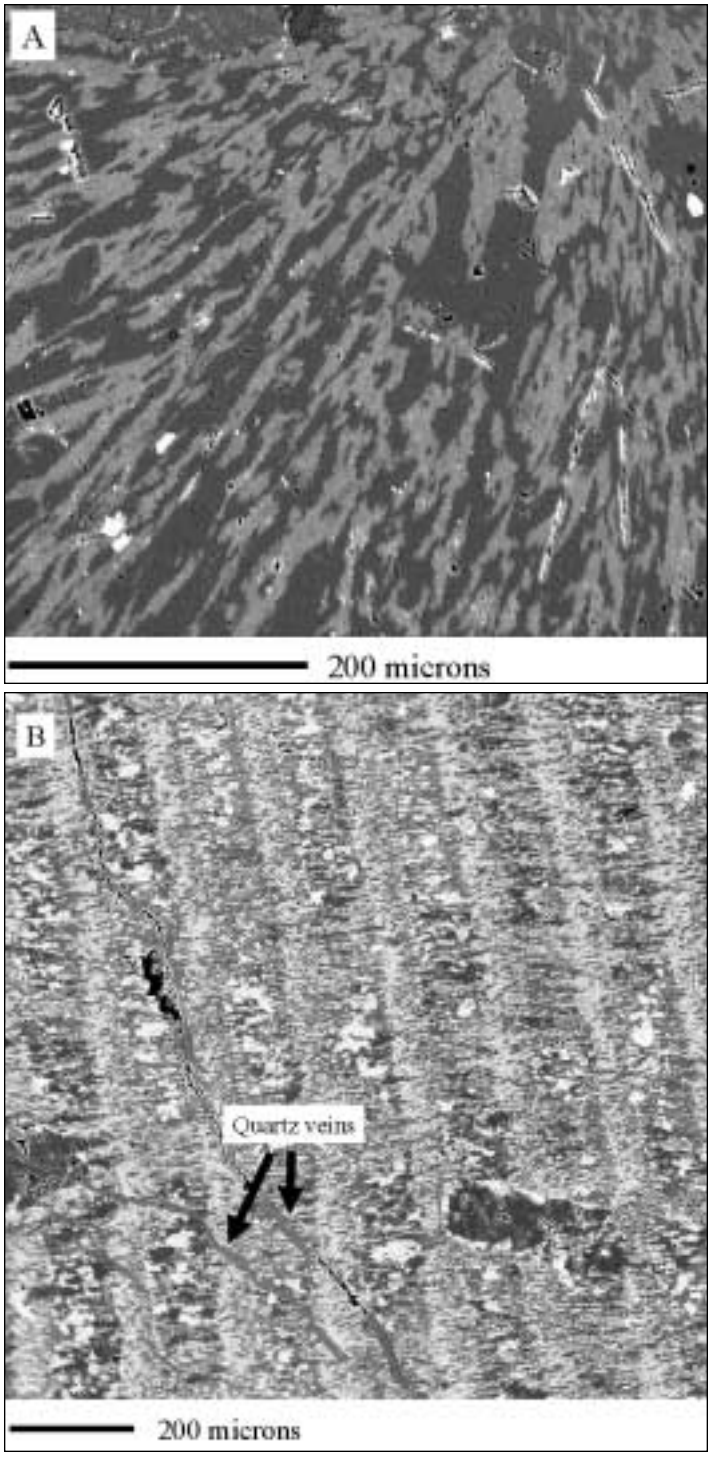

FIGURE 8—Backscattered electron images of polished samples of a Rockhound spherulite. **A**. Intimately intergrown quartz, feldspar, and magnetite. The darkest gray shade represents quartz, lighter gray represents feldspar, and the white represents magnetite. **B**. Banded intergrowth of dominantly feldspar (brighter bands) and dominantly quartz bands (darker bands). White areas are magnetite. Quartz veins crosscutting the banded crystallization can be seen.

a hollow center that can be filled later by silica. The vapor bubbles would have formed as a result of crystallization of quartz, feldspar, and magnetite, which contain no water, from rhyolitic magma, which contains a small amount of dissolved water at atmospheric pressure (Taylor, 1986). Calculations of the volume of water vapor that could have formed from anhydrous crystallization suggest that the volume would be more than enough to generate the size of hollow cavities seen in spherulites. The reason that some spherulites are hollow and others are not may be related to the rate and depth of crystallization and to the resultant ability or inability of vapor bubbles to nucleate and coalesce.

The agate, chalcedony, and quartz veins and open-space-fillings within voids in the spherulites formed later by multiple cycles of hydrothermal fluids. Hydrothermal fluids are a mixture of late-stage fluids escaping the magma and local ground water. The fluids contain some elements from the original magma and also dissolved minerals from the country rock. The amount of ions that the fluid can dissolve depends upon pH, temperature, pressure, and composition of the fluid. The hydrothermal fluids move through fractures in the rocks, which crosscut the igneous textures, and form veins or banded agate, chalcedony, and quartz. Some of these fluids seep through microscopic pores and into spherulites and gas pockets in the volcanic rocks, and they precipitate crystals along the walls of the cavity, forming geodes and geode-like spherulites. Other fluids seep through fractures and gas and other void spaces in the spherulites. Because of their formation by multiple hydrothermal events, each thunderegg provides clues as to its unique formation.

Different temperatures and fluid compositions would account for the variety of textures found within any given thunderegg or geode. By carefully studying the crystal fill and textures in spherulites and geodes, geologists can piece together the different processes through time that formed them. The banding found within some spherulites and geodes consists of multiple layers of different colored agate, chalcedony, and locally quartz, and may have been formed by fluids supersaturated in silica (Fournier, 1985a). Supersaturated solutions are solutions that contain excessive silica in solution. The presence of silica minerals within the thundereggs and geodes indicates that the fluids were saturated in silica. Saturated fluids are fluids that contain enough silica in solution without precipitating silica minerals. When a silica-saturated solution cools slowly, crystalline quartz is deposited at approximately 200°–340° C (Fournier, 1985a). Rapid cooling of a silica-saturated fluid allows supersaturated solutions to form that precipitate chalcedony or amorphous silica. These supersaturated fluids are unstable and quickly deposit thin layers of chalcedony or amorphous silica, typically at lower temperatures (<200° C). The fluid loses silica due to precipitation and becomes saturated with silica but as the fluid continues to cool rapidly, it becomes supersaturated with silica again. An increase in salinity (such as NaCl) increases the solubility of silica at higher temperatures and also produces saturated silica solutions (Fournier, 1985a). Supersaturation of the fluids can also occur by mixing of different hydrothermal fluids, especially with different pHs, and by reaction of hydrothermal fluids with volcanic gases.

The different colors of the bands are a result of trace amounts of impurities, such as iron (red), manganese (black, pink), cobalt (blue, violet-red), copper (green, blue), chromium (orange-red), nickel (green), etc. Faceted quartz crystals indicate that the fluids were somewhat supersaturated with silica and that precipitation occurred under relatively slow-changing conditions (Fournier, 1985a).

Not all geodes are spherulites formed by magmatic processes; other natural processes form some geodes. Lower-temperature ground water percolates through the cooled volcanic rocks and dissolves additional minerals. These fluids are typically low temperature (<200° C), although locally higher-temperature (200°–300° C) ground waters may be present, especially adjacent to the volcanic vents. These fluids move through microscopic pores in the rock by a process called "diffusion." During diffusion, some ions in the fluid collect into void spaces and gas pockets in the rock, whereas other ions cannot pass through. This collection of ions surrounding these void spaces may actually, in some cases, form the hard outer shell that is characteristic of geodes. The outer shell may be strengthened by the precipitation of some ions that were excluded during crystallization of agate, chalcedony, and quartz and concentrated in the remaining fluid. Fluids also enter the void spaces through fractures. The void spaces may have orig-

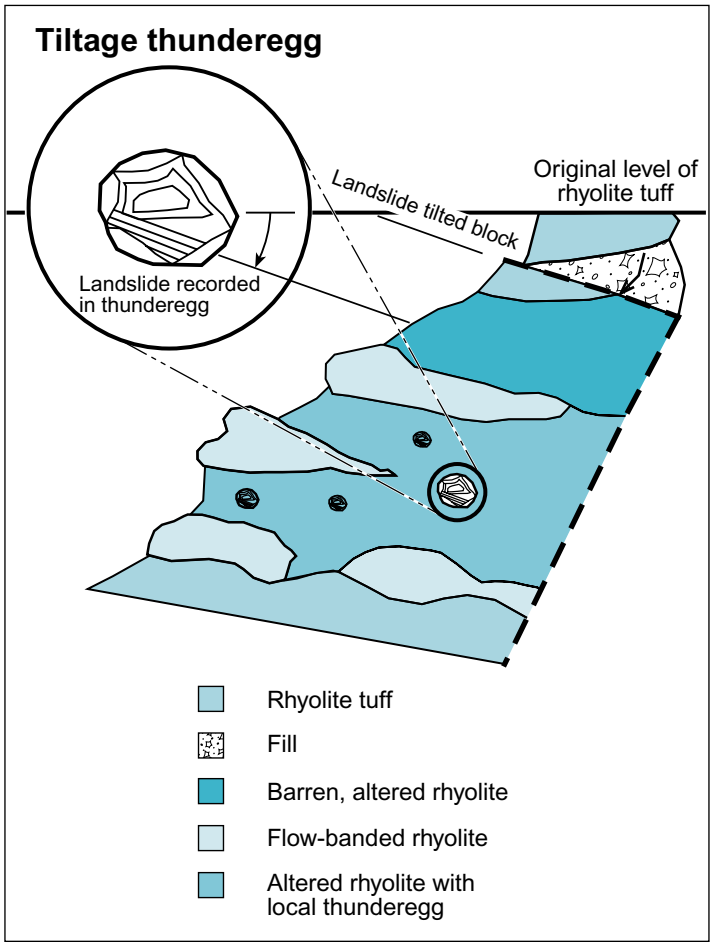

FIGURE 9—Schematic cross section of formation of tiltage spherulite (modified from Colburn, 1999).

inally formed by gas pockets within the magma or by prior dissolution of spherulites or other features within the volcanic rock.

The presence of calcite in some thundereggs and geodes indicates another episode of physical and chemical conditions (Fournier, 1985b). Calcite typically cannot crystallize from a silicic magma; therefore, the calcite must form from hydrothermal fluids. In most waters, heating of the fluids causes calcite to precipitate, and cooling of the fluids without boiling will cause calcite to dissolve. Calcite can also precipitate when a fluid quickly loses pressure and boils immediately (i.e. flashes) as a result of loss of CO_2 (Fournier, 1985b). Geologists must carefully examine the textures, determine the concentrations of the fluids, calculate the pressures and temperatures, and decide which process occurred in a specific thunderegg or geode.

Tiltage thundereggs, locally found at Rockhound State Park, are filled with horizontal layers of agate and chalcedony that are overlain by concentric-banded agate and chalcedony; the contact between the layered and banded agate resembles an angular unconformity (Fig. 9). These thundereggs record either small local landslides or tilting of local fault blocks within the Little Florida Mountains while the crystals were precipitating from the fluid (Fig. 10; Shaub, 1979; Colburn, 1999).

Other events can modify or even destroy thundereggs and geodes. As the spherulite forms, the expanding magmatic vapor can rupture and break the spherulite, forming fractures that may later fill with agate, chalcedony, or quartz and form vein-like features instead of thundereggs (Colburn, 1999). Similar vein-like features occur if the geode was fractured or broken before the hydrothermal fluids precipitated. Localized fracturing or faulting of thundereggs and geodes can occur during crystallization, and the fractures can be cemented together by other hydrothermal fluids. Later-stage ground waters can dissolve portions of the thunder-

FIGURE 10—Tiltage spherulite (photo by Robert Colburn).

eggs and geodes instead of precipitating minerals.

Thundereggs and geodes cannot be distinguished from one another until they have been broken apart. The beauty of a thunderegg or geode is locked inside the hard, rough-textured outer shell. All it takes to look for thundereggs and geodes is a rock hammer, pick, shovel, brush, chisel, collecting bag or pack, and persistence and patience. For more information on how to orient, where to collect, and how to slab thundereggs, see Colburn (1999).

Summary

Although Rockhound State Park is known for rock and mineral collecting, it also offers picnicking, camping, and hiking. The park allows the visitor to truly experience the desert Southwest with scenic views of Basin and Range topography and abundant desert wildlife and plants.

Acknowledgments. Special thanks are given to the personnel of Rockhound State Park and Carlos Valdez for their help and to Jack and Ali Kamm for the bird lists at Rockhound State Park. Discussions with Robert Colburn, who provided some of the photos, contributed additional insights into the origin of thundereggs. Richard Chamberlin, Steve Cary, Christy Comer, and Nancy McMillan reviewed this manuscript. Peter Scholle, Director, New Mexico Bureau of Mines and Mineral Resources and State Geologist, is acknowledged for his support and encouragement of this project.

References

Akizuki, M., 1983, An electron microscopic study of anorthoclase spherulites: Lithos, v. 16, no. 4, pp. 249–254.

Clemons, R. E., 1982, Geology of Florida Gap quadrangle, Luna County, New Mexico: New Mexico Bureau of Mines and Mineral Resources, Geologic Map 52, scale 1:24,000.

Clemons, R. E., 1984, Geology of Capitol Dome quadrangle, Luna County, New Mexico: New Mexico Bureau of Mines and Mineral Resources, Geologic Map 56, scale 1:24,000.

Clemons, R. E., 1998, Geology of the Florida Mountains, southwestern New Mexico: New Mexico Bureau of Mines and Mineral Resources, Memoir 43, 112 pp.

Clemons, R. E., and Brown, G. A., 1983, Geology of Gym Peak quadrangle, Luna County, New Mexico: New Mexico Bureau of Mines and Mineral Resources, Geologic Map 58, scale 1:24,000.

Clemons, R. E., Christiansen, P. W., and James, H. L., 1980, Southwestern New Mexico: New Mexico Bureau of Mines and Mineral Resources, Scenic Trips to the Geologic Past, no. 10, 119 pp.

References continued on page 86.

Colburn, R., 1999, The formation of thundereggs (lithophysae): Robert Colburn, CD-ROM, 385 pp.

Davis, B. K., and McPhee, J., 1996, Spherulites quench fractures and relict perlite in a Late Devonian rhyolite dike, Queensland, Australia: Journal of Volcanology and Geothermal Research, v. 71, pp. 1–11.

Dunbar, N. W., Jacobs, G. K., and Naney, M. T., 1995, Crystallization processes

Charlie Maxwell, October 1984, in the Black Range, New Mexico. Photo courtesy of Mimi Oakman Dickinson.

Charles Henry Maxwell

1923–2000

Charlie Maxwell was a familiar visitor around the Bureau of Mines. Although Charlie made his home in Lakewood, Colorado, he traveled often to New Mexico. Usually he was en route to his hometown, Las Palomas, or to Truth or Consequences, although it was still known as Hot Springs in 1941 when Charlie graduated from high school there. One trip each year in November coincided with the New Mexico Mineral Symposium.

During his 37-year career with the U.S. Geological Survey, Charlie undertook many mapping and resource-evaluation projects in New Mexico, Brazil, Kentucky, Wyoming, and Colorado. Charlie spoke fluent Portuguese and Spanish and worked for 5 years in Brazil, a research project that culminated in the 1972 publication of USGS Professional Paper 341J, *Geology and ore deposits of the Alegria district, Minas Gerais, Brazil*, an important contribution to the understanding of the stratigraphy, structure, and mineral resources of the region. From 1980 to 1988 Charlie headed a project to study the resource potential, mineralogy, and geochemistry of the Black Range tin district. Publication in 1986 of *Geologic map of El Malpais lava field and surrounding areas, Cibola County, New Mexico*, a 1:62,500-scale sheet that covers 950 mi^2, includes the first detailed mapping of some of the flow units south of Grants.

For many years Charlie made generous donations of minerals to the Mineral Museum of the New Mexico Bureau of Mines and Mineral Resources. In 1996, Charlie loaned a sizable collection of fine Brazilian cut gemstones, which enabled the museum to create a gem display for the first time. Among the faceted stones are aquamarine, various tourmalines, topaz, andalusite, chrysoberyl, and many varieties of quartz—aventurine, amethyst, rose, and smoky quartz. The focus of the display is a 32-pound clear-to-blue, gem-quality partial crystal of topaz from Minas Gerais, Brazil, and five faceted clear and blue stones taken from the large topaz.

Charlie was a classic field geologist, doing his mapping and resource studies by walking the hills and acutely observing everything around him. He looked for his facts in the rocks rather than speculating about how things should fit a theoretical model. Charlie will be remembered for his outstanding professional career and additionally by his friends for his wit and charm and for his generosity in sharing his expertise with professionals and amateurs alike.

The Editors wish to thank Mimi Oakman Dickinson, Virgil Lueth, Robert Eveleth, Marie Huizing, and Robert Gait, whose contributions make this memorial to Charlie more complete.

The following article was originally printed in *Rocks & Minerals* in 1992.

A selected New Mexico bibliography follows page 73.

WHO'S WHO in Mineral Names

Robert I. Gait
Department of Mineralogy
Royal Ontario Museum
100 Queen's Park
Toronto, Ontario, Canada M5S 2C6.

Dr. Robert I. Gait, an executive editor of Rocks & Minerals, *is curator of mineralogy at the Royal Ontario Museum.*

MAXWELLITE was named in honor of Charles Henry Maxwell by Dr. Eugene Foord and his coworkers at the U.S. Geological Survey (USGS); the description was published in *Neues Jahrbuch für Mineralogie* (Foord et al. 1991). In a private communication to the author, Dr. Foord wrote: "Charles Maxwell does not have his Ph.D. degree (M.S. from Univ. of New Mexico) but he knows more than 10 normal Ph.D.'s put together."

Maxwell (known as Charlie to his friends and colleagues) has spent forty years studying New Mexico geology and mineralogy, and so it is fitting that a new species from New Mexico should be named for him. In dedicating the 1989 New Mexico Geological Society *Guidebook* to Maxwell, his colleague Orin J. Anderson remarked that a more knowledgeable proponent of New Mexico and its diverse geology would be difficult to find.

Charles Maxwell was born in Las Palomas, New Mexico, into a family whose life in that state began in the 1870s with the arrival of his grandfather, Alexander J. Maxwell. Originally from the Dumfries area of Scotland, Alexander met a German immigrant, Anna Katarin Walther, and they were married in Deming in 1886. They soon moved and began operating saloons in the old mining towns of Kingston and Hermosa. William Henry Maxwell, Charles's father, was born in 1889. The family then moved in 1893 to Las Palomas, where they ran a general store, boarding house, farm, and cattle ranch. William went into the freight-hauling business, operated a blacksmith shop, and subsequently ran a garage and service station. He married Annie L. Stirling, a Texas native, in Las Palomas in 1921.

Two years later, on 9 July, they became the proud parents of Charles Henry Maxwell. His mother said that he collected "pretty rocks" as soon as he was able to walk. Perhaps the Maxwell family's connections with New Mexico mining towns first sparked the interest that turned into his passion for rocks and minerals. By the

time he finished graduate school at the University of New Mexico he had a large collection of minerals, many museum quality. Maxwell subsequently donated most of his collection to the University of New Mexico as well as to other museums and individuals. His knowledge of mineral localities, especially in New Mexico, is legendary, and he is always ready to share it with anyone who is interested.

Maxwell attended Hot Springs High School (1938-41) and went on to graduate from the University of New Mexico with a B.S. degree, majoring in geology and minoring in biology. In 1952, he received his M.S. degree with the very same major and minor. His master's thesis is entitled "Pleonaste [*pleonaste* is an old term for a variety of spinel] crystals from an olivine basalt, Caballo Mountains, New Mexico." While still studying at the university, he did X-ray and blowpipe analysis of minerals for the state of New Mexico, taught the laboratory part of courses in mineralogy, and assisted in optical mineralogy and petrography. In the summer of 1952, he had a part-time job with Shell Oil Company (Houston, Texas) doing X-ray and differential thermal analysis and microscopic studies in basic research on carbonate rocks.

MAXWELLITE, ideally $NaFe^{3+}(AsO_4)F$, a sodium iron fluoro-arsenate, was found at the Squaw Creek tin prospect, Catron County, and at another tin deposit at Willow Spring Draw, Sierra County, New Mexico. The mineral is monoclinic with space group Aa or A2/a. The crystals, up to 1 mm and in clusters up to 3 mm across, are medium to dark red with a medium to pale orange streak, blocky to short prismatic, exhibiting the following forms in decreasing order of importance {013}, {526}, {$\bar{5}$26}, and {011}. Its density is 3.90, and its Mohs hardness is 5 to 5.5. It has a vitreous luster, a good cleavage on {110}, and an irregular to conchoidal fracture. Associated minerals are squawcreekite, quartz, tridymite, sanidine, pseudobrookite, hematite, Fe- and Sb-bearing cassiterite, chernovite-(Y), and gasparite-(Ce). It is related to durangite and tilasite.

Maxwell's career with the USGS began in 1952. His first project was field mapping and preparing a report on the schröckingerite deposits of Sweetwater County, Wyoming; it was the forerunner of numerous similar projects. In 1965, while working with the Strategic Studies Section, Branch of Military Geology (Washington, D.C.), he devised a system of graphs to translate refraction of UHF transmission and the curvature of the earth to the plane of topographic maps, making it possible to read directly—with a straight edge—the line-of-sight coverage. This system was widely used for the preliminary site planning for microwave facilities.

From 1973 onward, he was chief of several major geological and resource evaluation projects undertaken by the USGS. Between 1978 and 1980, he headed the study of El Malpais lava field and surrounding areas in Cibola County. This included the first detailed mapping of over 400 square miles of Quaternary basalt flows, containing ten flow units, for resource evaluation. Among the guidebooks, maps, and open-file reports that came out of this project, Maxwell's map (published in 1986) is an outstanding achievement. It covers an area of 950 square miles—at a scale of 1:62,500—including 400 square miles never before mapped. This is the first accurate and detailed map of the flow units in the basalt field to the south of Grants. It also made possible new Cretaceous correlations and is a major contribution to the geologic knowledge of the region that is now El Malpais National Monument.

On a visit to Denver in 1990, I had the privilege of meeting Maxwell, who recounted some of his experiences in El Malpais lava field. He waxed eloquent about the walk-through lava tunnels and how wonderful little frozen lava "stalactites" could be seen in some of them. His enthusiasm is infectious, and I cannot wait to visit this national monument that came into being partly at his instigation.

Yet another of his major undertakings was the study of the Black Range tin district carried out under his supervision between 1980 and 1988. The objectives were to determine the resources and potential resources, the mineralogy and geochemistry of the veins, and the genesis of the deposits; to prepare detailed maps of the major deposits; to produce a reconnaissance map of the 500-square-mile tin belt; and to relate the several types of tin deposits to the geology. At least eight papers and abstracts resulted from this study; a major report in preparation contains several aspects for tin mineralization that are not generally known, notably the persistent substitution of antimony, lead, and arsenic for tin in cassiterite. Also of importance was the recognition, for the first time, of the fact that rather than being a single system, the tin mineralization is part of the complex, cyclic chemistry and paragenesis of several overlapping types of mineralization.

He is a member of the New Mexico Geological Society and the Geological Society of America and has been a member of the Rocky Mountain Association of Geologists (1954–56), Sociedada Brasiliera de Geologia (1956–61), the Mineralogical Society of America (1960–75), and the Geological Society of Washington (1963–70).

Maxwell's bibliography contains over eighty entries and is still growing. It contains over twenty geologic maps (most of them of New Mexico); of the remaining sixty, many relate to base or precious metals deposits and radioactive and strategic minerals. The New Mexico Geological Society published eight of his works. It is of special note that he was not only the chief of many of these projects, but that he also did the field work himself. Although he retired in 1989, he is still actively involved as a volunteer emeritus with the USGS and with the New Mexico Bureau of Mines and Mineral Resources. At present, he has several papers and maps in various stages of preparation and editing, including one with Foord on the tin deposits of the Black Range. He and Foord are also working on the description of yet another new fluoro-arsenate from Durango, Mexico. Maxwell's geologic map of El Morro quadrangle, a cooperative effort with Orin Anderson, is also reaching publication stage.

Besides having had an outstanding professional career, Maxwell is an accomplished artist, an avocation and hobby that he acquired early on and one he has maintained up to the present. Although he favors landscapes, he also creates naturalist, impressionist, and objective abstracts; he works with watercolors, some oils, and pencil. His art has received awards at local shows, including one Best of Show award. Another of his hobbies is HO model railroading, and he is especially interested in "scratch-built" models. It is clear that Charles Maxwell is a man of considerable intellect, drive, and energy, whose contributions to science and art are most remarkable.

Maxwell married Jacqueline Perkinson of Albuquerque in 1952; they have three children: Florence Ann (b. 1953), Patricia Alece (b. 1954), and William Alexander (born in Brazil in 1960). The Maxwells have been divorced since 1973.

Acknowledgments—I would like to express my special thanks to Charlie Maxwell, who provided me with a perfect set of data from which I was able to write this biography. Dr. Eugene Foord kindly provided me with the galley proofs of his paper prior to publication and made it possible for me to contact Charlie Maxwell directly.

Reference

Foord, E. E., P. F. Hlava, J. J. Fitzpatrick, R. C. Erd, and R. W. Hinton. 1991. Maxwellite and squawcreekite, two new minerals from the Black Range tin district, Catron County, New Mexico, U.S.A. *Neues Jahrbuch für Mineralogie, Monatshefte,* Heft 8: 363–84.

Rocks & Minerals, v. 67, no. 5, pp. 332–334, September/October, 1992. Reprinted with permission of the Helen Dwight Reid Educational Foundation. Published by Heldref Publications, 1319 18th Street NW, Washington, D.C. 20036-1802.

Maps

Anderson, O. J., Maxwell, C. H., and Lucas, S. G., in press, Geology of Fort Wingate quadrangle, McKinley County, New Mexico: New Mexico Bureau of Mines and Mineral Resources, Geologic Map 74, scale 1:24,000.

Anderson, O. J., and Maxwell, C. H., 1991, Geology of El Morro quadrangle, Cibola County, New Mexico: New Mexico Bureau of Mines and Mineral Resources, Geologic Map 72, scale 1:24,000.

Maxwell, C. H., 1990a, Geologic map of the Broom Mountain quadrangle, Cibola County, New Mexico: U.S. Geological Survey, Geologic Quadrangle Map GQ–1666, scale 1:24,000.

Maxwell, C. H., 1990b, Geologic map of the Cubero quadrangle, Cibola County, New Mexico: U.S. Geological Survey, Geologic Quadrangle Map GQ–1657, scale 1:24,000.

Maxwell, C. H., and Oakman, M. R., 1990, Geologic map of the Cuchillo quadrangle, Sierra County, New Mexico: U.S. Geological Survey, Geologic Quadrangle Map GQ–1686, scale 1:24,000.

Maxwell, C. H., 1988, Geologic map of the Marmon Ranch quadrangle, Cibola County, New Mexico: U.S. Geological Survey, Miscellaneous Field Studies Map MF–2049, scale 1:24,000.

Maxwell, C. H., 1986, Geologic map of El Malpais lava field and surrounding areas, Cibola County, New Mexico: U.S. Geological Survey, Miscellaneous Investigations Series, Map I–1595, scale 1:62,500.

Maxwell, C. H., Heyl, A. V., Ellis, C. E., and Scott, D. C., 1984, Mineral resource potential map of the Ryan Hill Roadless Area, Socorro County, New Mexico: U.S. Geological Survey, Miscellaneous Field Studies Map MF–1634–A, scale 1:50,000.

Heyl, A. V., Maxwell, C. H., and Davis, L. L., 1983, Geology and mineral deposits of the Priest Tank quadrangle, Sierra County, New Mexico: U.S. Geological Survey, Miscellaneous Field Studies Map MF–1665, scale 1:24,000.

Maxwell, C. H., Wobus, R. A., and Light, T. D., 1983, Mineral resource potential map of the Manzano Wilderness, Valencia and Torrance Counties, New Mexico: U.S. Geological Survey, Miscellaneous Field Studies Map MF–1464–C, scale 1:50,000.

Maxwell, C. H., and Wobus, R. A., 1982a, Geologic map of the Manzano Wilderness, Valencia and Torrance Counties, New Mexico: U.S. Geological Survey, Miscellaneous Field Studies Map MF–1464–A, scale 1:50,000.

Maxwell, C. H., and Wobus, R. A., 1982b, Geochemical and geophysical maps of the Manzano Wilderness, Valencia and Torrance Counties, New Mexico: U.S. Geological Survey, Miscellaneous Field Studies Map MF–1464–B, scale 1:50,000.

Maxwell, C. H., and others, 1982, Mineral resource potential map of the Manzano Wilderness, Valencia and Torrance Counties, New Mexico: U.S. Geological Survey, Miscellaneous Field Studies Map MF–1464–C, scale 1:50,000.

Maxwell, C. H., 1981a, Geologic map of the El Malpais Instant Study Area and adjacent areas, Valencia [now Cibola] County, New Mexico: U.S. Geological Survey, Miscellaneous Field Studies Map MF–1375–A, scale 1:62,500.

Maxwell, C. H., 1981b, Aeromagnetic map of the El Malpais Instant Study Area and adjacent areas, Valencia [now Cibola] County, New Mexico: U.S. Geological Survey, Miscellaneous Field Studies Map MF–1375–B, scale 1:62,500.

Maxwell, C. H., 1979, Geologic map of the East Mesa quadrangle, Valencia [now Cibola] County, New Mexico: U.S. Geological Survey, Geologic Quadrangle Map GQ–1522, scale 1:24,000.

Maxwell, C. H., 1978, Map showing appraisal of mineral resource potential of RARE II proposed roadless areas in national forests, New Mexico (exclusive of coal, oil, gas, and construction materials): U.S. Geological Survey, Open-file Report 78–859, scale 1:500,000.

Maxwell, C. H., 1977a, Preliminary geologic map of the McCartys quadrangle, Valencia [now Cibola] County, New Mexico: U.S. Geological Survey, Open-file Report 77–380, scale 1:24,000.

Maxwell, C. H., 1977b, Preliminary geologic map of the Crow Point quadrangle, Valencia [now Cibola] County, New Mexico: U.S. Geological Survey, Open-file Report 77–323, scale 1:24,000.

Maxwell, C. H., 1977c, Preliminary geologic map of the Los Pilares quadrangle, Valencia [now Cibola] County, New Mexico: U.S. Geological Survey, Open-file Report 77–240, scale 1:24,000

Maxwell, C. H., 1976, Geologic map of the Acoma Pueblo quadrangle, Valencia [now Cibola] County, New Mexico: U.S. Geological Survey, Geologic Quadrangle Map GQ–1298, scale 1:24,000.

Maxwell, C. H., and Heyl, A. V., 1976, Preliminary geologic map of the Winston quadrangle, Sierra County, New Mexico: U.S. Geological Survey, Open-file Report 76-858, scale 1:24,000.

Papers

Maxwell, C. H., 1989, Bandera Crater; in Anderson, O. J., Lucas, S. G., Love, D. W., and Cather, S. M. (eds.), Southeastern Colorado Plateau: New Mexico Geological Society, Guidebook 40, p. 65.

Maxwell, C. H., Nowlan, G. A., Bankley, V., and Hannigan, B. J., 1989a, Mineral resources of the Rimrock, Sand Canyon, Little Rimrock, and Pinyon Wilderness Study Areas, Cibola County, New Mexico: U.S. Geological Survey, Bulletin 1734–G

Maxwell, C. H., Nowlan, G. A., Bankley, V., and Hannigan, B. J., 1989b, Mineral resources of the Petaca Pinta Wilderness Study Area, Cibola County, New Mexico: U.S. Geological Survey, Bulletin 1734–H

Anderson, O. J., Lucas, S. G., Love, D. W., Maxwell, C. H., and Chamberlin, R. M., 1989, Third-day road log, from Gallup to Upper Nutria, Ramah, El Morro, and Grants; in Anderson, O. J., Lucas, S. G., Love, D. W., and Cather, S. M. (eds.), Southeastern Colorado Plateau: New Mexico Geological Society, Guidebook 40, pp. 49–66.

Chamberlin, R. M., Anderson, O. J., Lucas, S. G., Maxwell, C. H., and Love, D. W., 1989, Second-day road log, from Grants to El Malpais, Fence Lake, Zuni Pueblo, and Gallup; in Anderson, O. J., Lucas, S. G., Love, D. W., and Cather, S. M. (eds.), Southeastern Colorado Plateau: New Mexico Geological Society, Guidebook 40, pp. 25–48.

Maxwell, C. H., Anderson, O. J., Lucas, S. G., Chamberlin, R. M., and Love, D. W., 1989, First-day road log, from Albuquerque to Mesita, Laguna, Acoma, McCartys, and Grants; in Anderson, O. J., Lucas, S. G., Love, D. W., and Cather, S. M. (eds.), Southeastern Colorado Plateau: New Mexico Geological Society, Guidebook 40, pp. 1–24.

Brown, S. D., and Maxwell, C. H., 1988, Mineral resources of the Manzano Wilderness Study Area, Torrance County, New Mexico: U.S. Geological Survey, Open-file Report 88–0296, 10 pp.

Maxwell, C. H., Foord, E. E., Oakman, M. R., and Harvey, D. B., 1986, Tin deposits in the Black Range tin district; in Clemons, R. E., King, W. E., and Mack, G. H. (eds.), Truth or Consequences region: New Mexico Geological Society, Guidebook 37, pp. 273–281.

Maxwell, C. H., and Oakman, M. R., 1986, A Pennsylvanian unconformity in the Mud Springs Mountains; in Clemons, R. E., King, W. E., and Mack, G. H. (eds.), Truth or Consequences region: New Mexico Geological Society, Guidebook 37, pp. 4–5.

Osburn, G. R., Harrison, R. H., Eggleston, T. L., Lozinsky, R. P., and Maxwell, C. H., 1986, First-day road log, from Truth or Consequences to Sierra Cuchillo, Winston graben, Winston, south Fork Cuchillo Negro Creek, Fluorine, and central Black Range; in Clemons, R. E., King, W. E., and Mack, G. H. (eds.), Truth or Consequences region: New Mexico Geological Society, Guidebook 37, pp. 1–19.

Foord, E. E., Oakman, M. R., and Maxwell, C. H., 1985, Durangite from the Black Range, New Mexico, and new data on durangite from Durango and Cornwall: Canadian Mineralogist, v. 23, pt. 2, pp. 241–246.

Maxwell, C. H., and Ellis, C. E., 1984, Ryan Hill Roadless Area, New Mexico; in Marsh, S. P., Kropschot, S. J., and Dickinson, R. G. (eds.), Wilderness mineral potential—assessment of mineral-resource potential in U.S. Forest Service lands studied 1964–1984: U.S. Geological Survey, Professional Paper 1300, pp. 827–829.

Maxwell, C. H., and Light, T. D., 1984, Manzano Wilderness, New Mexico; in Marsh, S. P., Kropschot, S. J., and Dickinson, R. G. (eds.), Wilderness mineral potential—assessment of mineral-resource potential in U.S. Forest Service lands studied 1964–1984: U.S. Geological Survey, Professional Paper 1300, pp. 820–822.

Maxwell, C. H., 1982a, El Malpais; in Grambling, J. A., and Wells, S. G. (eds.), Albuquerque country II: New Mexico Geological Society, Guidebook 33, pp. 299–301.

Maxwell, C. H., 1982b, Mesozoic stratigraphy of the Laguna–Grants region; in Grambling, J. A., and Wells, S. G. (eds.), Albuquerque country II: New Mexico Geological Society, Guidebook 33, pp. 261–266.

Bigsby, P. R., and Maxwell, C. H., 1981, Mineral resource potential of the El Malpais Instant Study Area and adjacent areas, Valencia [now Cibola] County, New Mexico: U.S. Geological Survey, Open-file Report 81–557, 23 pp., scale 1:62,500.

Maxwell, C. H., and Heyl, A. V., 1980, Mineralization and structure of mineral deposits in the Hermosa, Chloride, and Phillipsburg areas, New Mexico: Laboratory of Global Tectonics and Metallogeny, Bulletin, v. 1, no. 2, pp. 129–133.

Maxwell, C. H., 1976, Stratigraphy and structure of the Acoma region, New Mexico; in Woodward, L. A., and Northrop, S. A. (eds.), Tectonics and mineral resources of southwestern North America: New Mexico Geological Society, Special Publication 6, pp. 95–101.

Abstracts

Foord, E. E., Hlava, P. F., Fitzpatrick, J. J., and Maxwell, C. H., 1987, Three new minerals from Squaw Creek, stolzite from Nugget Gulch, and tilasite from Willow Springs Draw, Black Range tin district, New Mexico (abs.): New Mexico Institute of Mining and Technology, 8th annual New Mexico Mineral Symposium, Symposium Proceedings, pp. 25–27.

Foord, E. E., and Maxwell, C. H., 1986, Mineralogy of the Black Range tin district, Sierra and Catron Counties, New Mexico (abs.): New Mexico Institute of Mining and Technology, 7th annual New Mexico Mineral Symposium, Symposium Proceedings, pp. 6–8.

Oakman, M. R., Foord, E. E., and Maxwell, C. H., 1984, Durangite from the Black Range, New Mexico, and Coneto, Durango, Mexico (abs.): Mineralogical Society of America, symposium.

Heyl, A. V., Bozion, C. N.,and Maxwell, C. H., 1975, Silver resources of New Mexico (abs.); in Seager, W. R., Clemons, R. E., and Callender, J. F. (eds.), Las Cruces country: New Mexico Geological Society, Guidebook 26, p. 340.

Maxwell, C. H., and Heyl, A. V., 1975, Mineralization and structure of mineral deposits in the Hermosa, Chloride, and Phillipsburg areas, New Mexico (abs.); in Seager, W. R., Clemons, R. E., and Callender, J. F. (eds.), Las Cruces country: New Mexico Geological Society, Guidebook 26, pp. 341–342.

Abstracts

New Mexico Geology recognizes the important research of students working in post-graduate MS and PhD programs. The following abstracts are from recently completed MS theses and PhD dissertations that pertain to the geology of New Mexico and neighboring states.

New Mexico Institute of Mining and Technology

SPATIAL VARIABILITY OF DESERT LOESS ON THE CARRIZOZO LAVA FLOW, SOUTH-CENTRAL NEW MEXICO, by *Shari L. Bauman*, 1999, MS thesis, Department of Earth and Environmental Science, New Mexico Institute of Mining and Technology, Socorro, NM 87801, 106 pp.

The Carrizozo lava flow is an ideal isochronous (5 ka) surface to examine the influences of climate, provenance, and surface-cover types on the abundance of and physical and chemical composition of loess deposits, and the early pedogenic process occurring within the deposits. The Carrizozo lava flow is 75 km long. Its complex surface topography provides catchments for eolian material accumulation, as well as for the development of a range of surface-cover types (i.e. desert pavement, grasses and cacti, and juniper trees). The Carrizozo lava flow is surrounded by various lithologies within the Tularosa Basin, and dust transport is by southwestern prevailing winds.

Surface-cover type influences the loess composition in two ways: (1) by influencing the moisture content and thus the accumulation of chemical constituents in the soil profile during pedogenesis and (2) by preferentially trapping material. In general, higher concentrations of CaO, MgO, S, soluble salts, chloride, and calcium carbonate are found in the south and are indicative of provenance effects. Strong correlations in chemistry coupled with the prevailing wind direction suggest that the evaporite gypsum dune deposit of White Sands and the dolomitic rocks from the San Andres Mountains influence the dust composition.

The Carrizozo dust flux average of 0.54 $g/cm^2/ka$ is very comparable to those found in the southwestern United States and in similar desert environments around the world. The non-pedogenic calcium carbonate chemical composition of the Carrizozo loess is similar to the regional shale standard (NASC), local crustal composition, and to soils developing on the Potrillo volcanic field in southern New Mexico. As expected, high deviation in chemistry is observed when compared to the Carrizozo basalt composition, indicating that the soils are indeed of eolian origin and not basalt weathering products.

Furthermore, surface-cover type, provenance, and wind direction affect the abundance of and physical and chemical composition of the Carrizozo lava flow loess deposits, and the early developmental stages of pedogenesis. The Carrizozo lava flow has provided an opportunity to investigate the spatial variability associated with these factors, as well as the remarkable uniformity of the eolian material and accumulation over the last 5,000 yrs.

STRUCTURAL AND THERMOCHRONOLOGICAL CONSTRAINTS ON THE MOVEMENT HISTORY OF THE MONTOSA FAULT, CENTRAL NEW MEXICO, by *Rose-Anna Behr*, 1999, MS thesis, Department of Earth and Environmental Science, New Mexico Institute of Mining and Technology, Socorro, NM 87801, 129 pp.

The 90-km-long Montosa fault bounds the east side of the Los Pinos and Manzano Mountains of central New Mexico. Overall fault strike is north-northeast, and dip is 55–70° west. The fault shows predominantly reverse separation and has been interpreted as Laramide in age. Local normal stratigraphic separation across the fault and normal-slip slickenlines on earlier reverse and strike-slip faults indicate that fault reactivation occurred during Neogene Rio Grande rift extension.

Lineations and kinematic indicators on minor fault planes and fold hinges were examined to constrain the direction of maximum shortening during formation of these structures and, by inference, the sense of slip on the Montosa fault. Three different directions of shortening were determined: east-west, northwest-southeast, and north-south. Other workers have reported that structures recording east-west shortening are cross-cut by those recording north-south shortening. East-west shortening would impart dextral reverse oblique-slip motion on the Montosa fault. The central portion of the fault shows strong evidence for northwest-southeast shortening, which would cause sinistral reverse oblique-slip motion on the Montosa fault. Along the north-central portion of the fault, minor planes and folds accommodated north-south shortening, which would result in sinistral reverse oblique-slip motion on the fault. East-west shortening was the most significant stage in the movement history of the Montosa fault, resulting in reverse separation, with a component of dextral strike-slip offset. The Montosa fault also shows evidence of normal reactivation during the Neogene Rio Grande rift formation.

Apatite fission tract (AFT) analysis was used to determine the thermal history of samples collected in several transects across the fault. Because the thermal history of a sample reflects the tectonic history, AFT data can be used to constrain the relative timing of faulting. AFT data from along the Montosa fault indicate that denudation in early Eocene to late Eocene time (55–35 Ma) resulted in cooling of the lower elevations of the Los Pinos Mountains. Samples from the lower elevations of the Manzano Mountains cooled in early Oligocene to early Miocene time (33–22 Ma), ascribable to exhumation following Laramide uplift and during the formation of the Rio Grande rift. The southern fault tip shows normal separation of sedimentary strata, which is attributed to reactivation during rift-related extension. Samples in this area did not cool until the late Oligocene to mid-Miocene (25–14 Ma). Broad track-length distributions suggest that all of the samples remained within the partial annealing zone (PAZ) for apatite (temperatures range from ~60° to ~120°C) for long periods of time where elevated temperatures caused fission tracks to shorten. Thermal modeling of the AFT ages and track-length distributions reveal that the samples remained in the PAZ for 10–30 m.y., then cooled quickly to surface temperatures.

AFT analysis did not show significant age variation across the fault, which indicates that faulting predated cooling; therefore, movement on the Montosa fault during the Laramide orogeny must have occurred at temperatures greater than ~120°C. Any normal fault reactivation during rift formation also occurred at temperatures greater than 60°–120° C or was too minimal to be recorded by AFT.

DEFORMATION WITHIN A BASEMENT-CORED ANTICLINE: TEAPOT DOME, WYOMING, by *Scott P. Cooper,* 2000, MS thesis, Department of Earth and Environmental Science, New Mexico Institute of Mining and Technology, Socorro, NM 87801, 274 pp.

Teapot Dome is an asymmetric, doubly plunging, basement-cored, Laramide-age anticline. A systematic study of natural fractures within the Cretaceous Mesaverde Formation at Teapot Dome, Wyoming, indicates that lithology and structural position control outcrop fracture patterns. Lithology controls fracture, deformation band, and fault patterns in the following ways: (1) fracture intensity increases with increased cementation; (2) fracture spacing increases proportionally with bed thickness within two sandstone facies but not in carbonaceous shales where fracture spacing is inversely proportional to bed thickness; (3) coal cleats are generally oblique, by up to 20°, to fractures in sandstones; (4) most fractures in sandstone units terminate at contacts with shale layers; (5) deformation bands occur almost exclusively in a poorly cemented, high-porosity, beach-sand facies; and (6) normal faults within well-cemented sandstones are generally expressed as fracture zones, whereas the same faults within poorly cemented sandstones are diffuse zones of subparallel deformation bands.

Three primary through-going fracture sets were documented at Teapot Dome. The oldest fracture set is oblique to the fold hinge. The vast majority of these fractures strike northwest to west-northwest. A small number of these oblique fractures strike roughly north-northeast. Fractures that strike oblique to the fold hinge appear to predate folding. The most common fractures, which are found throughout the fold, are bed-normal extension fractures striking subparallel to the fold hinge. A third set consists of bed-normal extension fractures striking perpendicular to the fold hinge. In many areas this fracture set is spatially related and subparallel to northeast-striking, normal, oblique-slip faults. The normal, oblique-slip faults are common along the eastern limb, but more than 90% of these faults terminate before intersecting the western limb. Conjugate fractures, deformation bands, and faults, oriented such that they have a vertical bisector to the acute angle and striking subparallel to the axis of the anticline, are common in the southwestern limb and southern arc of the anticline. Hinge-parallel and hinge-perpendicular fractures and faults are probably broadly contemporaneous with basement-involved thrusting and folding at Teapot Dome, as suggested by their spatial relationship to the fold. Further observations suggest that fault-related, hinge-perpendicular fractures are generally the same age as hinge-parallel fractures, and that northeast-striking, normal, oblique-slip faults are oriented roughly perpendicular to the fold hinge, even where it bends, and terminate toward the southwest limb of the anticline. The oblique movement recorded on some of these northeast-striking faults may be related to differential movement across individual segments of the basement-involved thrust.

Based on the Teapot Dome natural fracture data set, a three-dimensional conceptual model

of fractures associated with basement-cored anticlines suggests significant horizontal permeability anisotropy. Depending on structural position and the interaction between fracture sets, the direction of maximum permeability can be either parallel or perpendicular to the fold hinge.

EXPERIMENTAL EVIDENCE OF HYPERFILTRATION INDUCED PRECIPITATION OF HEAVY METALS, by *Gina DeRosa*, 1999, MS thesis, Department of Earth and Environmental Science, New Mexico Institute of Mining and Technology, Socorro, NM 87801, 126 pp.

It has long been known that clays and shales have membrane properties. A semipermeable membrane is defined as a material that will permit the passage of some molecules, but not others. When a shale membrane partially rejects solute, a concentration polarization layer (CPL) forms at the higher-pressure membrane face. Non-equilibrium thermodynamic calculations for conditions of reasonable hydraulic gradient, aquitard hydraulic conductivity, and pollutant heavy-metal concentration suggest that it should be possible for concentrations of heavy-metal solute in the CPL to reach supersaturation, resulting in the precipitation of heavy-metals. The purpose of this research was to test this concept. Eight hyperfiltration experiments were conducted with undersaturated heavy-metal solutions of varying composition. Of these eight, six succeeded in precipitation of heavy metal on the high-pressure face of the membrane. The heavy metals of interest included lead, copper, and cobalt.

In order for solute sieving to occur, there must be a head difference across the shale aquitard. Such head differences can occur as the result of rapid sedimentation of fine-grained materials or lateral tectonic compression. Head differences observed in perched and artesian aquifer systems are sufficient to drive the phenomenon. Additional theoretical calculations indicate that much lower pressure-head gradients than those used in these experiments will drive hyperfiltration in natural systems, resulting in the precipitation of heavy metals as described in this study.

The experiments demonstrate that clay-membrane induced precipitation of heavy metals can occur when undersaturated solutions pass through membranes. Mathematical analysis coupled with the findings of this study suggest that hyperfiltration may induce heavy-metal precipitation in the subsurface where contaminated aquifers are bounded by membrane-functioning shales.

TRACE-ELEMENT CONTROL ON NEAR-INFRARED TRANSPARENCY OF PYRITE, by *Jerzy Kulis*, 1999, MS thesis, Department of Earth and Environmental Science, New Mexico Institute of Mining and Technology, Socorro, NM 87801, 271 pp.

Pyrite from various localities has been analyzed, by means of infrared microscopy, FTIR spectroscopy, bulk geochemical analysis, and electron microprobe analysis for correlations between trace-element contents and transparency in near-infrared ($\lambda \leq \sim 2.0$ µm). Additionally, FTIR spectra were taken in the temperature range from 28°C to 400°C to identify mechanisms responsible for degradation of the transparency of pyrite at high temperatures.

The transparency of pyrite at room temperature was found to be highly variable, with a sedimentary and fine-grained pyrite being mostly opaque in the analyzed spectral range. Although fluid inclusions are present in pyrite, relatively few of them are transparent enough to be suitable for microthermometric measurements, and their prevalent opacity can be attributed to the high refractive index of pyrite and the resulting refraction of IR light from the inclusion walls.

Six distinct absorption features, caused by imperfections in pyrite, have been identified in the IR spectra: (1) raised baseline; (2) prominent absorption tail of the main absorption edge; (3) high-absorption area, with a steep low-energy slope, below the main absorption edge; (4) symmetric absorption peak centered at 2.0 µm; (5) asymmetric absorption peak with a maximum at ~2.0 µm, with a steeper low-energy slope; and (6) gradual increase in absorption, below the main absorption edge, with longer wavelengths. The first three absorption features have been linked to the presence of large-scale mechanical defects in pyrite (e.g., cracks, grain boundaries, solid inclusions, surface imperfections), and they might be caused by reflection, refraction, and absorption (by foreign minerals) of the incident IR light. The remaining absorption features are likely produced by crystal-lattice imperfections, which affect the electronic structure of pyrite. Strong experimental evidence indicates that Co is responsible for the symmetric absorption peak in pyrite at 2.0 µm. Theoretical calculations suggest that this peak is most likely caused by $^2E \rightarrow {}^4T_1(F)$ crystal-field transitions of a low-spin Co^{2+}, with $B \cong 0.050$ eV and $\Delta \cong 1.65$ eV. Co^{2+} occurs in a solid solution in pyrite as a stoichiometric substitution for Fe^{2+}, and it probably enters pyrite as a deep-level imperfection, close to the bottom of the energy gap of pyrite. The last absorption feature listed above correlates with As; however, there is no theoretical evidence to support that correlation.

The main absorption edge of pyrite shifts gradually toward longer wavelengths with an increase in temperature. The coefficient of this shift is equal to -0.50 meV/°C in the analyzed temperature range from 28°C to 400°C. The resulting high-temperature degradation in the IR transparency of pyrite can be minimized by keeping the thickness of a sample to a minimum and/or by increasing the spectral range of the IR detector being used.

GEOCHEMICAL CHARACTERIZATION OF GEOLOGICALLY COMPLEX MOUNTAIN FRONT AQUIFERS: PLACITAS, NEW MEXICO, by *William J. LeFevre*, 1999, MS thesis, Department of Earth and Environmental Science, New Mexico Institute of Mining and Technology, Socorro, NM 87801, 209 pp.

Characterization of ground-water flow across geologically complex mountain-front recharge areas can be confounded by an intricate network of structural and stratigraphic controls. Standard exploration methods are inadequate because the hydrologic nature of geologic discontinuities may be difficult to discern and the collection of representative data may be prohibitively expensive. The use of geochemical techniques as a primary tool for characterizing ground-water flow and recharge in geologically complex terrain is demonstrated on the eastern margin of the Albuquerque Basin at the north end of the Sandia Mountains in New Mexico, where structural and stratigraphic controls produce hydrologic discontinuities and aquifer compartmentalization. The regional distribution of geochemical parameters such as radioisotopic dating, stable isotope analyses, major ion analyses, ground-water temperature, and dissolved oxygen concentration, differs significantly from the distribution predicted by a standard basin model and illustrates the heterogeneity and complexity of ground-water flow in the study area.

Local scale analysis of the geochemical results from ground-water, surface-water, and precipitation sampling permits the identification of recharge areas, discharge areas, preferential ground-water flow pathways, and barriers to ground-water flow. Comparison of stable isotope analyses on ground water and precipitation suggests that most ground water is recharged in the Sandia Mountains by infiltration of precipitation and runoff that is produced by winter-type storms originating over the northern Pacific Ocean. The Madera Limestone that caps the Sandia Mountains produces ground water that is typical of recharge areas and has a low temperature, low TDS concentration, and high dissolved oxygen concentration (Madera-type water). Madera-type water is also produced by isolated Mesozoic aquifers between the mountains and the Albuquerque Basin, and downgradient of basin-bounding faults, suggesting that some faulted and compartmentalized aquifers have a good hydraulic connection to the Madera Limestone, and also that local infiltration of surface water is a significant source of recharge to the basin-fill aquifer. An evaporation-altered stable isotope composition and a high tritium concentration in Madera-type ground water near Las Huertas Creek and other arroyos suggest that ground water from the mountains is redistributed across the study area, and to the Albuquerque Basin, by ephemeral arroyos and Las Huertas Creek, and that infiltration from Las Huertas Creek is the single most important source of ground-water recharge within the study area. Mesozoic aquifers between the Sandia Mountains and the Albuquerque Basin generally produce ground water with higher temperatures, higher TDS concentrations, and higher dissolved oxygen concentrations than the Madera Formation, suggesting that ground-water flow from the Sandia Mountains to the Albuquerque Basin is generally blocked by basin-margin faults and by tilted and rotated fault blocks that orient the bedding planes of sedimentary units normal to ground-water flow. Several instances of Madera-type water produced by Mesozoic aquifers suggest that ground-water flow across basin margin faults is permitted where permeable sandstone formations are in fault contact with the Madera Limestone and at the highly faulted junction of the Placitas fault zone and the San Francisco fault . Anomalous ground-water ages and temperatures, stable isotope compositions, and dissolved oxygen concentrations along the San Francisco fault suggest that this fault, and other faults in the Madera Limestone, may act as discrete ground-water flow paths.

The results of this thesis illustrate that geochemical techniques can be a valuable primary tool for characterizing ground-water flow through geochemically complex mountain front aquifers. Measurements of the stable isotope and major ion composition, temperature, and dissolved oxygen concentrations were the most useful parameters measured during this study, and prior knowledge of the geology was critical to the hydrogeologic investigation.

PROBABILISTIC SEISMIC HAZARD IN NEW MEXICO AND BORDERING AREAS, by *Kuo-wan Lin*, 1999, PhD dissertation, Department of Earth and Environmental Science, New Mexico Institute of Mining and Technology, Socorro, NM 87801, 194 pp.

Presented in this dissertation is a catalog of magnitude 2.0 or greater earthquakes for New Mexico and bordering areas for the time period 1962–1998. This catalog contains 925 events (215 inside the Socorro Seismic Anomaly [SSA]) and covers the region longitude 101° west to 111° west and latitude 31° north to 38° north. Significant contributions to this catalog came from Los Alamos National Laboratory, U.S. Geological Survey, University of Texas at El Paso, University of Texas at Austin, and Texas Tech University. The unique features of this catalog include reassignment of magnitudes using a duration scale tailored to the region, and relocation of epicenters using the SEISMOS program. A major factor in improving locations was the development of an innovative subroutine that calculates a reliable first estimate of the epicenter for input into the SEISMOS program. The subroutine is based on a modified G matrix and fuzzy logic. Inclusion of it in the location process avoids problems encountered when using data from small aperture networks or when confronted with earthquake phase readings containing large errors, both rather frequent occurrences with the catalog events.

Probabilistic seismic hazards for the region based on the catalog are presented in maps of 10% and 2% probability of exceedance in a 50-yr period. The hazard maps show moderate to low seismic hazards for the region, with the highest level of ground acceleration, ~ 0.18g, inside the SSA (10% probability of exceedance in a 50-yr period). Along the major population corridor of the state from Albuquerque to Santa Fe, the peak ground acceleration is ~ 0.08g, which generates Modified Mercalli Intensity (MMI) VI effects. The magnitude contribution curves for selected areas show that earthquakes with magnitude 4.5–5.5 contribute the most to seismic hazards. Structural damage is not expected to modern buildings from earthquakes in this strength range but non-structural damage can be significant.

Sensitivity studies for the probabilistic seismic hazard analyses indicate that the hazard estimates for New Mexico are stable. Among controlling factors, the maximum likelihood slope B in the recurrence model is the most important factor for estimating rates for earthquakes in the magnitude range 4.0–6.5. A recurrence relationship based on preinstrumental data 1868–1961 for the SSA is in reasonably good agreement with the rate based on instrumental data 1962–1998. The recurrence rates based on active faults in the Rio Grande rift and the SSA suggest that the active faults in these regions do not significantly affect hazard estimates for a short return interval of 500 yrs.

TRANSPARENCY AND MICROTHERMOMETRY OF PYRITE-HOSTED FLUID INCLUSIONS, by *Shannon E. Logan* (nee *Lindaas*), 1999, MS thesis, Department of Earth and Environmental Science, New Mexico Institute of Mining and Technology, Socorro, NM 87801, 55 pp.

Pyrite, a common gangue mineral, is often associated with ore minerals within sulfide ore deposits. In the past, fluid inclusion microthermometry has been limited to transparent minerals. Unlike most transparent gangue minerals, pyrite is a sulfide, and as such, it may give a closer approximation than quartz, calcite, or fluorite to physical conditions at the time of ore deposition. Analysis of opaque minerals, such as pyrite, using a near-infrared camera, can broaden the sample base when applying microthermometry to the study of ore genesis.

Ninety-three doubly polished pyrite thick sections were made from 35 deposits worldwide. Pyrite transparency was quantified and intramineral features were identified using a near-infrared camera and microscope. Microthermometric analyses were made on 55 fluid inclusions within the pyrite sections.

Pyrite transparency is dependent on the formation environment and careful sample preparation. Pyrite-hosted fluid inclusions and available microthermometric measurements are scarce; of the 55 fluid inclusions found, 24 yielded salinity measurements, and 10 yielded homogenization temperatures. Microthermometric analysis on pyrite-hosted fluid inclusions is possible; however, workable fluid inclusions are limited to specific depositional environments.

AN ATTEMPT TO DATE FLUID INCLUSIONS IN QUARTZ: IMPLICATIONS FOR THE ^{40}AR/^{39}AR METHOD, by *Sarah A. W. Lundberg*, 1999, MS thesis, Department of Earth and Environmental Science, New Mexico Institute of Mining and Technology, Socorro, NM 87801, 212 pp.

The primary aim of this work was to investigate the possibility of dating fluid inclusions in quartz veins from the Capitan pluton, south-central New Mexico with the ^{40}Ar/^{39}Ar method. Because quartz is such an abundant vein mineral, the ability to use the ^{40}Ar/^{39}Ar method to date quartz would allow a wide range of ore deposit systems to be dated. Vein quartz from Capitan is considered to be deposited from primary magmatic waters and is cogenetic with vein adularia, which provides a tight constraint on the age of the quartz veins. The fluid inclusion populations are exceptionally well characterized. The inclusions have been shown to be remarkably abundant, highly saline, and relatively large. Samples of different grain sizes from several prospect pits were analyzed using furnace, laser, and in vacuo crushing as argon extraction methods. ^{40}Ar/^{39}Ar age spectra from vein adularia show argon loss profiles. The plateau ages obtained from the adularia range from 25.80 ± 0.22 to 31.60 ± 2.00 Ma, which agree well with the known age of the pluton. Ages determined from ^{40}Ar/^{39}Ar analysis of quartz exhibit a wide range of behavior. In addition to anomalous old ages typical of samples containing excess ^{40}Ar (^{40}Ar$_E$), anomalously young ages were observed in seven samples. The young ages were measured at the high temperature degassing steps, which implies they are a result of material contained within the quartz, rather than some form of contamination. In vacuo crushing of the quartz released up to 83% of the ^{39}Ar. A substantial part of the ^{40}Ar$_E$ was removed, but some remained in the samples after crushing. The remaining ^{40}Ar$_E$ in the samples, measured by post in vacuo crush step-heating, resulted in ages older than the emplacement age of the pluton. The ^{40}Ar$_E$ appears to be distributed throughout the quartz, not associated with one phase in particular, and was very difficult to quantify. As a result of the distribution of the ^{40}Ar$_E$, the quartz yielded relatively high precision plateau ages in the high temperature steps, which are as old as 81.7 ± 4.1 Ma. The Cl/K ratios measured during ^{40}Ar/^{39}Ar analysis are remarkably homogeneous and agree well with the results from the crush-leach analysis, obtained for the vein quartz (Campbell et al., 1995), which implies that the bulk quartz, as opposed to sylvite or feldspar, is being measured during ^{40}Ar/^{39}Ar analysis. Quartz was thought to be a neutral substrate, which would not contribute to the argon budget of the inclusions. This was not the case. The quartz was found to be heterogeneous on the micron level, containing many small solid inclusions of salts and other K-bearing phases. Complexity of K and Ar distribution in the quartz prohibits reliable dating of the fluid inclusions in Capitan quartz.

ELECTROKINETIC ION TRANSPORT THROUGH UNSATURATED SOILS: THEORY AND APPLICATION, by *Earl D. Mattson*, 1999, PhD dissertation, Department of Earth and Environmental Science, New Mexico Institute of Mining and Technology, Socorro, NM 87801, 305 pp.

Previous studies of electrokinetic ion and water transport have generally disregarded its application to remediation of unsaturated soils due to a lack of theoretical understanding, numerical predictive capabilities, and suitable electrodes. The research focus of this dissertation is on the electromigration of ions in unsaturated soils. Electrokinetic transport theory, three-dimensional numerical model development, comparison of model predictions to experimental results, and a surfactant-coating procedure for the anode electrode casings are all described in the dissertation.

An electromigration transport model was developed based on a modified Nernst-Planck equation describing the electromigration and diffusive flux of ions in a porous medium and on the equation of continuity. A steady-state electric potential field was assumed, an assumption valid for highly buffered soils or when the electrode electrolysis reactions are neutralized. The model also assumed that advective water movement through the soil due to either electric or hydraulic potentials was negligible. The transport and continuity equations were implemented in the model using public domain ground-water flow (MODFLOW) and transport (MT3D) numerical codes that were modified to allow prediction of ion transport due to an electric potential field.

Effective ionic mobility and diffusion parameters for porous media were calculated using a tortuosity function based on a closed-form solution of an equation describing electrical conductivity dependence on moisture content. The effect of ionic strength on ionic mobility was estimated using the activity coefficient calculated by the Davies equation.

One-dimensional laboratory experiments that measured anionic dye electromigration rates as a function of moisture content were used to verify the model. Laboratory experiments were conducted using a 10-mA, constant-current condition. Predicted red dye No. 40 migration rates matched the experimental data very well. Both the numerical simulations and the experimental results showed a maximum electromigration velocity at moisture contents less than satura-

tion. This maximum is believed to be due to competing effects between current density and tortuosity.

A six-month field demonstration was conducted to examine ion electromigration through heterogeneous unsaturated sandy soils. Acetate electromigration transport in the field demonstration indicated preferential transport through soil layers exhibiting higher moisture content and electrical conductivity.

Modeling was used to assess the effects of spatial heterogeneities on electromigration transport at the field-scale. The measured soil properties of the field demonstration were conceptualized as a layered system or as a homogeneous system. The layered model had three layers where each layer was assigned a moisture content and electrical conductivity value. The homogeneous model represented a single homogeneous profile with average properties of the layered model. Numerical results from these models suggest that spatial heterogeneities in soil properties must be accounted for in order to predict electromigration transport in a heterogeneous soil profile. The numerical predictions of the layered model qualitatively matched observations from the field experiments.

A surfactant-coating procedure for ceramic electrode casings was developed that eliminates excess electro-osmotic flow from the anode into unsaturated soils. Anode porous ceramic casings were treated with hexadecyltrimethylammonium at concentrations above the critical micelle concentration. Laboratory experimental results suggested the surfactant coating formed a bilayer on the ceramic surface, reversed the zeta potential and, hence, the electro-osmotic flow direction within the treated-ceramic pores. A six-month field demonstration confirmed the stability and effectiveness of the surfactant treatment on the porous ceramic.

The results of this dissertation illustrate the importance of moisture content and its relationship to electrical conductivity on electromigration transport, and the importance of including spatial heterogeneity in electrokinetic transport models. The steady-state electric potential field assumption allowed soil spatial variability effects on electromigration to be incorporated in a three-dimensional transport model. Electrokinetic transport models assuming homogeneous soil parameters will not adequately predict ion transport pathways at the field-scale in heterogeneous soil profiles.

GEOLOGY AND GEOCHEMISTRY OF WASTE ROCK PILES IN THE HILLSBORO MINING DISTRICT, SIERRA COUNTY, NEW MEXICO, by *Erik A. Munroe*, 1999, MS thesis, Department of Earth and Environmental Science, New Mexico Institute of Mining and Technology, Socorro, NM 87801, 144 pp.

In New Mexico, there are more than 100,000 abandoned mine waste rock piles with variable mineralogical and geochemical compositions. To better understand the environmental consequences of metal mobility in regions of minimal precipitation, a mineralogical and geochemical study was implemented for four mine waste rock piles and their drainage systems in the Hillsboro mining district.

A sampling strategy was developed to geochemically characterize four mine waste rock piles representing four different mineral deposits: a placer gold waste rock pile (Site A), a Laramide polymetallic vein waste rock pile (Site B), a carbonate-hosted Pb–Zn waste rock pile (Site C), and a carbonate-hosted Ag–Mn waste rock pile (Site D). In addition, another Laramide polymetallic vein waste rock pile (Site E) was studied to compare physical and chemical characteristics specifically with Site B. To determine the appropriate grain size range to be sampled, six grain size fraction ranges (2–1 mm, 1–0.5 mm, 0.5–0.25 mm, 0.25–0.125 mm, 0.125–0.063 mm, and <0.063 mm) were analyzed by FAAS and XRF. The <0.25 mm grain size fraction (encompassing the three smaller grain size fraction ranges) was used to sample the mine waste rock piles because it was determined to typically contain the highest metal concentrations. Using grid patterns unique to each of the waste rock piles, three homogenized samples were obtained using sampling densities of 15, 30, and 45 sample cells. Chemical analyses by FAAS and XRF determined that these mine waste rock piles can be adequately geochemically characterized by homogenizing samples collected from a grid pattern containing 15–30 samples.

An examination of metal mobility from the waste rock piles indicates that metals are moving as mineral grains, suspended material, and dissolved material. Chemical metal mobility is higher in the Laramide polymetallic vein waste rock piles (Site B and Site E) than in the carbonate-hosted waste rock piles (Site C and Site D). This may be a result of pyrite-bearing waste rock piles (Site B and Site E) generating sulfuric acid that can increase metal availability to the environment. Site C and Site D, however, have less chemical movement due to the abundance of calcite. Physical movement of material from these sites is the primary cause for the metals in downgradient stream sediments.

Secondary mineral rinds play a major role in the release of metals to the environment. Iron sulfate, iron oxide, and iron oxyhydroxide form rinds on the chalcopyrite and pyrite. Pyrite oxidation rinds preferentially partition arsenic. Oxidation rind thickness varies depending on mineralogy, mineral residence time in the waste rock pile, and hydrothermal history associated with the different deposits. Strong precipitation events may flush out metals partitioned in the outer rinds of oxidized sulfide grains. However, hydrothermal oxidation of some mineral grains like galena may be "armored" by cerussite. This leads to a significant decrease in the lead concentration available for chemical transport in the environment. Dissolved material may precipitate soluble salts onto grains in waste rock piles and stream sediments.

Agitation tests indicate copper and zinc are preferentially partitioned in the suspended material during a simulated precipitation event. Primary clays present in the stream sediments were smectite, illite, and illite/smectite mixed-layer clays. Metal movement in a semi-arid environment is governed by local drainage characteristics, mineralogy, and grain size.

CHARACTERIZATION OF VADOSE ZONE IN-SITU MOISTURE CONTENT AND AN ADVANCING WETTING FRONT USING CROSS-BOREHOLE GROUND PENETRATING RADAR, by *Lee T. Paprocki*, 2000, MS thesis, Department of Earth and Environmental Science, New Mexico Institute of Mining and Technology, Socorro, NM 87801, 120 pp.

The need for effective methods of containing and remediating contamination has become increasingly important as our reliance on ground water for drinking water and the occurrence of contaminated vadose zone sites has increased. Flow and transport within the vadose zone is dependent upon the in-situ moisture-content distribution, which is often inadequately characterized by sparse hydrological measurements. Cross-borehole ground penetrating radar (GPR) is a high resolution, rapid-acquisition geophysical method that can obtain detailed measurements of the subsurface. Ground penetrating radar estimates the velocity of the electromagnetic (EM) waves in the subsurface. This velocity can be converted to an image of moisture content because it depends primarily upon the moisture content (Topp et al., 1980).

At a vadose zone field site the feasibility of using cross-borehole GPR to image the two-dimensional in-situ moisture-content distribution was tested. Then, during an infiltration experiment, cross-borehole GPR was tested to see if it could accurately image the advancing wetting front. GPR measurements were taken along an 11-m profile, consisting of five boreholes, with a 3- by 3-m infiltrometer in the center that emitted water at a rate of 2.7 cm / d. Two-dimensional GPR moisture-content images were produced for preinfiltration and infiltration conditions. The GPR images were compared to neutron moisture-content measurements and to two stratigraphic columns. The neutron measurements were collected in the same five boreholes, and the stratigraphic columns were constructed from continuous core samples taken several meters from the boreholes.

Overall, the GPR two-dimensional in-situ moisture-content distribution image correlated well with the neutron-probe and the stratigraphic-column data. By taking multiple data sets, one is able to quantify the GPR repeatability error. The average traveltime error was 1.08 ns, which in a general sense translated to an average moisture-content error of ±2%. Both errors were calculated by taking two standard deviations. The overall error was highest in areas of high moisture content and low ray density. Results indicate that the GPR moisture-content figures represent a smoothly varying image that maintains the general trend of the moisture-content distribution as compared to the neutron-probe and stratigraphic-column data. Equipment failures led to inaccurate estimation of moisture content in at least two data sets. However, this study showed that cross-borehole GPR can be an effective and feasible technique for characterizing the vadose zone.

SEQUENCE STRATIGRAPHY AND SEISMIC-GUIDED ESTIMATION OF LOG PROPERTIES OF THE SECOND SAND MEMBER OF THE BONE SPRING FORMATION, DELAWARE BASIN, NEW MEXICO, by *Robin A. Pearson*, 1999 MS thesis,, Department of Earth and Environmental Science, New Mexico Institute of Mining and Technology, Socorro, NM, 124 pp.

Seismic attributes have the potential to significantly improve reservoir property predictions in interwell areas if care is taken to ensure that the results are geologically and geophysically reasonable as well as statistically significant. This study illustrates how an integrated, volume-based attribute analysis can be used to determine reservoir properties and evaluate infill drilling targets via a case study of an oil and gas field producing from the Second Sand Member of the Bone Spring Formation along the north-

ern slope of the Delaware Basin, New Mexico. The Second Sand is a stratigraphically complex submarine fan deposit, and more traditional horizon- and interval-based attribute analysis techniques have been unable to predict porosity with the desired accuracy.

Based on an integrated analysis of well logs, cores, and 3-D seismic data, a combination of high frequency sea-level changes, variations in sediment supply, and tectonic activity have resulted in a submarine fan deposit that is largely confined to a small intraslope basin and that can be subdivided into a basin-floor fan, a slope fan, and a modified lowstand wedge. The best reservoir quality is found in the slope fan. The porosity distribution was successfully predicted using a combination of five seismic attributes. Although the predicted porosity distribution is complex, it appears to be geologically reasonable with high porosities (>10%) tending to occur in what is believed to be a channel fairway, and zones of extremely low porosity being associated with faults. Three potential drilling targets were identified within the slope fan and were assigned risk factors based on the geologic setting, production history, and statistical significance. These results have implications for the way in which other attribute studies are done and for Bone Spring exploration elsewhere.

PETROGRAPHY, DIAGENESIS AND RESERVOIR QUALITY OF THE UPPER SPRABERRY FORMATION, TEXAS, by *Claudio J. Saleta*, 1999, MS thesis, Department of Earth and Environmental Science, New Mexico Institute of Mining and Technology, Socorro, NM 87801, 196 pp.

The Spraberry Formation is part of the submarine fan and deep marine deposits of the Midland Basin. The unit consists of very fine grained sandstones, siltstones, shales, and carbonate mudstones. These rocks show different degrees of lamination, bioturbation, convolute bedding, and a complex mineralogy.

The Spraberry reservoirs are naturally fractured, with very low matrix permeability that ranges from 0.1 to 1.0 md. Most of the reservoir fluid conductivity is due to the presence of a broad fracture system, wherein hydrocarbons stored in the pore space of the rock matrix flow at very low rates. The rock framework directly influences permeablilty, capillary pressure, and wettability characteristics of the reservoirs. For this reason, the interaction between rock matrix, natural fractures, and fluid flow must be well understood.

Small-scale lithofacies from thin-section and core-plug petrophysics were described for core intervals analyzed in the upper Spraberry Formation. The analysis of these lithofacies included observation of their petrographic properties as well as results from fluid-flow experiments for each lithofacies type. The Spraberry Formation contains two clean and porous sandstone lithofacies, one carbonate mudstone, and one dolomitic-cemented siltstone; two clay-rich lithofacies were also found using thin-section analysis. Among all lithofacies present, the clean and porous sandstones show good reservoir quality, whereas other lithofacies exhibit poor or total lack of porosity and permeability. The main diagenetic processes affecting the unit are as follows: quartz cementation, clay precipitation, carbonate cementation, grain and cement dissolution, and fracture formation and mineralization.

Rock properties vary gradually from reservoir rocks to non-reservoir rocks following two main trends: (1) increasing organic and argillaceous content with decreasing porosity, and (2) increasing carbonate sediments and cements with decreasing porosity. Both trends show a strong relationship to grain density, which in turn, suggests that lithological variability is an important control on reservoir properties. Water and oil saturation is also strongly controlled by lithofacies variability rather than a single water/oil contact controlled by gravity forces. The fluid distribution is probably mainly controlled by pore-throat diameter, pore-throat distribution, pore morphology, capillary pressures, and wetting behavior of the rock fluid system. In general, it is observed that the very small sizes of pores and pore throats make capillary forces strong enough to hold fluids tightly to the pore system. Thus, gravity forces are less dominant in controlling the distribution of fluid saturation. Core-plug fluid-flow data suggest that fluid distribution is controlled by the wetting behavior of the different minerals that form each lithofacies along the stratigraphic sequence. Fine-grained lithofacies such as dolostones and argillaceous siltstones show high percentages of water saturation, whereas low water saturation is associated with clean, very fine sandstones and siltstones richer in hydrocarbons.

A PORE-SCALE EXPERIMENT TO EVALUATE ENHANCED VAPOR DIFFUSION IN POROUS MEDIA, by *Thomas S. Silverman*, 1999, MS thesis, Department of Earth and Environmental Science, New Mexico Institute of Mining and Technology, Socorro, NM 87801, 117 pp.

A pore-scale experiment was performed to determine whether the rate of water vapor diffusion through a pore throat is enhanced by the presence of liquid trapped in the pore throat. The experiment demonstrated that enhanced vapor diffusion (EVD), first presented by Philip and de Vries (1957), exists on a pore scale and does not require a thermal gradient. A diffusion cell with two vapor reservoirs bridged by a single "pore throat" was used to test EVD. Using a brine-concentration-induced vapor pressure gradient, we demonstrate that the rate of water vapor transport through a liquid-filled pore throat is enhanced relative to the flux through a gas-filled pore throat. The enhancement is shown to be a quadratic function of liquid-island length. An ancillary experiment with two parallel pore throats showed that water vapor is transported simultaneously through both gas- and liquid-filled pore throats if both are available. The vapor flux through each pore in the dual-pore-throat diffusion cell is inversely proportional to the resistance of the gas- or liquid-filled pore throat. Lastly, an isotopic tracer test was performed to compare the rates of deuterium transfer through gas- or liquid-filled pore throats. The rate of deuterium transfer to the downgradient reservoir is faster in the presence of a liquid-filled pore throat despite the slower self-diffusion coefficient of deuterium through liquid than through gas.

LABORATORY INVESTIGATION OF PERMEABILITY UPSCALING, by *Vincent C. Tidwell*, 1999, PhD dissertation, Department of Earth and Environmental Science, New Mexico Institute of Mining and Technology, Socorro, NM 87801, 224 pp.

Parameterization of flow and transport models is often complicated by the inability to make measurements at the desired scale of analysis. This disparity in scale necessitates the use of some averaging or upscaling model to compute the effective media properties from the measured data. Although numerous theoretical models have been proposed, physical data with which to test these upscaling models are sparse and limited in scope. Here, we develop and employ a novel minipermeameter test system, which we call the Multi-Support Permeameter (MSP), to physically investigate permeability upscaling. The MSP allows precise, rapid, nondestructive measurement of permeability over a range of different sample supports (i.e., sample volumes). Measurements are made over different sample supports, subject to consistent boundary conditions and flow geometries, by simply varying the size of the minipermeameter tip seal. Experiments progress by collecting thousands of measurements from each face of meter-scale blocks of rock with each of five different tip seals (0.15, 0.31, 0.63, 1.27, and 2.54 cm radius), plus a single large (7.62 cm) tip seal designed to integrate over the entire sampling domain. Upscaling is manifest in the acquired data by changes in key permeability statistics with increasing sample support.

Permeability upscaling experiments are conducted on four blocks of rock, each exhibiting differing physical attributes: (1) Berea Sandstone, a faintly laminated fluvial-deltaic sandstone, (2) Massillon Sandstone, a conspicuously cross-stratified sandstone from a high-energy fluvial or near-shore environment, (3) Topopah Spring Tuff, a densely-welded, devitrified tuff, and (4) Tiva Canyon Tuff, a poorly welded tuff. Over 150,000 permeability measurements corresponding to six different sample supports have been collected from these four rock samples.

By comparing and contrasting results, we explore how traits distinguishing each rock sample influence the statistical and upscaling characteristics of the permeability. Results indicate that differences in the physical attributes of each rock sample give rise to measurable differences in the spatial permeability patterns, permeability distributions, and semivariograms. Results also yield clear evidence of permeability upscaling for each rock sample and each statistic investigated. Specifically, as the sample support increases the sample variance always decreases according to a power-law relation, the semivariogram range increases linearly, while small-scale (i.e., smaller than the minipermeameter tip seal) structural features are sequentially filtered from the permeability maps and semivariograms. Although each of the samples exhibits qualitatively similar upscaling trends, distinct differences are also evident. Differences between samples are manifest in the rate at which a given statistic upscales, the absolute change in the value of the statistic, and in the sense (i.e., increasing versus decreasing) of the mean upscaling. These differences are most evident between samples of differing genetic origin (e.g., sandstones versus tuffs).

To aid in the interpretation of the permeability upscaling, comparisons are made with a series of published theoretical models. The selected models differ according to the assumptions made about the nature of the permeability distribution, spatial structure, and uniformity/non-uniformity of the imposed flow field. Results suggest that the differences in the upscaling exhibited by the four rock samples

can be explained on the basis of the spatial patterns distinguishing each, particularly the spatial correlation of the higher permeability fraction. We also find the permeability upscaling to be strongly influenced by the non-uniform flow conditions imposed by the minipermeameter measurements. As such, these data clearly demonstrate that permeability upscaling is not an intrinsic property of a porous medium but rather depends on the characteristics of its measurement. In an effort to empirically quantify the measurement characteristics of the MSP, spatial weighting functions are calculated from the multi-support permeability data via linear filter theory.

ATR-FTIR ANALYSIS OF ADSORPTION FROM CRUDE OIL COMPONENTS ONTO MINERAL SURFACES, by *Susan M. Von Drasek*, 1999, MS thesis, Department of Earth and Environmental Science, New Mexico Institute of Mining and Technology, Socorro, NM 87801, 208 pp.

Rock-fluid interactions, or wettability, influence both the rate and amount of oil produced by the displacement of oil by water in a conventional waterflood. Although most reservoir minerals are intrinsically water-wet, their wetting properties can be altered by complex interactions among crude oil components, brine, and reservoir minerals.

Most studies of crude oil/brine/rock (COBR) interactions have relied upon measurements that quantify the end result of exposure of high-energy surfaces to brine and oil including measurements of contact angles on smooth mineral surfaces and imbibition phenomena in porous media. Less work has focused on chemical analysis of the adsorbing species because of the difficulties posed by complex mixtures of organic compounds and small amounts of material. Reducing complexity by eliminating water or substituting model organic compounds for crude oils has failed to reproduce wettability conditions that represent those that result from COBR interactions.

Acidic and/or basic species in crude oils are expected to display the greatest tendency to interact with mineral surfaces and alter wetting. In this work, the use of an ATR-FTIR technique has been evaluated, as a potential tool, for quantifying the adsorption of species with polar functional substituents from the oil onto mineral surfaces.

Six crude oils with varying chemical properties, including a wide range of acid and base numbers, were analyzed by ATR-FTIR using a ZnSe prism. Oil selection was guided by the results of earlier studies that used traditional methods to assess their wettability-altering potential. Oil spectra by the ATR technique adequately reproduced those obtained with standard sample preparation methods, although absorbance levels were weaker. Spectra of all the oils were dominated by C–H stretching and bending of aliphatic groups with only minor differences between oils.

ATR-FTIR confirmed adsorption of organic material on mica and clay surfaces exposed first to brine, then to oil. Evidence of enrichment in aromatic or polar material was impossible to discern, however, due to the strong substrate signal in regions of particular interest and to the relatively weaker signal from the adsorbed organic material. The technique does provide significant insight into the fate of water that is present on the surfaces before exposure to oil that may prove useful in understanding the mechanisms of COBR interactions.

ARSENIC GEOCHEMISTRY OF STREAM SEDIMENTS ASSOCIATED WITH GEOTHERMAL WATERS AT LA PRIMAVERA GEOTHERMAL FIELD, MEXICO, by *David Welch*, 1999, MS thesis, Department of Earth and Environmental Science, New Mexico Institute of Mining and Technology, Socorro, NM 87801, 91 pp.

The purpose of this study is to determine factors controlling the mobility of arsenic under natural conditions and is part of a reconnaissance study on arsenic speciation of geothermally impacted stream waters. Stream sediments and algae were collected at 20 sample locations along the Rio Salado watershed and its tributaries at La Primavera geothermal field near Guadalajara, Mexico. Sediments were analyzed by several partial extractions to determine: (1) the amount of arsenic available to the environment and its partitioning into different size fractions, (2) the species of arsenic present in sediments, (3) the sedimentary phases that are associated with arsenic, and (4) the relationship between arsenic sediment chemistry and water chemistry. In addition, Rio Grande sediments, collected near Socorro, New Mexico, were analyzed for As, Mn, Fe, and percent total organic carbon (%TOC) for comparison with La Primavera sediments. In carrying out these objectives, a modified method of ion-exchange chromatography is used for speciation of As(III), As(V), monomethylarsonate (MMA), and dimethylarsinate (DMA) in sediment extracts.

Total arsenic in sediments available to the environment ranges between 3 and 16 ppm and is highest in the silt-clay fraction. Arsenic is present primarily as inorganic forms that account for over 90% of the total; MMA and DMA are detectable in small amounts. Algae from La Primavera contains between 18 and 68 ppm arsenic (dry weight) with similar proportions of inorganic and organic forms.

The primary sedimentary phases that are associated with arsenic and control its mobility are oxides and hydroxides of iron and manganese and organic carbon. Arsenic concentration is positively correlated with manganese and %TOC and shows no direct correlation with Fe; however, evidence suggests that iron oxides are also enriched in arsenic. The positive correlation between arsenic and %TOC suggests that plants and algae may represent a significant sink in some natural settings.

Sediment arsenic concentrations showed no correlation with surface water concentrations. Though sediment-water heterogeneity may account for this lack of correlation, evidence indicates that sediment arsenic concentrations are determined by the amount of organic matter, iron and manganese oxides and hydroxides present, not the concentration of arsenic in surface waters.

Comparison of sediment-water data from the Rio Grande to that of La Primavera showed arsenic to be more mobile in La Primavera waters with relatively less being retained in the sediments. This is most likely due to lower concentrations of iron, occurring as iron oxides and hydroxides in La Primavera sediments, but could also occur if the capacity of the sediments to take up arsenic has been exceeded.

SOLUTE MIXING IN A FRACTURE JUNCTION UNDER EQUAL AND UNEQUAL FLOW CONDITIONS, by *J Sidney Wise*, 1999, MS thesis, Department of Earth and Environmental Science, New Mexico Institute of Mining and Technology, Socorro, NM 87801, 84 pp.

I conducted a series of experiments using a physical model of a fracture junction with simple geometry. The flow conditions in the experiments included equal flow, where the flow rates in all four fracture branches were identical; unequal flow, where the flow rates in the two inflow fractures were different but the flow rates in adjacent inflow and outflow branches were identical; and forced mixing (a type of unequal flow), where water from one of the inflow branches crossed to the opposite side of the junction and mixed with water from the other inflow branch. Forced mixing occurred because the flow rate in one inflow branch was greater than the flow rate in the adjacent outflow branch, resulting in overflow to the opposite outflow branch. The goal of the experiments was to determine how the mixing behavior of a solute would be affected by the Peclet number at the junction in each of these flow conditions.

In the case of equal flow, the present work verifies the findings of Li (1995), showing that partial mixing occurs at Peclet numbers between approximately 1 and 200. Complete mixing occurs below this range, and streamline routing occurs above this range. Photomicrographs of the equal flow case illustrate the three types of mixing behavior and show that upstream diffusion occurs at low Peclet numbers. In the case of unequal flow without forced mixing, where the water from each inflow branch exits through the adjacent outflow branch, the transition between mixing states occurs at a lower range of Peclet numbers than in equal-flow conditions, so that complete mixing was not observed at a Peclet number of 1. In the case of forced mixing, the transition occurs at still lower Peclet numbers, too low to be observed in the present work.

WHOLE-ROCK OXYGEN ISOTOPE TRAVERSES ACROSS GOLD-BEARING AND BARREN STRUCTURES, LONE TREE COMPLEX, NEVADA, by *Christopher M. Young*, 1999, MS thesis, Department of Earth and Environmental Science, New Mexico Institute of Mining and Technology, Socorro, NM 87801, 104 pp.

The Lone Tree Complex includes the Lone Tree, North Peak, and Trenton Canyon deposits. These fine-grained gold deposits, hosted in Paleozoic sediments, are variations of Carlin-type deposits with ore zones being structurally controlled. Both gold-bearing and barren structures have hydrothermal alteration centered along faults that is indicated by an increase in modal percent of alteration minerals towards the structure. The alteration mineral assemblage is dominated by quartz, fine-grained white-phyllosilicates (sericite), oxidized sulfide (mainly pyrite), and locally, clays and chlorite.

Whole-rock oxygen isotope traverses across gold-bearing and barren structures record isotopic alteration resulting from deposition of alteration minerals and water-rock exchange. On a district-scale, oxygen isotopes are inconclusive at detecting ore zones. All gold-bearing traverses have depletions at the fault zone relative to background values, whereas barren traverses produced either an enrichment (North Peak) and a depletion (Lone Tree) at the fault zone. On a deposit-scale, correlation of oxygen

isotope composition and ore zones can be made. Gold-bearing structures are associated with more oxygen isotope alteration (change relative to background values) than the barren structures. At Lone Tree, North Peak, and Trenton Canyon gold-bearing quartz was isotopically lighter than the barren quartz, respectively, by 8.8 ‰, 4.1 ‰, and 9.9 ‰.

Calculated oxygen isotope composition and fluid inclusion data indicate multiple sources of fluid for deposits of the Lone Tree Complex. A regional, barren formation water is documented by temperature and salinity measurements in inclusions and calculated oxygen isotope compositions from the three deposit areas. This formation water ranges in both salinity and oxygen isotope composition, respectively, from 3.0 to 18.0 eq. wt.% NaCl and from 8.5 to 13.1 ‰, and ranges in homogenization temperature from 170° to 310°C, with the upper range resulting from mixing with a higher temperature magmatic fluid at Lone Tree.

At Lone Tree, a magmatic source for gold-bearing fluid is suggested by the range in homogenization temperatures from 280° to 400°C and salinity from 12.0 to 39.0 eq. wt.% NaCl (Kamali, 1996). Calculated oxygen isotope composition of gold-bearing fluid (6.5%) supports this conclusion. Ranges in salinity and homogenization temperature for gold-bearing and barren sample suggest mixing between the gold-bearing and barren fluids. Trenton Canyon gold-bearing fluids had calculated $\delta^{18}O$ of 0.0 ‰, indicating an evolved meteoric fluid. This meteoric fluid, ranging in homogenization temperature from 210° to 350°C and salinity from 2.6 to 5.7 eq. wt.% NaCl, can be approximated by mixing the Lone Tree magmatic fluid and a local meteoric water (from -6.0 to -9.0 ‰) established at Twin Creeks and Getchell deposits (Groff, 1996). Further mixing of this fluid with the barren formation water lowers salinity and homogenization temperatures from values expected by a true meteoric-magmatic mixing trend. Gold-bearing fluid at North Peak had calculated $\delta^{18}O$ value of 8.5 ‰. Mixing between meteoric water and regional barren formation water produces the oxygen isotope composition, along with ranges in homogenization temperature (170°–270°C) and salinity (3.7–14.0 eq. wt.% NaCl). As with the Lone Tree and Trenton Canyon deposits, salinity and homogenization temperatures at North Peak from gold-bearing and barren samples indicate mixing between the barren and gold-bearing fluids.

New Mexico State University

CONGLOMERATIC DEPOSITION WITHIN THE CRETACEOUS CORDILLERAN FORELAND BASIN: REDDICK CANYON CONGLOMERATE OF CENTRAL UTAH, by *Jennifer M. Jones*, 1999, MS thesis, Department of Geological Sciences, New Mexico State University, Las Cruces, NM 88003, 91 pp.

The Cordilleran foreland basin formed in Aptian through Campanian time. Clastics deposited in the basin were sourced by erosion unroofing of the Sevier orogenic belt to the west. The Sevier orogenic belt includes folded synorogenic deposits that include the Indianola Group, of which the Reddick Canyon conglomerate is part. The Reddick Canyon conglomerate is composed dominantly of large cobble to boulder-size quartzite clasts.

The Reddick Canyon conglomerate is divided into three units, 1, 2, and 3, which are defined in the stratigraphic section studied. Unit 1 is interpreted to have been deposited in a fan-delta environment. Unit 2 developed on the proximal to upper mid-fan environment. Unit 3 contains deposits that are indicative of mid-fan to distal-fan environments.

Three major controls influenced deposition of the Reddick Canyon conglomerate. The first control was lithology of source bedrock. Widely exposed Precambrian and Cambrian quartzite strata provided large resistant clasts to the depositional site. These strata are presently exposed in the upper plate of the Canyon Range thrust currently located 40 km west of the Reddick Canyon conglomerate. The second control is the tectonic evolution of thrust belt. The clasts found in the Reddick Canyon conglomerate are very large, well rounded, and as much as 1 m in diameter suggesting that 40 km of transport is unlikely. Distance from the source, overall rounding of clasts, and clast size suggest repeated recycling of clasts from the thrust belt to the basin. It is therefore likely that other as yet unknown thrusts located between the Canyon Range and the Gunnison Plateau contributed to deposition of the Reddick Canyon conglomerate. The third control was the evolution of the foreland-basin system. Decreasing stratigraphic dips upsection in a single measured section in the northern part of the study area suggest that the Reddick Canyon conglomerate records foredeep disruption and subsequent deposition in a wedge-top depozone. Disruption had not yet begun in the southern part of the study area, because no significant change in stratigraphic dips is observed there. Thus, the southern part of the study area was located in the foredeep depozone throughout deposition of Reddick Canyon conglomerate.

PROVENANCE, GEOMETRY, LITHOFACIES, AND AGE OF THE UPPER CRETACEOUS WAHWEAP FORMATION, CORDILLERAN FORELAND BASIN, SOUTHERN UTAH, by *Stonnie L. Pollock*, 1999, MS thesis, Department of Geological Sciences, New Mexico State University, Las Cruces, NM 88003, 117 pp.

In the southern part of the Cordilleran foreland basin, Upper Cretaceous fluvial strata of the Wahweap Formation record three major river systems with different headwaters. Exposed along the flanks of the southern High Plateaus and Kaiparowits Plateau of southern Utah, the Wahweap Formation consists of four informal members. The lower and middle members were deposited by north- and northeast-flowing meandering and anastomosing rivers that transported feldspar-rich volcanic-lithic detritus from a basement source in the Mogollon highlands and a volcanic source from the Delfonte Volcanics in southeastern California. The upper member was deposited by northeast-flowing rivers that transported sedimentary lithic detritus from Paleozoic sedimentary rocks uplifted in the Sevier thrust belt in southern Nevada. The uppermost capping sandstone member was deposited by east- and southeast-flowing braided rivers that transported quartzose detritus derived from Paleozoic and Mesozoic sedimentary rocks of the Sevier orogenic belt. Although not directly dated, the Wahweap Formation overlies the Santonian Straight Cliffs Formation and underlies the middle-late Campanian Kaiparowits Formation.

The lower, middle, and upper members were deposited in an actively subsiding foredeep setting with abundant accommodation space. The capping sandstone member was deposited in wedge-top basins that were carried by eastward advancing thrust sheets of the Sevier thrust belt. Thickness trends of the Wahweap Formation and stratigraphically adjacent units indicate that the foreland basin was partitioned during or after Wahweap deposition. The capping sandstone member thins in a downdip direction from 150 m in the Henrieville Basin to 30 m in the Kaiparowits Basin. In the updip direction it is present locally as paleovalley deposits in the Paunsaugunt Basin beneath the Eocene Claron Formation west of the Paunsaugunt fault and thicker quartzose units in the Markagunt Basin. I infer that the Paunsaugunt fault, most recently with Neogene normal offset, and other associated Neogene and Laramide structures are inverted Campanian thrust faults. Uplift along thrust-tip anticlines resulted in the formation of wedge-top basins and concomitant erosion of and partitioning of the foreland basin.

DEPOSITIONAL FACIES ANALYSIS OF THE LATE PENNSYLVANIAN, LOWER HOLDER FORMATION PHYLLOID ALGAL MOUND COMPLEXES, SACRAMENTO MOUNTAINS, NEW MEXICO, by *Mark A. Rivera*, 1999, MS thesis, Department of Geological Sciences, New Mexico State University, Las Cruces, NM 88003, 143 pp.

This study has focused on the delineation of intramound sequence stratigraphy in order to understand vertical and lateral mound growth patterns. Because other phylloid algal mound complexes hold million to billion barrel fields within the mid continent and southwestern U.S. and the former U.S.S.R., it is important to understand how phylloid algal mound growth is affected by change in accommodation.

Fourteen lithofacies and 10 depositional sequences were recognized and correlated within the Upper Pennsylvanian lower Holder Formation phylloid algal bioherms of the Sacramento Mountains, New Mexico. These facies include mound core phylloid algal boundstones, mound flank skeletal wackestones and packstones, and off-mound conglomerate, sandstone, siltstone, shale, and algal-peloid-rich wackestone and packstone. Detailed sequence stratigraphic correlation of 10 depositional sequences within Yucca and Dry Canyons reveals that sequence thickness and vertical facies successions vary relative to biohermal buildups.

Variation in facies patterns, both laterally and vertically, has been attributed to the variable growth of mound core boundstones in response to generation and destruction of short-term accommodation space. Vertical relief of abnormal subaerial exposure surfaces developed on top of individual phylloid algal mounds indicates potential sea-level fluctuations of 54 m and possibly as high as 100 m. Furthermore, estimates of sequence durations for Late Pennsylvanian time suggest that these fluctuations occurred for a period of 400,000 yrs. Therefore, lower Holder bioherm complexes experienced changes in accommodation of at least 54 m that

were glacioeustatically controlled and short term.

Bioherm accretion varied as a function of both spatial (lateral) location relative to mound core buildups, and evolutionary (nucleation, acme, and mature phases) positions. Sequences accumulated during the nucleation stage of mound growth developed during late stages of falling sea level (LHST to VLHST) and display a "catch-down" character. Acme stage sequences developed during sea level rise (TST to EHST) and display a "keep-up" phase of deposition followed by a "catch-down" phase of deposition. Sequences developed during the acme evolutionary phase are characterized by (1) vertical aggradation of mound core boundstone, (2) abrupt vertical and lateral facies transitions ("Non-Waltherian"), and (3) significant syndepositional topography. Mature stage sequences grew atop significant bathymetric relief and are characterized by deposition of late highstand rise to early fall, "catch-down" sequences.

DEPOSITIONAL ENVIRONMENTS AND PROVENANCE OF THE CENOZOIC GILA CONGLOMERATE OF THE DUNCAN AND CANADOR PEAK QUADRANGLES, SOUTHWESTERN NEW MEXICO, by *Shane V. Smith*, 1999, MS thesis, Department of Geological Sciences, New Mexico State University, Las Cruces, NM 88003, 103 pp.

Lithofacies distribution, paleocurrent, and provenance data are used to define the evolution of the Cenozoic Gila Conglomerate in the Basin and Range tectonic province of the Duncan and Canador Peak quadrangles, southwestern New Mexico. Crustal extension in this part of the Basin and Range resulted in fault-block mountains and complementary basins filled with up to 315 m of conglomerate, sandstone, siltstone, and mudstone of the Gila Conglomerate. The Gila Conglomerate is divided into upper and lower stratigraphic units that are separated by an angular unconformity. The lower unit consists of strongly consolidated conglomerate, sandstone, and mudstone, and the upper unit consists of unconsolidated to poorly consolidated siltstone, mudstone, and sandstone with uncommon conglomerate. Three mappable members were identified in these two units including the Wilson Mine and Nichols Canyon members of the lower Gila Conglomerate and the Pearson Mesa member of the upper Gila Conglomerate.

The Gila Conglomerate of the Duncan and Canador Peak quadrangles shows a two-stage evolution. The initial stage was the deposition of the late Oligocene(?) to early Miocene Wilson Mine and Nichols Canyon members, which consist of 240 m of sediment deposited in distal alluvial-fan, alluvial-flat, and lacustrine environments. Clast composition and paleocurrent directions indicate a provenance for both members to the southeast in the southern Big Burro Mountains. This initial stage was followed by uplift and tilting of the strata of these two members. The second stage was the deposition of the Pliocene to Pleistocene(?) Pearson Mesa member, which consists of 75 m of alluvial-flat and distal to mid alluvial-fan lithofacies, in a northwest-trending, northeast-tilted, internally drained half graben. Clast composition and paleocurrent directions indicate a provenance for this member to the north in the Riley Peaks area. There is no evidence of an ancestral Gila River during the time of deposition of the Gila Conglomerate.

FIELD, PETROGRAPHIC, AND ISOTOPIC DISCRIMINATION OF SHALLOW, AUTHIGENIC CARBONATE OF THE PLIO–PLEISTOCENE PALOMAS BASIN OF SOUTHERN NEW MEXICO, by *Leandro Treviño, Jr.*, 1999, MS thesis, Department of Geological Sciences, New Mexico State University, Las Cruces, NM 88003, 78 pp.

In the Plio–Pleistocene Palomas half-graben of southern New Mexico, shallow authigenic carbonate is commonly found in both the footwall-derived and hanging wall-derived facies of the Palomas Basin. Site investigation and sample collection on a basin-wide scale has resulted in the identification of nine types of shallow, authigenic carbonate that can be classified into four categories. Pedogenic or soil carbonate is found on the hanging wall- and footwall-derived alluvial fans. Carbonate that precipitates at or near the water table consists of nodular mudstones found in the hanging wall-derived alluvial fan and the axial fluvial system; nodules and tubules in eolian sand and gully bed cementation are common to the hanging wall- and footwall-derived alluvial fan. Carbonate precipitating at or near the land surface produces groundwater carbonate with capillary fringe restricted to the hanging wall- and footwall-derived alluvial fans; thick shallow ground-water carbonate and calcareous root mats are found only in the hanging wall-derived alluvial fan. Concretions, found only in the axial fluvial system, and sparry cement, found in all environments within the basin, develop below the water table.

Subtle but discernible changes in the vertical fabric, presence or absence of peds, root traces, and bounding surfaces help differentiate among different forms of carbonate. In the case of non-pedogenic carbonates, the base of the indurated carbonate bedding is sharply defined and parallel to the overall bedding, resulting in a laterally extensive sheet-like deposit. In contrast, pedogenic carbonate exists as nodular or massive horizons with gradational bases. Unless eroded before burial, pedogenic carbonate is overlain by an argillic B horizon characterized petrographically by clay coatings (argillans) around grains and/or peds.

Stable carbon isotopes further differentiate carbonate in footwall-derived alluvial fan strata and associated axial-fluvial fan strata from that in hanging wall-derived strata. This is likely the result of vegetation differences or the presence of Paleozoic carbonate rocks in the catchment and as clasts in the footwall-derived detritus. Stable oxygen isotopes help differentiate among different forms of carbonate on the footwall fan.

STRATIGRAPHY, SEDIMENTOLOGY, AND PROVENANCE OF THE GILA CONGLOMERATE NEAR LAKE ROBERTS, NEW MEXICO, by *Gregory J. Wheeler*, 1999, MS thesis, Department of Geological Sciences, New Mexico State University, Las Cruces, NM 88003, 125 pp.

Southwestern New Mexico has experienced middle and late Cenozoic crustal extension in the Basin and Range and southern Rio Grande rift. In addition, there is a narrow Transitional Zone between the Basin and Range/Rio Grande rift and the largely undeformed Colorado Plateau that has also experienced late Cenozoic crustal extension. The most studied and best-understood province is the Rio Grande rift, which is generally considered to have developed in two stages. By comparison to the southern Rio Grande rift, there has been very little research directed toward understanding the extensional history of the Transitional Zone, primarily because of a lack of detailed geologic maps and few studies of the syntectonic/synvolcanic sedimentary unit, the Gila Conglomerate. Thirty-six outcrops, four standard petrographic thin sections, and one stratigraphic column of the Gila Conglomerate were analyzed in the Lake Roberts area. From this study, the Lake Roberts, Purgatory Chasm, Meerschaum Canyon, Skates Canyon, and Turkey Cienega Canyon members were classified as a part of the Gila Conglomerate near Lake Roberts, New Mexico.

The analysis of the stratigraphy and sedimentology of the Gila Conglomerate has provided the pieces necessary for understanding the evolution of the Sapillo Basin through time. Early, middle, and late stages have been identified for the Sapillo Basin. The early stage of the Sapillo Basin corresponds to those members of the Gila Conglomerate that directly overlie the Bearwallow Mountain Basalt, including the Lake Roberts, the lower part of the Meerschaum Canyon, and Skates Canyon members. During its early stage, the Sapillo Basin was a half graben, bordered on the north by the Copperas Peak fault and Buck Hannen and Loco Mountains, which constituted the footwall. The principal difference between the early and middle stages of the Sapillo Basin was progradation into the basin of the Purgatory Chasm member. The late stage of evolution of the Sapillo Basin corresponds to the time of deposition of the Turkey Cienega Canyon member.

This study also showed that the east-trending Copperas Peak fault north of Lake Roberts was active during the deposition of the Gila Conglomerate. The paleocurrent direction, clast shape and size, and sedimentary structures of the Meerschaum Canyon member reveal that this fault was active during deposition of the Gila Conglomerate.

University of New Mexico

EVALUATION OF AQUIFER RECHARGE USING A MASS-BALANCE MODEL AND CONSERVATIVE TRACERS, SANDIA NATIONAL LABORATORIES/KIRTLAND AIR FORCE BASE, ALBUQUERQUE, NEW MEXICO, by *Jerry K. Bird*, 1998, MS thesis, Department of Earth and Planetary Sciences, University of New Mexico, Albuquerque, NM 87131, 115 pp.

Recharge in arid and semi-arid climates is difficult to evaluate with traditional soil-physics and water-budget calculations that can provide estimates off by as much as an order of magnitude. The use of conservative tracers is an accepted method of evaluating mixing processes, residence time, recharge source, and recharge volume. This study uses the mass-balance model NETPATH and the conservative tracers Cl^-, Br^-, and ^2H to investigate potential recharge at Sandia National Laboratories/Kirtland Air Force Base

(SNL/KAFB), Albuquerque, New Mexico.

NETPATH is a U.S. Geological Survey model developed to evaluate mixing percentages of two or more initial waters and the mass-balance changes required along suspected hydrologic flow paths. I modeled mixing scenarios in four specific study areas at SNL/KAFB to evaluate ground-water flow. Single species conservative-tracer models were used to identify potential mixing proportions for well and spring pairs located near known or suspected preferential pathways. These pairs were also evaluated by NETPATH mass-balance models. Modeling scenarios that produce similar results with NETPATH and conservative-tracer models are considered the most robust. Although this type of modeling does not provide unique solutions, it can be used in conjunction with other hydrologic investigations to evaluate mixing processes occurring in an aquifer.

My results do not provide quantitative recharge estimates; however, they do provide qualitative evidence for mixing within the aquifer. Recent pumping has heavily perturbed local ground-water flow. The geochemical signatures observed in the study area may be reflective of the regional flow system prior to anthropogenic influences, but cannot be confirmed with this data set. Some results support other workers who have suggested that a concentrated, deep-basin water is upwelling near the basin-bounding fault system and mixing with a dilute recharge water in the basin. The source of this dilute water cannot be specified, but modeling results suggest that recent river and/or arroyo recharge as well as alluvial mountain-front recharge are possibilities. One simple model suggests that mixing of two sources east of the fault system will produce the geochemical signature observed in wells completed in the regional aquifer west of the faults.

SYNCHRONOUS PLUTONISM, METAMORPHISM, AND DEFORMATION OF THE 1.65 GA MANZANITA PLUTON, MANZANITA MOUNTAINS, NEW MEXICO, by *Cynthia L. Brown*, 1999, MS thesis, Department of Earth and Planetary Sciences, University of New Mexico, Albuquerque, NM 87131, 82 pp.

The 1.65 Ga Manzanita pluton and its aureole record an interaction of Paleoproterozoic plutonism, deformation, and metamorphism in New Mexico. Field observations and microscopic analysis indicate that the pluton was emplaced during regional northwest-southeast shortening. Synchronous plutonism and contact metamorphism are indicated by an increase in temperature from regional metamorphic greenschist grade rocks to contact metamorphic amphibolite grade rocks. Peak contact metamorphic temperatures and pressures of 600°–620°C and 2–3 kbar are shown by assemblages with Fe-rich andalusite + K-feldspar + biotite + quartz + white mica + oxides. Synchronous deformation and metamorphism are indicated by contact metamorphic mineral-matrix relationships including the growth of garnet before, during, and after development of the regional S_2 foliation, sillimanite that is both randomly oriented and aligned along S_2, and hornblende that is dynamically recrystallized along S_2. Synchronous plutonism and regional deformation are indicated by parallel magmatic and solid-state fabrics; dynamic recrystallization of feldspar indicating high-T solid-state deformation; variably deformed dikes and veins that cross-cut and are also folded by regional foliation; and dike orientations consistent with a regional kinematic framework of northwest-southeast shortening.

Recent radiometric dating constrains the timing of synpluton tectonism. The Manzanita pluton has been dated by U–Pb–zircon techniques at 1,645 ± 16.0 Ma. In addition a post-S_2 rhyolite dike to the south of the pluton cooled through 300°C at 1,428 ± 2.0 Ma, determined by $^{40}Ar/^{39}Ar$ techniques. Hornblende in the contact aureole of the pluton yields variable $^{40}Ar/^{39}Ar$ ages of circa 1.40 Ga and 1.67 Ga; variable ages are interpreted as hornblende growth at 1.65 Ga and reheating at 1.40 Ga to 400°–500°C.

ZIRCON DISSOLUTION, by *Katheryn B. Helean*, 1998, MS thesis, Department of Earth and Planetary Sciences, University of New Mexico, Albuquerque, NM 87131, 132 pp.

Zircon, $ZrSiO_4$, has been proposed as a host phase for excess weapons Pu. The chemical durability of zircon must be quantified so that the performance can be assessed. One consequence of immobilizing radioactive elements in the structure of zircon is that the structure loses atomic-scale periodicity due to self-irradiation caused by α-decay events. A unique aspect of zircon is that natural analogues exist for all stages of the expected structural degradation, from crystalline to amorphous, hydrous zircon. Previous studies of crystalline zircon failed to quantify the dissolution rates in water using static test methods. A high-temperature Soxhlet extractor, therefore, was designed to measure the forward rate of zircon dissolution at temperatures in the range of 120°–250°C. The forward dissolution rates for zircon based on the Si release rates are : 4.1×10^{-4} g m^{-2} day^{-1} at 250°C, 1.7×10^{-4} g m^{-2} day^{-1} at 200°C, and 7.1×10^{-5} g m^{-2} day^{-1} at 120°C. The Arrhenius activation energy for the zircon dissolution reaction is 23 kJ/mol. The dissolution of amorphous, hydrous "gel-zircon" was measured using a static test method. The forward dissolution rate for "gel-zircon" based on the U release profile is 8.5×10^{-3} g m^{-2} day^{-1} at 90°C. Using the Arrhenius relationship, the forward dissolution rate for crystalline zircon was extrapolated to 90°C from the data collected in this study. The forward dissolution rate for crystalline zircon at 90°C, 4.6×10^{-5} g m^{-2} day^{-1}, is two orders of magnitude lower than the forward rate for "gel-zircon." Based on these data, zircon would make a chemically durable host phase for excess weapons Pu. A 100 μm zircon crystal would survive 150,000 yrs in an open aqueous system at 90°C.

PROTEROZOIC MULTISTAGE (~1.1 AND ~0.8 GA) EXTENSION IN THE GRAND CANYON SUPERGROUP AND ESTABLISHMENT OF NORTHWEST AND NORTH-SOUTH TECTONIC GRAINS IN THE SOUTHWESTERN UNITED STATES, by *J. Michael Timmons*, 1999, MS thesis, Department of Earth and Planetary Sciences, University of New Mexico, Albuquerque, NM 87131, 66 pp.

The Grand Canyon Supergroup records a prolonged history of intracratonic rifting and sedimentation in rift basins during two or more distinct tectonic/depositional events in the late-Meso and Neoproterozoic. Mesoproterozoic Unkar Group deposition took place between 1.2 and 1.1 Ga during northeast-southwest extension on domino-style normal faults during Grenville northwest-directed contraction. The Neoproterozoic Chuar Group was deposited in a north-south rift basin, synchronous with movement on the Butte fault during east-west extension. Syntectonic sedimentation is documented by sedimentary patterns and sedimentary structures, including growth syncline and intraformational faults, within the Chuar Group. Neoproterozoic faults locally reactivate and cross-cut older Mesoproterozoic faults. Laramide monoclines have northwest and north-south segments that reactivate Unkar- and Chuar-age structures and are used to infer extent of each extensional event. We suggest that 1.1 Ga northwest structures and 0.8 Ga north-south structures have persisted into the Phanerozoic as important regional grains that influenced subsequent tectonism.

STREAM POWER AND INCISION OF FIVE MIXED ALLUVIAL-BEDROCK STREAMS, NORTHERN NEW MEXICO, by *David K. Mitchell*, 2000, MS thesis, Department of Earth and Planetary Sciences, University of New Mexico, Albuquerque, NM 87131.

The validity of modeling fluvial bedrock incision rates with the stream power law is evaluated on five northern New Mexico streams: the Rio Pueblo de Taos, Rio Hondo, Red River, Comanche Creek, and Jemez River. Fluvial terraces within these basins provide an excellent spatial and temporal record of fluvial bedrock incision. The stream power law follows the general form, $Z = kA^mS^n$, where Z is the incision rate, k is a constant that incorporates bedrock erodibility, A is drainage area (a proxy for discharge), S is channel gradient, and m and n are exponents that scale the relative importance of discharge and slope to incision. Five versions of the stream power law, with different m and n values and/or slight modifications to the general law, are tested. This study represents one of the first rigorous tests of the stream power law with field-measured discharge and slope data.

Stream power models generally reproduce field-measured incision rates within ≈10–20%. No single version of the stream power law consistently outperforms other models, although tributary junction analysis suggests an m/n ratio of 0.4, similar to the ratio of 0.5 for a unit stream power (m=0.5, n=1) or shear stress (m=0.33, n=0.66) model. Stream power models calculated using map-measured data match known incision rates as well as field-parameterized stream power models. Thus, substituting drainage area for discharge, a common technique of the map-based metric approach, may be valid because drainage area may represent the cumulative effects of many discharge events over geologic time. Stream power models reproduce incision rates measured over hundred-thousand-year time scales better than incision records from shorter or longer time scales. Shorter-term records (10^4–10^5 yr) are sensitive to local variabilities such as migrating knickpoints, whereas drainage-basin characteristics likely have changed for longer-term (10^6 yr) records.

Channel widths, valley-bottom widths, and controls on channel gradient and discharge generation are examined in the context of the parameters of the stream power law. Channel widths vary nearly as a function of the square root of

discharge. This relationship is similar to the relationship known for purely alluvial streams and those used in bedrock stream power models. Discharge-area relationships show that local geologic controls on discharge can cause significant differences in discharge production between adjacent basins. A comparison of New Mexico gage data with Washington State gage data shows that local geologic controls on discharge generation are more significant in semiarid New Mexico.

A discharge threshold that controls the effect of rock type on channel gradients is quantified. Above this threshold sufficient discharge is generated to maintain incision in the face of base-level fall, regardless of rock type. The discharge of threshold underscores the difficulty in calibrating the proportionality constant *k*, which likely varies spatially in response to rock-type changes and temporally in response to changes in discharge generation.

A combination of field and laboratory geomorphic, sedimentologic, and sedimentary petrographic methods are employed to document the sources of basin-fill sediment, the character and relative amount of sediment produced on local hillslopes through time, the hillslope weathering and transport processes occurring through time, and the role that rock type has played in regional landscape evolution. Results of these studies indicate rock type is the dominant control on sediment yield and landscape development in tectonically inactive, dry landscapes. Hillslope processes and products in the study area have been consistent through time, but process rates have varied greatly, indicating that orbital-scale climate cyclicity can be, but is not always, well expressed in the stratigraphy of continental basins.

A LONG-TERM RECORD OF CLIMATE-CONTROLLED HILLSLOPE SEDIMENTATION, by *Joel L. Pederson*, 1999, PhD dissertation, Department of Earth and Planetary Sciences, University of New Mexico, Albuquerque, NM 87131, 235 pp.

Rare exposures of buried hillslopes and colluvium are found in the upper Miocene and Pliocene basin-fill records of two extensional basins in southeastern Nevada. Study of the stratigraphy, sedimentology, and petrology of these hillslope deposits, along with the Quaternary record and modern slopes of the study area, produces a long-term record of variable hillslope-sediment production and delivery to piedmonts as a function of climate change. Though rare, ancient colluvium exists in the stratigraphic record, and its study is the most direct method of linking hillslope processes to basin depositional systems. Results enhance our ability to interpret the sedimentologic record, particularly in terms of climate controls, and clarifies the applications of arid-environment geomorphic research to sedimentology and basin analysis.

The upper Miocene and Pliocene Muddy Creek Formation and Pliocene Panaca Formation of southeastern Nevada are analogous in their role as late-stage (post-tectonic) basin fill deposited prior to basin integration and incision. The Muddy Creek Formation exposed in Table Mesa Basin consists of three members defined by sharp changes in depositional style. The lower member, dominated by internally-drained spring travertine and saline lacustrine deposits, underlies a relatively sharp, undulating contact with mostly extrabasinally-derived red, siliciclastic alluvium of the middle member. The middle member of the Muddy Creek Formation coarsens upward at its top in a gradational contact with the locally-derived coarse fluvial upper member, which, in turn, is truncated at its top by QTg gravel deposited after external drainage was established. The Panaca Formation consists of distal deposits of pond and littoral/marsh environments and medial and proximal alluvial-slope, fluvial, eolian, and colluvial deposits. Alluvial-slope deposits account for much of the exposed fill in the Panaca Basin, and its fine-grained, roughly parallel-bedded, and commonly massive character probably led to previous interpretations of these deposits as lacustrine.

A petrologic weathering index for sand, clay-mineral data, and stratigraphic relations all indicate that, in the Neogene, episodes of greater production and delivery of colluvium from hillslopes in the study area were marked by more intense chemical weathering and thus greater effective moisture. Strata that record only limited colluviation, less intense weathering, and piedmonts dominated by eolian processes very likely correspond to drier conditions. The climate-driven hillslope and piedmont landscape changes evident in these older stratigraphic records corroborate the conceptual model developed by Quaternary researchers for arid environments. Quaternary models of arid landscape change can therefore be used to interpret the stratigraphic record at least back into the Miocene, but though the mode of response is consistent through the record, the magnitude of sedimentologic response has varied greatly.

A HIGH-RESOLUTION PETROGRAPHIC STUDY OF THE CRETACEOUS FERRON SANDSTONE, COYOTE BASIN, UTAH: INTEGRATING PETROLOGY AND PETROPHYSICS, by *Karen N. Roche*, 1999, MS thesis, Department of Earth and Planetary Sciences, University of New Mexico, Albuquerque, NM 87131, 110 pp.

A high-resolution petrographic study is combined with laboratory measurements of porosity and permeability to characterize a fluvial-channel deposit in the Upper Cretaceous Ferron Sandstone. Thin sections were made of samples from four wells and five outcrop transects within a study volume 40.00 m × 16.5 m × 12.50 m deep. Five distinct sandstone units were defined for this volume, all of which are represented in the sampling. Thin-section macroporosity values range from 18.4% to 1.6% in outcrop samples and from 14.8% to 0.4% in core samples. Porosity determined from petrographic examination differs significantly from laboratory determinations. In most cases the petrographically determined measurements were approximately half of the volume of the bulk laboratory determination. The thin-section porosity counts suggest that up to half of the measured bulk porosity in some of the sandstones is comprised of interstitial clays, which lower the effective porosity of those units. Thin-section macroporosity values are found to correlate very well ($r^2 = 0.80$) with Hassler cell permeability values in core samples. The porosity measurements performed in the laboratory do not correlate as well with the Hassler cell permeability measurements ($r^2 = 0.59$).

The most significant factor in terms of porosity reduction is calcite cement. The degree of cementation is highly variable, ranging from 19.0% to 0.2% in outcrop samples and 20.8% to 0.4% in core samples. Authigenic, pore-filling kaolinite also contributes to porosity reduction. Incipient quartz overgrowths are present but do not contribute significantly to porosity reduction.

The differences between core and outcrop samples are due to weathering effects. The most important difference is the porosity (and therefore permeability) increase in the outcrop samples due to the dissolution of calcite cement.

STRATIGRAPHIC CYCLICITY AND MUD MOUND FORMATION IN MIDDLE CAMBRIAN DEEP-WATER CARBONATES, MARJUM FORMATION, HOUSE RANGE, WESTERN UTAH, by *Anna C. Snider*, 1999, MS thesis, Department of Earth and Planetary Sciences, University of New Mexico, Albuquerque, NM 87131, 126 pp.

The Middle Cambrian Marjum Formation (~400 m thick) in the House Range of western Utah is composed of deep-water carbonates, which were deposited in the axis of the House Range embayment. Within the Marjum Formation, there are three scales of cyclicity recognized, including (1) limestone-marl rhythmites (~5 cm thick), (2) rhythmite-mound cycles (3–30 m thick), and (3) large-scale sequences (145–190 m thick).

Rhythmites are composed of thin rhythmically interbedded, laterally continuous, limestone and marl layers. Limestone layers are composed of dark, laminated pelletal lime mudstone (~3 cm thick), and marl layers (~2 cm thick) are composed of laminated, argillaceous, dolomitized, pelletal lime mudstone; both lithologies contain rare agnostid trilobites and sponge spicules. Fine-grained carbonate and siliciclastic material in rhythmites is detrital in origin and was deposited in quiet, dyserobic waters, below storm-wave base. Alternations of limestone and marl layers are interpreted as the result of millennial-scale paleoclimatic fluctuations, which influenced changes in fluvial/ eolian influx and/or changes in the location or intensity of storms.

Rhythmite-mound cycles (3–30 m thick) are composed of limestone-marl rhythmites overlain by stromatactis-bearing carbonate mud mounds (0.5–1.5 m thick at crest). Mud mounds are composed of bioturbated pelletoidal lime mudstone with sparse trilobite wacke/packstone lenses and abundant spar-filled stromatactis-like structures. Mud mounds were precipitated in situ in deeper waters with some contribution from detrital carbonate and terrigenous sediment. Lime mud and pelletoids precipitated from highly alkaline waters produced by bacterial decay of siliceous sponges and microbial mats. The mud mounds are interpreted to have developed during a 10^4–10^5 year sea-level rise when the carbonate "factory" retrograded and the supply of fine, detrital carbonate material to the basinal regions decreased. During sea-level fall/lowstand, an increase in detrital carbonate influx due to carbonate factory progradation resulted in deposition of limestone–marl rhythmites.

Three large-scale siliciclastic-carbonate sequences (145–190 m thick) are recognized in the Wheeler Shale and Marjum Formations and are composed of shale and marl-dominated rhythmite facies grading into carbonate-dominated intervals. These sequences correlate to time-equivalent shallow-water carbonates that exhibit similar scale sequences interpreted to have formed in response to 3rd-order (1–3 m.y.)

eustatic sea-level changes. This across-platform correlation suggests the Wheeler–Marjum sequences were also formed in response to eustatic changes.

DEXTRAL TRANSCURRENT DEFORMATION OF THE EASTERN MARGIN OF THE COLORADO PLATEAU (USA) AND THE MECHANICS OF FOOTWALL UPLIFT ALONG THE SIMPLON NORMAL FAULT (SWITZERLAND/ITALY), by *Timothy F. Wawrzyniec*, 1999, PhD dissertation, Department of Earth and Planetary Sciences, University of New Mexico, Albuquerque, NM 87131

Two independent studies employ kinematic analysis of minor-fault populations to address large-scale tectonic problems. The first addresses the nature of transcurrent deformation along the eastern margin of the Colorado Plateau. The work is based on a combined fault kinematic and paleomagnetic investigation of rocks affected by faulting during the Laramide orogeny and younger Rio Grande rifting. The second evaluates the mechanics of footwall uplift along the Simplon low-angle normal fault in the Alps, by combining a fault kinematic study with fluid inclusion analysis of kinematically referenced fluid inclusion arrays.

Chapter 1 proposes a new model to describe the tectonic history of the eastern margin of the Colorado Plateau. The margin extends from southern New Mexico to northern Colorado and has experienced both Laramide-style deformation and Rio Grande rift extension. Limited age information on minor fault populations indicates that the eastern margin of the plateau has experienced a prolonged history of dextral transpression followed by dextral transtension.

Chapters 2 and 3 address the nature of extension along the Simplon low-angle normal fault (southern Switzerland and northern Italy). Structural and fluid-inclusion analysis indicates that at least part of the footwall of the Simplon shear zone experienced footwall uplift via a rolling hinge mechanism, and that the observed style of deformation and the transition from ductile to brittle deformation during the exhumation of mid-crustal rocks is in part influenced by the composition of syn-kinematic fluids. Specifically, faulting at mid-crustal depths is associated with the occurrence of carbonic fluids. Different wetting characteristics of carbonic versus aqueous fluids probably influenced the mechanical behavior of the rocks during exhumation. A comparative analysis of the Simplon shear zone with the Brenner shear zone (Chapter 3), a low-angle extensional structure located in the eastern Alps, reveals remarkable similarities. The uniformity of structural style along these two structures is likely due to (1) external tectonic controls, and (2) introduction of carbonic fluids into these shear zones at mid-crustal depths to aid in formation of a sub-vertical simple shear rolling hinge to accommodate footwall uplift during extensional unloading of the footwall rocks.

A FLUVIAL RECORD OF ROCK UPLIFT ALONG THE JEMEZ LINEAMENT, GREAT PLAINS OF NORTHEASTERN NEW MEXICO, by *Paul A. Wisniewski*, 1999, MS thesis, Department of Earth and Planetary Sciences, University of New Mexico, Albuquerque, NM 87131, 118 pp.

Post-Laramide rock uplift in the western United States has been the subject of a long-standing debate, fueled in part by deep fluvial incision into the world's second largest orogenic plateau. Studies of late Cenozoic landscape evolution in the Rocky Mountains have focused on deeply incised fluvial systems, which have been touted as critical evidence for post-Laramide epeirogeny. Debate persists about whether this plateau achieved its current elevation during the Laramide orogeny or more recently in the late Cenozoic. The latter of these models has broad implications for the mechanisms that uplift rocks after compression and crustal thickening has ceased. Efforts to elucidate a rock uplift signal from fluvial systems are complicated by numerous non-tectonic mechanisms, such as climate change, that also drive river incision and have typically contributed little to our understanding of post-Laramide rock-uplift processes.

This study presents new incision data from a well-constrained reach of a Rocky Mountain front–Great Plains river that is uniquely situated to isolate the effects of post-Laramide rock uplift. The Canadian River of northeastern New Mexico is one of four major Great Plains rivers draining the eastern slope of the Rocky Mountain front. This river has carved a deep (~300 m), narrow canyon through Mesozoic strata at a location where its profile is broadly convex and crosses the Jemez lineament, a well-known, northeast-trending line of late Cenozoic volcanism. The numerically dated (^{14}C and $^{40}Ar/^{39}Ar$) fluvial terrace and volcanic stratigraphy in this canyon reach constrain rates of fluvial bedrock incision. Incision is maximized in the canyon reach where it has been relatively steady at ~0.06 mm/yr (60 m/m.y.) over the past ~4.5 Ma. Canyon reach terraces are correlated to produce paleo-long profiles that are increasingly convex with profile age and converge to the modern channel profile both upstream and downstream of the canyon reach. Similar terrace profiles are currently unknown for well-studied streams in the adjacent Rio Grande rift where rates of incision can be greater by a factor of three. These observations of the study area are best explained by invoking a slow but steady rate of rock uplift during the late Cenozoic beneath the Canadian River along a northeast-trending axis coincident with the Jemez lineament. Recently acquired geophysical data, including upper mantle velocity structure, suggest that hot asthenospheric mantle is rising diapirically beneath the southern Rockies and is subsequently funneled along compositional and structural heterogeneities at the base of the lithosphere. The Jemez lineament has long been recognized as one of these heterogeneities, and the Canadian River incision data likely indicate rates of rock uplift for the mantle processes acting at its base. If rates of incision and rock uplift for the Canadian River are representative for the southern Rockies in general, then they place constraints on the timing and degree of high-standing topography for the western Cordillera.

MULTIPHASE THERMAL MODELING IN VOLCANIC AND CONTACT METAMORPHIC TERRANES, by *Gordon N. Keating*, 2000, PhD dissertation, Department of Earth and Planetary Sciences, University of New Mexico, Albuquerque, NM 87131.

This dissertation presents the results of unique numerical models of hydrothermal systems in unsaturated pyroclastic rocks. A simple one-dimensional, radial conductive finite-difference heat-flow model is demonstrated to be an adequate tool for investigating possible thermal conditions in a limited contact metamorphic aureole that developed around a large mafic intrusion in unsaturated, silicic host rocks at Grants Ridge, New Mexico. A modified version of the Los Alamos National Laboratory code, FEHM, is presented that has a unique capability of simulating multiphase (air + H_2O) flow under the high-temperature conditions near intrusive The modified equations of state (EOS) for water and air are valid in the ranges $10° < T < 1500°C$, $0.00123 < P < 1000$ MPa, and $10° < T < 1500°C$, $0.00123 < P < 22$ MPa, respectively.

Two applications of the FEHM code are presented. A two-dimensional model of multiphase flow near a magmatic intrusion was constructed to characterize the cooling history of part of a late-Miocene mafic intrusive complex at Paiute Ridge, Nevada, USA. The results of the model were combined with paleomagnetic data to estimate that the rate of change of the transitional part of the geomagnetic field during a reversal was 0.06–0.13 degrees/year.

Multiphase cooling processes in cooling ash-flow tuffs (ignimbrites) were investigated using a set of FEHM models. The results of these models identify important factors in the cooling history, including the presence of a saturated zone in the shallow substrate, geometry of the substrate-ignimbrite interface (e.g., buried valleys), and welding zonation and fumarole structures within the ignimbrite. In addition, the models shed light on conditions that may give rise to the development of secondary explosions in ignimbrites. Finally, the model results indicate that superheated vapor from the boiling zone at the base of the ignimbrite, flowing upward through the core, may provide the necessary water mass in the upper zones of the ignimbrite to account for reported oxygen-isotope exchange in the Bishop and Chegem Tuffs, rather than requiring high meteoric infiltration on the surface of the ignimbrite, as previously proposed.

Geographic Names

U. S. Board on Geographic Names

Cañada del Agua—arroyo, 0.8 km (0.5 mi) long, heads 3.5 km (2.2 mi) southwest of Rainsville at 35°58'10"N, 105°14'48"W, trends southwest 1.6 km (1 mi) before joining Cañon del Agua, 1.6 km (1 mi) north-northwest of the community of La Cueva; Spanish name meaning "little valley of water"; Mora County, NM; T20N R16E, NMPM; 35°57'21"N, 105°15'16"W; USGS map, Mora 1:24,000 (mouth of feature).

Montoya Pasture—flat, 4.8 km (3 mi) by 4 km (2.5 mi), elevation 2,057 m (6,749 ft), in Gila National Forest/Gila Wilderness, located southeast of the confluence of Diamond Creek and the East Fork Gila River, 8 km (5 mi) east of the Gila Cliff Dwellings National Monument; named for Donaciano Montoya, who homesteaded and ranched in the area in the early 20th century; Catron County, NM; T12S R13W, NMPM; 33°14'30"N, 108°09'05"W; USGS map, Gila Hot Springs 1:24,000 (central point); *not* Montoya Ranch.

Perra Peak—summit, elevation 3,586 m (11,765 ft), in Carson National Forest, 1.6 km (1 mi) south-southwest of Lobo Peak, 2.3 km (1.4 mi) north of Gallina Peak, 4.5 km (2.8 mi) east-northeast of Kiowa Village; Spanish name meaning "female dog"; Taos County, NM; sec. 4 T27N R13E, NMPM; 36°35'54"N, 105°33'03"W; USGS map, Arroyo Seco 1:24,000.

Puerto del Venado Alazán—gap, 0.8 km (0.5 mi) west of State Route 21, 2.5 km (1.6 mi) west of Rainsville, 4.2 km (2.6 mi) north-northeast of La Cueva; Spanish name meaning "port of the red elk"; Mora County, NM; T20N R16E, NMPM; 35°58'43"N, 105°14'14"W; USGS map, Rainsville 1:24,000.

—Dave McCraw
NMBMMR Correspondent

in an artificial magma: Variations in crystal shape, growth rate, and composition with melt cooling history: Contributions to Mineralogy and Petrology, v. 120, pp. 412–425.
Farnham, L. L., 1961, Manganese deposits of New Mexico: U.S. Bureau of Mines, Information Circular 8030, 176 pp.
Fournier, R. O., 1985a, The behavior of silver in hydrothermal solutions; *in* Berger, B. R., and Bethke, P. M. (eds.), Geology and geochemistry of epithermal systems: Reviews in Economic Geology, v. 2, pp. 45–62.
Fournier, R. O., 1985b, Carbonate transport and deposition in the epithermal environment; *in* Berger, B. R., and Bethke, P. M. (eds.), Geology and geochemistry of epithermal systems: Reviews in Economic Geology, v. 2, pp. 63–72.
Jacobs, G. K., Dunbar, N. W., Naney, M. T., and Williams, R. T., 1992, In-situ vitrification: Observations of petrological processes in a man-made magmatic system: EOS, Transactions of the American Geophysical Union, v. 73, pp. 401–411.
Julyan, R., 1996, The place names of New Mexico: University of New Mexico Press, Albuquerque, 385 pp.
Kiely, J. M., and James, W. C., 1988, Diagenesis of the fanglomerate of Little Florida Mountains (Miocene), southwestern New Mexico; *in* Mack, G. H., Lawton, T. F., and Lucas, S. G. (eds.), Cretaceous and Laramide tectonic evolution of southwestern New Mexico: New Mexico Geological Society, Guidebook 39, pp. 175–184.
Lasky, S. G., 1940, Manganese deposits in the Little Florida Mountains, Luna County, New Mexico; a preliminary report: U.S. Geological Survey, Bulletin 922-C, pp. 55–73.
Lofgren, G., 1970, Experimental devitrification rate of rhyolitic glass: Geological Society of America, Bulletin, v. 81, pp. 553–560.
Lofgren, G., 1971, Spherulitic textures in glassy and crystalline rocks: Journal of Geophysical Research, v. 76, no. 23, pp. 5635–5648.
McAnulty, W. N., 1978, Fluorspar in New Mexico: New Mexico Bureau of Mines and Mineral Resources, Memoir 34, 64 pp.
McLemore, V. T., 1996, Copper in New Mexico: New Mexico Geology, v. 18, pp. 25–36.
McLemore, V. T., Sutphin, D. M., Hack, D. R., and Pease, T. C., 1996, Mining history and mineral resources of the Mimbres Resource Area, Doña Ana, Luna, Hidalgo, and Grant Counties, New Mexico: New Mexico Bureau of Mines and Mineral Resources, Open-file Report 424, 252 pp.
Northrop, S. A., and LaBruzza, F. A., 1996, Minerals of New Mexico: University of New Mexico Press, Albuquerque, New Mexico, 356 pp.
Shaub, B. M., 1979, Genesis of thundereggs, geodes, and agates of igneous origin: Lapidary Journal, v. 32, pp. 2340–2354, 2548–2566.
Stanley, F., 1962, The Deming, New Mexico, story: F. Stanley, P.O. Box 107, Nazareth, Texas, 20 pp.
Taylor, B. E., 1986, Magmatic volatiles: isotopic variation of C, H, and S; *in* Valley, J. W., Taylor, H. P., and O'Neil, J. R. (eds.), Stable isotopes in high temperature geological processes; Reviews in mineralogy: Chelsea, Michigan, Mineralogical Society of America, pp. 185–225.
Weber, R. H., 1980, Rockhound: New Mexico Geology, v. 2, pp. 59–60.

—Virginia McLemore and Nelia Dunbar

Book review

***Hydrogeology in practice—a guide to characterizing ground-water systems*, by William J. Stone, 1999, Prentice-Hall, Upper Saddle River, NJ 07458, ISBN 0-13-899154-5 (pbk)**

With this book Stone bridges the gap between the academic and the applied worlds of hydrogeology. Despite its shortcomings, this book should be on the shelf of every practicing ground-water scientist. I've divided this review into three parts: the book's content and organization, the reasons I believe it's worth your consideration, and the changes that I would recommend for the second edition.

Content and structure

After the preface, the book consists of fourteen chapters, a glossary, five appendices, and an index. References conclude each chapter. After the introductory chapter, Stone created four parts. Chapters 2, 3, and 4, "Compiling geologic information," "Characterizing the geologic setting," and "Geologic materials as aquifers," make up Part I, *The geologic setting*.

Chapters 5, 6, and 7, "Compiling hydrologic information," "Characterizing hydrologic conditions," and "Hydrologic impact of the geologic setting," make up Part II, *The hydrologic system*.

Chapters 8 and 9, "Conceptual hydrogeologic models" and "Writing hydrogeologic reports," make up Part III, *Synthesis*.

Chapters 10 through 15, "Water supply," "Ground-water contamination," "Hydrologic monitoring," "Water problems in mining," "Ground-water modeling," and "Final suggestions," make up Part IV, *Applications*.

The book contains 104 illustrations and 25 tables.

Appendix A is "Guide to logging cuttings/core," Appendix B is a sample "Well-inventory data sheet," Appendix C lists "Elements of an ideal conceptual hydrogeologic model," Appendix D is a sample "Well-construction data sheet," and Appendix E includes "Miscellaneous conversions, equivalents, and formulas."

Pluses

For New Mexico ground-water scientists and engineers the book contains 48 illustrations and 9 tables of New Mexico examples. Moreover chapters 10 through 14 each contain case histories that involve the illustrations and tables used in earlier chapters to help explain the themes of the individual chapters. Thus we have early examples of specific topics that are tied together in the case histories. A good idea and well executed.

Chapter 9, "Writing hydrogeologic reports," explains the need for and how to write concise reports. Having read hundreds of reports, I can only say that I wish that most of their authors had read this chapter before they made me suffer from their poor organization, needless duplication, and soporific prose.

Stone's Chapter 15, "Final suggestions," is worth the price of the book. His suggestions are remember the basics, use intuition, apply models wisely, be right, maintain professionalism, practice good writing, and keep learning. Everyone involved from the boss to the newest employee should read this chapter at least every six months to remind themselves what professional ground-waterists are all about.

Minuses

Things I would like to see in the next edition include:

• A discussion of the water table and the role of hydraulic head with cross sections showing head distribution as a function of depth. Only one cross section in the book shows isohead lines; the others use arrows to depict the direction of ground-water flow, if they depict it all.

• A discussion of the difference in use and construction of wells and piezometers would help many readers appreciate ground-water behavior in three dimensions.

• The use of more cross sections to better illustrate features portrayed on more than one map.

• A discussion of the preparation of isopach and structure maps (p. 21), stressing their dualistic nature. The thickness contoured by isopach maps should be exactly the same as that determined from the equivalent structure maps. Too often these maps are drawn independently and never checked for conformability.

• Stone has included a detailed justification of the word "aquifer." Not necessary. Besides, hydrogeologists will come to learn that the term doesn't really carry its weight. Water-bearing and water-yielding rocks are more useful terms.[1]

• In his chapter on report writing, Stone advocates a format sometimes known as the mystery format. The problem, the method, the results, and the conclusion. Reports read better and require virtually no executive summary, when they state the conclusions in the first paragraph. For example here's a first sentence that gets a client's attention and cooperation:

"This report explains why XYZ Company has polluted a segment of the ground-water environment and how a simple six-well remedial well field with six monitoring wells will solve the problem."

• Although the book is subtitled *A guide to characterizing ground-water systems*, it doesn't deal adequately with the difference between working in recharge and discharge areas. Instead it tends to deal with areas the size of contour maps. The next edition should describe ground-water systems and how the principles apply to them.

Closure

This book brings together ideas from multiple sources. It's a good stab at a much-needed subject. Buy it. Use it. Tell Stone about your pet peeves, and let's help make the second edition the "final answer."

[1]I know my view on this point isn't shared by many

Service/News

**Only starred items (*) are available from New Mexico Bureau of Mines and Mineral Resources*

New publications

Open-file reports

NMBMMR

(web site: http://geoinfo.nmt.edu/)

***444a**—Field logs of borehole drilled for nest piezometers, Montesa Park site, Bernalillo County, New Mexico, by R. M. Chamberlin, B. D. Allen, J. W. Hawley, S. D. Connell, and M. Heynekamp, 1999, 16 pp., 4 tables, 2 figs. $5.20

***444b**—Field logs of borehole drilled for nested piezometers, Sierra Vista West Park site, Bernalillo County, New Mexico, by R. M. Chamberlin, P. B. Jackson, S. D. Connell, M. Heynekamp, and J. W. Hawley, 1999, 30 pp., 4 tables, 3 figs. $8.00

***444c**—Field logs of borehole drilled for monitoring well at Dome Road site, Cañada de Cochiti Grant, Sandoval County, New Mexico, by R. M. Chamberlin, P. B. Jackson, and S. D. Connell, 1999, 30 pp. $8.00

***446**—Hydrocarbon source rock evaluation, A. G. Hill No. 1 Federal A well, sec. 27 T9N R19E, Guadalupe County, New Mexico, by G. S. Bayliss, 2000, 11 pp., 5 tables, 1 fig., 1 appendix. $3.20

***447**—Reservoir rock evaluation of Pennsylvanian sandstones, El Paso San Juan 29-5 No. 50 well and Phillips San Juan Deep 30-06 No. 112Y, Rio Arriba County, New Mexico, by Reservoirs Inc., 2000, 88 pp., 10 tables, 10 figs., 26 plates. $19.60

***448**—Hydrocarbon source facies characterization, Pennsylvanian-age sediment penetrated by the El Paso Natural Gas Company No. 50 San Juan 29-5 well, Rio Arriba County, New Mexico, by G. S. Bayliss, 2000, 94 pp., 4 tables, 3 figs. $20.80

***449**—Hydrocarbon source facies character of sediments penetrated by the Shell Oil Company No. 1 Isleta Central well, Valencia County, New Mexico, sec. 7 T7N R2E, by G. S. Bayliss, 2000, 59 pp., 4 tables, 1 appendix. $13.80

***450**—Hydrocarbon source facies character of sediments penetrated by the Shell Oil Company No. 1 Santa Fe well, Sandoval County, New Mexico, sec. 18 T13N R3E, by G. S. Bayliss, 2000, 53 pp., 4 tables, 5 figs., 1 appendix. $12.60

USGS

(web site: http://pubs.usgs.gov/)

99–0386—"Can't see the geology for the ground clutter"—shortcomings of the modern digital topographic base, by D. J. McCraw; *in* D. R. Soller (ed.) Digital Mapping Techniques '99 Workshop Proceedings, 1999, pp. 21–25.

99–0404—Digital aeromagnetic data from the Sandoval–Santa Fe, Belen, and Cochiti airborne surveys; covering areas in Rio Arriba, Sandoval, Santa Fe, Socorro, and Valencia Counties, New Mexico, by U.S. Geological Survey, Sander Geophysics, and Geoterrex–Dighem, 1999, CD-ROM.

Other publications

Austin, G. S., and Barker, J. M., 1998, What geologists should know about cement and concrete; *in* Bélanger, M., Clark, T., and Jacob, H-L., Proceedings of the 33rd forum on the geology of industrial minerals: Canadian Institute of Mining, Metallurgy, and Petroleum, Special Volume 50, pp. 101–113.

Barker, J. M., Austin, G. S., and Santini, K., 1999, What geologists (and perhaps others) should know about marketing industrial minerals, rocks, and materials; *in* Johnson, K. S. (ed.), Proceedings of the 34th forum on the geology of industrial minerals, 1998: Oklahoma Geological Survey, Norman, Circular 102, pp. 281–295.

Brandvold, L. A., and McLemore, V. T., 1998, A study of the analytical variation of sampling and analysis of stream-sediments from areas contaminated by mining and milling: Journal of Geochemical Exploration, v. 64, pp. 185–196.

Broadhead, R. F., 1999, Underdeveloped oil fields—Upper Pennsylvanian and lower Wolfcampian carbonate reservoirs of southeast New Mexico: Carbonates and Evaporites, v. 14, no. 1, pp. 84–105.

Broadhead, R. F., 1999, Underdeveloped oil fields in Upper Pennsylvanian and Lower Permian carbonates of southeast New Mexico—initial development missed major reserves: The Leading Edge, September, pp. 1012, 1014–1017.

Cataldi, R., Hodgson, S. F., and Lund, J. W. (eds.), 1999, Stories from a heated earth—our geothermal heritage: Geothermal Resources Council, Davis, CA, 588 pp.

Coose, K. E., and Austin, G. S., 1999, Variations in New Mexico concrete through time; *in* Johnson, K. S. (ed.), Proceedings of the 34th forum on the geology of industrial minerals 1998: Oklahoma Geological Survey, Norman, Circular 102, pp. 181–187.

Heynekamp, M. R., Goodwin, L. B., Mozley, P. S., and Haneberg, W. C., 1999, Controls on fault-zone architecture in poorly lithified sediments, Rio Grande rift, New Mexico—implications for fault-zone permeability and fluid flow; *in* Haneberg, W. C., Mozley, P. S., Moore, J. C., and Goodwin, L. B. (eds.), Faults and subsurface fluid flow in the shallow crust: American Geophysical Union, Washington, DC, Geophysical monograph 113, pp. 27–49.

Heywood, C. E., 1998, Piezometric-extensometric estimations of specific storage in the Albuquerque Basin, New Mexico; *in* Borchers, J. W. (ed.), Land subsidence; case studies and current research; proceedings of the Dr. Joseph F. Poland symposium on land subsidence: Association of Engineering Geologists, Special Publication 8, pp. 435–440.

Knesel, K. M., Davidson, J. P., and Duffield, W. A., 1999, Evolution of silicic magma through assimilation and subsequent recharge; evidence for Sr isotopes in sanidine phenocrysts, Taylor Creek Rhyolite, New Mexico: Journal of Petrology, v. 40, no. 5, pp. 773–786.

Love, D. W., Whitworth, T. M., Davis, J. M., and Seager, W. R., 1999, Free-phase NAPL-trapping features in intermontane basins: Environmental & Engineering Geoscience, v. V, no. 1, pp. 87–102.

Machette, M. N., 1998, Contrasts between and short- and long-term records of seismicity in the Rio Grande rift; important implications for seismic-hazards analysis (abs.); *in* Lund, W. R. (ed.), Proceedings volume, Basin and Range province seismic-hazards summit: Utah Geological Survey, Miscellaneous Publication 98-2, p. 25.

Minor, S. A., and Sawyer, D. A., 1999, Structural evolution of a rift border fault zone–La Bajada fault zone, Rio Grande rift, northern New Mexico (abs.): Geological Society of America, Abstracts with Programs, 1999 annual meeting, v. 31, no. 7, p. 112.

Reiter, M., 1999, Stress analyses of a simple fault asperity; *in* Amadei, Kranz, Scott, and Smeallie (eds.), Rock mechanics for industry: Balkema, Rotterdam, pp. 391–397.

Reiter, M., 1999, Hydrogeothermal studies in New Mexico and implications for groundwater resources: Environmental & Engineering Geoscience, v. V, no. 1, pp. 103–116.

Reiter, M., 1999, Hydrogeothermal studies on the southern part of Sandia National Laboratories/Kirtland Air Force Base—data regarding ground-water flow across the boundary of an intermontane basin; *in* Haneberg, W. C., Mozley, P. S., Moore, J. C., and Goodwin, L. B. (eds.), Faults and subsurface fluid flow in the shallow crust: American Geophysical Union, Washington, DC, Geophysical monograph 113, pp. 207–222.

Sigda, J. M., Goodwin, L. B., Mozley, P. S., and Wilson, J. L., 1999, Permeability alteration in small-displacement faults in poorly lithified sediments, Rio Grande rift, central New Mexico; *in* Haneberg, W. C., Mozley, P. S., Moore, J. C., and Goodwin, L. B. (eds.), Faults and subsurface fluid flow in the shallow crust: American Geophysical Union, Washington, DC, Geophysical monograph 113, pp. 51–68.

Utah Geological Association, 2000, Geology of Utah's parks and monuments: Utah Geological Association, Publication 28, 550 pp.

Whitworth, T. M., Haneberg, W. C., Mozley, P. S., and Goodwin, L. B., 1999, Solute-sieving-induced calcite precipitation on pulverized quartz sand—experimental results and implications for the membrane behavior of fault gouge; *in* Haneberg, W. C., Mozley, P. S., Moore, J. C., and Goodwin, L. B. (eds.), Faults and subsurface fluid flow in the shallow crust: American Geophysical Union, Washington, DC, Geophysical monograph 113, pp. 149–158.

Upcoming geologic meetings

Conference title	Dates	Location	Contact for more information
17th Annual Gem and Mineral Show	Sept. 2–4	Silver City, NM	Jim Lett, (505) 338-3216
Denver Gem and Mineral Show	Sept. 14–17	Denver, CO	www.denvermineralshow.com
Rocky Mountain Section AAPG Annual Meeting	Sept. 17–20	Albuquerque Hilton Albuquerque, NM	Albuquerque Geological Society Paul A. Catacosinos, paulcat@attglobal.net (505) 299-3544
Association of Engineering Geologists Annual Meeting	Sept. 19–26	San Jose, CA	Bob Tespel, bobtepe@packbell.net aegweb.org
Environmental Sedimentology Research Conference: Hydrogeology of Sedimentary Aquifers	Sept. 24–27	Santa Fe, NM	Dr. Matt Davis, Dept. of Earth Sciences Univ. of New Hampshire, Durham, NH 03824 (603) 862-4199, matt.davis@unh.edu
American Institute of Professional Geologists	Oct. 10–14	Pfister Hotel Milwaukee, WI	Wisconsin Section of AIPG webmaster@aipgwis.org
AFNMS/RMFMS Show and Conference	Oct. 12–15	Moab, UT	Dean Richardson, (801) 595-6750
New Mexico Geological Society 51st Fall Field Conference	Oct. 18–21	Lordsburg, NM	Dr. Timothy F. Lawton, Dept. of Geo. Sciences New Mexico State University, Las Cruces, NM 88003 (505) 646-4910, tlawton@nmsu.edu
Chaparral Rockhounds Gem & Mineral Show	Oct. 21–22	Roswell, NM	(505) 622-3130
Remote Sensing 2000: From Spectroscopy to Remotely Sensed Spectral Observation	Oct. 22–25	Corpus Christi, TX	R. Muttiah, Blackland Research Center 720 East Blackland Rd., Temple, TX 76502 (254) 770-6659, muttiah@brc.tamus.edu
Rocky Mountain Association of Geologists, and Denver Association of Petroleum Landmen, and Denver Geophysical Society	Nov. 7	Denver Convention Denver, CO	Rocky Mountain Association of Geologists 820 16th St., Ste. 505, Denver, CO 80202 (303) 573-8621, RMAGdenver@aol.com
21st New Mexico Mineral Symposium	Nov. 11–12	Macey Center Socorro, NM	Virgil W. Lueth, NMBMMR Socorro NM 87801 (505) 835-5140
GSA Annual Meeting	Nov. 13–16	Sparks Convention Center, Reno, NV	GSA Meetings Dept., (800) 472-1988 meetings@geosociety.org
American Geophysical Union Fall Meeting	Dec. 15–19	San Francisco, CA	AGU Meetings Dept., (800) 966-2481 meetinginfo@agu.org
Symposium on Volcanoes and Volcanology in New Mexico	Feb. 17, 2001	New Mexico Museum of Natural History and Science Albuquerque, NM	L. S. Crumpler, NMMNHS 1801 Mountain Road NW Albuquerque, NM 87104 lcrumpler@nmmnh.state.nm.us fax: (505) 841-2866

NEW MEXICO GEOLOGY

Science and Service

New Mexico Bureau of Mines and Mineral Resources
New Mexico Institute of Mining and Technology
801 Leroy Place
Socorro, New Mexico 87801-4796